# Universitetet i Stavanger

**Faculty of Science and Technology**

# MASTER'S THESIS

| Study program/Specialization:<br><br>Petroleum Geosciences Engineering | Spring semester, 2017<br><br>Open Access |
|---|---|
| Writer: Andrés Felipe Cedeño Motta | <br><br>_____<br>Writer's signature |

| Faculty supervisors: Alejandro Escalona Varela – Sverre Ekrene Ohm |
|---|
| External supervisor(s): |

| Thesis title: |
|---|
| Geochemical analysis of oils from Barbados and basin modeling of Paleozoic units in the southern Llanos basin, Colombia |

| Credits (ECTS): 30 |
|---|

| Keywords:<br><br>Caribbean region<br>Hydrocarbon potential<br>Barbados accretionary prism, Tobago forearc basin<br>Geochemical characterization<br>Southern Llanos basin<br>2D basin modeling | <br><br>Pages: 137<br><br>Enclosure: USB<br><br><br>Stavanger, July 14th 2017 |

# Geochemical analysis of oils from Barbados and basin modeling of Paleozoic units in the southern Llanos basin, Colombia

**By**
**Andrés Felipe Cedeño Motta**

## Master Thesis

Presented to the Faculty of Science and Technology
University of Stavanger

**University of Stavanger**
**July, 2017**

# Acknowledgements

# *Geochemical analysis of oils from Barbados and basin modeling of Paleozoic units in the southern Llanos basin*

## Abstract

This study evaluates two separate areas using different approaches that help improve knowledge regarding their hydrocarbon potential: 1 - A frontier region lying between the junction of the Barbados accretionary prism and the Tobago basin; 2. - A mature basin such as the southern Llanos basin in Colombia. Both areas are located within the hydrocarbon-rich southern Caribbean margin.

Commercial oil production from The Woodbourne oil field and the presence of migrated petroleum in outcropping rocks onshore Barbados prove the existence of a working petroleum system in the region. Barbados petroleum is suggested (Lawrence et al., 2002; Burggraf et al., 2002; Leahy et al., 2004; Hill and Schenk, 2005) to have been generated by facies similar to the Upper Cretaceous carbonate rich La Luna Formation onshore South America, but it has so far not been proved. This study presents detailed organic geochemical observations on six crude oils, one seepage, and bitumen from seven outcrop samples, in order to investigate heterogeneities in petroleum composition, thermal maturity, and biodegradation, and to investigate the filling history of the Woodbourne field. The results were also compared with published geochemical data for other northern South American and Caribbean oils/source rocks. In addition, the hydrocarbon potential of four Paleogene source rocks was evaluated.

The geochemical data suggest that the petroleum present in Barbados can be divided into two compositional and maturity groups (group A and B). The petroleum in both groups was derived from Cretaceous shaly source rocks deposited in oxic-to-dysoxic marine environments with varying contribution of marine and land plants-derived organic matter. Group A petroleum was generated and expelled at low maturity levels (0.72-0.77%Ro), and was derived from predominantly marine organic matter. By contrast, petroleum in group B was generated at higher maturity levels (0.87-0.94%Ro), and was derived from a more proximal source rock influenced by terrestrial organic matter. These observations indicate the existence of two separate kitchens sourcing the Barbados petroleum.

Organic geochemical data also suggest that reservoirs at the Woodbourne field has received two pulses of oil. The first oil pulse represents a filling event believed to have charged the reservoirs after the Mid-Miocene uplift of the Barbados ridge. This oil was biodegraded in the reservoirs above 1000 meter depth. The second more recent pulse consists of very light hydrocarbons (n-C3 to n-C9). This oil probably got separated from the parental oil and escaped through faults and/or failing seals during/after the last tectonic event in the Pliocene. Both oils seem to be compositionally similar and to have the same maturity level.

Geochemical comparison of the Barbados sample set with Upper Cretaceous oils and source rocks from several basins in northern South America and Caribbean region indicates that Barbados petroleum was not derived from carbonate facies typical of La Luna Formation or its equivalent in eastern Venezuela The Querecual Formation. Finally, Rock-Eval pyrolysis data indicate that the studied Paleogene source rocks have poor generation potential.

On the other hand, hydrocarbons exploration in the Llanos basin began in the 1980's. Exploration trends have focused exclusively on the Cretaceous-Cenozoic foreland plays, and no hydrocarbons sourced by Paleozoic rocks have yet been discovered. Forward 2D basin modeling was performed along a profile to evaluate timing of hydrocarbon generation and expulsion and hydrocarbon phase from a potential Lower Ordovician source rock interval. The 2D model of the subsurface was constrained using a published interpretation of an E-W regional 2D seismic line, in which the basin sedimentary infill is divided into five tectono-stratigraphic sequences, and data from three exploration wells. Calibration data was available for the three wells, and included vitrinite reflectance and temperature data. Modeling results show that by Late Ordovician-Early Silurian a first major phase of transformation (average 60%) occurred in the deepest places of the basin. Later, Permian uplift and denudation most probably destroyed any hydrocarbon accumulation existing in the western and central parts of the basin. A second phase of generation begins in the Eocene-Paleogene and continues up to present day within the easternmost extension of the basin. This potential petroleum system has not undergone the degree of uplift, erosion, and destruction of reservoirs in the eastern part of the basin, making preservation of any petroleum accumulation much more feasible. Thus, potential for finding an alternative source of hydrocarbons in a mature basin exists in the eastern depocenters, where newly generated hydrocarbons (mainly gas) could coexist with older petroleum preserved from the first generation phase.

# Contents

# List of Figures

# List of Tables

# 1.     INTRODUCTION

Within the hydrocarbon-rich sedimentary basins of northern South America and southern Caribbean region, Upper Cretaceous rocks have been recognized to be the most prolific source for hydrocarbons (Talukdar et al., 1993). However, organic-rich intervals of Early Cenozoic age have also contributed to biogenic and thermogenic gas and oil accumulations in the onshore foreland basins and offshore basins of the Caribbean and Atlantic coasts of Colombia, Venezuela, and Trinidad (Escalona and Mann, 2011). Alternatively, Paleozoic sediments have been proposed as additional source rocks in the onshore Sub-Andean foreland basins of Colombia and Venezuela (Dueñas and Cesari, 2006).

In the northern South America region, diachronous and oblique collision between the Caribbean and the South American plates (Pindell and Barrett, 1990; Lugo and Mann, 1995; Mann et al., 2006) has resulted in a complex distribution of basins, source rocks, and active petroleum kitchens (Fig. 1.1.). Despite the complexity and variability in the nature of Caribbean basins, the two study areas evaluated in the present study are characterized by oils derived from Upper Cretaceous source rocks: 1) An offshore frontier region at the boundary between the Barbados accretionary prism and the Tobago basin where the distribution, thermal maturity, and facies variations of Upper Cretaceous source rocks, and their organic geochemical affinity with Caribbean oils and source rocks remain fundamentally unknown; and 2) A mature onland basin such as the southern Llanos basin where underexplored Paleozoic units might offer an alternative source of hydrocarbons. Petroleum from these two areas shows anomalously high extended tricyclic terpanes (ETR's). High ETR's as described by Holbard (1998) suggest oils sourced by Triassic-aged or older source rocks (Ohm et al., 2008). This fact would add credibility to presence of Paleozoic source rocks in the southern Llanos basin, but would be very controversial for Barbados oils.

Barbados is the eastern most island of the Lesser Antilles archipelago in the southeastern Caribbean region. The island lies at the leading edge of the Caribbean plate and emerges as the only subaerially exposed part of the Barbados accretionary prism (BAP). Oil production from the onshore Woodbourne field proves the existence of an active source rock (s) and a working petroleum system in the western margin of the Barbados accretionary prism (Hill and Schenk,

2005). The debate about the origin of the oil and gas produced on the Barbados Island and many offshore seepages has spanned for more than 30 years (starting with Larue et al., 1985). Most of the investigations have centered on identifying the source rock facies and their age (Larue et al., 1985; Speed et al., 1991; Babaie et al., 1992; Hill and Schenk, 2005). Recent geochemical work on Woodbourne oils indicates that they originated from an Upper Cretaceous La Luna-like marine source rock similar to the facies that generated some eastern Venezuelan oils (Lawrence et al., 2002; Burggraf et al., 2002; Leahy et al., 2004; Hill and Schenk, 2005). However, questions such as the spatial distribution, maturation levels, and the existence of multiple source rocks within the western margin of the Barbados accretionary prism and the easternmost extension of the Tobago basin still need to be addressed.

This study aims, first, to improve the understanding of the petroleum system in this region by characterizing source rock facies and maturity of petroleum occurrences onshore Barbados and also by documenting geochemical evidence to recognize differences between the Barbados oils and other northern South American and Caribbean oils that are known to be derived from Upper Cretaceous rocks.  Second, it attempts to evaluate the potential of terrigenous Paleogene geological units outcropping in the island. Bulk geochemical and biomarker analyses of six crude oils from Woodbourne field, one oil seepage, and four oil-stained sandstones from Barbados are performed, and the results are compared with published chromatographic data for northern South America and Caribbean source rocks and derived oils. Additionally, four Paleogene fine-grained, organic-rich samples are analyzed.

The southern Llanos basin, located between the Eastern Cordillera and the Guyana shield (Fig. 1.1 and 2.5), is the southernmost part of a major Andean foreland basin that represents the latest stage of a complex Paleozoic-recent multiphase evolution of eastern Colombia (Pindell et al., 1998; Moreno-Sanchez and Pardo-Trujillo, 2003; Escalona and Mann, 2011). The Llanos basin has been explored since the 1980's with four giant discoveries: Rubiales, Cano Limon, Cusiana and Cupiagua, but it has been comparatively unsuccessful in the southern area with only four minor heavy oil fields. Exploration trends have focused exclusively on the Cretaceous-Cenozoic foreland plays (Campos, 2011). However, older pre-foreland structures hosting up to 2km of Paleozoic-aged sediments may contain potential source rock intervals that will offer a regional context for
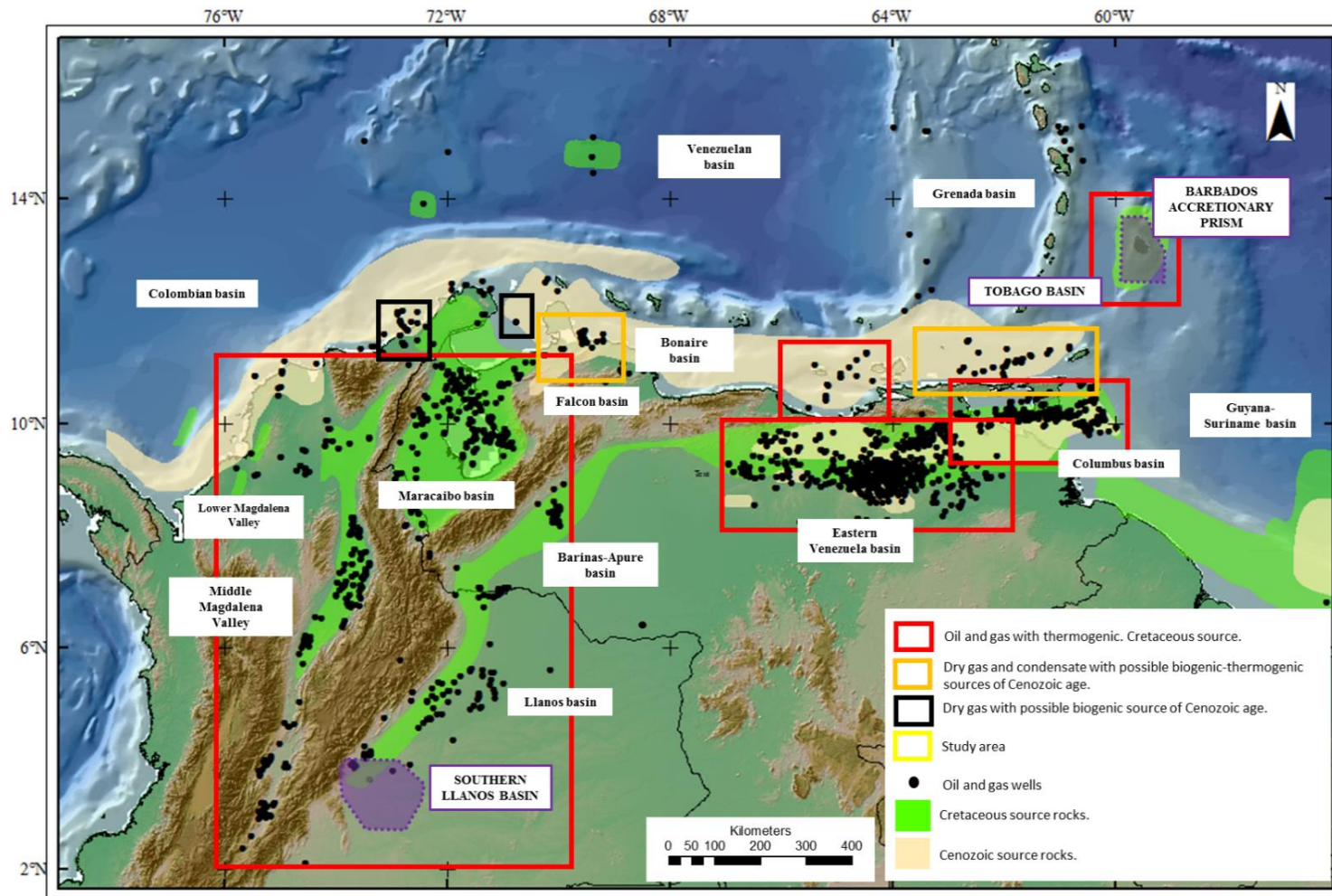
***Fig. 1.1.*** *Distribution of sedimentary basins of northern South America and southern Caribbean region. Distribution of producing oil and gas fields (Black dots). Red boxes show areas of thermogenic oil and gas derived from Cretaceous source rocks deposited in a passive margin setting; yellow boxes show dry gas and condensates with either a biogenic or thermogenic source of possible Tertiary age; black boxes show biogenic dry gas of possible Tertiary age. Green and yellow polygons represent the distribution of Cretaceous and Cenozoic source rocks respectively. Purple boxes outline the two study areas of this work. (Modified from Escalona and Mann, 2010).*

3

defining a new exploration play concept in areas where the Upper Cretaceous source rocks are absent and/or immature. Hydrocarbons sourced by Paleozoic rocks have not yet been discovered within the southern Llanos basin, and it has discouraged further exploration in pre-Mesozoic units to the extent that they are erroneously referred as the economic basement. Paleozoic units have, however, been proven to be efficient source rocks in various sub-Andean basins in the south of the continent (Dartora and Moretti, 2014). The present study uses 2D basin modeling to test timing and phase of hydrocarbons generation from a potential Paleozoic source rock interval. The study implements a recently proposed tectonostratigraphic evolution model of the basin by Moreno and Escalona (2015), as well as incorporates geochemical, maturity, and boundary condition parameters from published literature.

**Significance of this study**

Previous geochemical studies in the Barbados Island are topical and focused on geochemical characterization (Larue et al., 1985; Speed et al., 1991; Babaie et al., 1992; (Leahy et al., 2004; Hill and Schenk, 2005). However, there has not yet been an attempt to integrate the geochemical character of Barbados oils with source rocks and derived oils within the major sedimentary basins of northern South America and southern Caribbean region. This study differs largely from earlier works in that it performs geochemical comparison at a mega-regional scale, which is especially useful for constraining a more solid geochemical correlation between oils found in the leading edge of the Caribbean plate and oils and source rocks of similar age in the onland continental and offshore basins of the South American plate.

It should be kept in mind that Upper Cretaceous sediments are not a single homogenous entity, and that the environmental conditions during sedimentation most likely varied from north to south and from east to west. Thus, this comparison will provide valuable insights on the likely distribution of the source rock facies sourcing the Barbados petroleum and the possible presence of multiple source rocks. Paleogene source rocks are mature in the southernmost extension of the Tobago basin as proved by the discovery of condensates in the Venezuelan portion of the Tobago basin (Regueiro and Pena, 1996) where the heating effect of the rising Lesser Antilles arc may have had a positive impact on maturation (Escalona et al., 2011). Assessing the generation potential and thermal maturity of these units onshore Barbados will be critical for petroleum

exploration, in particular for establishing if hydrocarbons have been already expelled from these units.

No previous study has discussed the hydrocarbon potential of Paleozoic units in the southern Llanos basin. In this work, a 2D basin modeling study is taken on in an attempt to understand the spatial and temporal relation between the thermal maturation and uplifting of Paleozoic rocks and its implications in generation-migration-accumulation of hydrocarbons. Specifically, the modeling aims to test if pre-Mesozoic units might offer an alternative source of hydrocarbons to the Upper Cretaceous units where these are immature or virtually absent in the southern Llanos basin.

## 2.    GEOLOGICAL SETTING

The current structural configuration of northern South America results from the complex interaction between the subducting Pacific (Nazca) and Caribbean plates of oceanic affinity beneath South America, cored in this region by the continental Guyana Shield (Fig. 2.1.). The Nazca plate is subducted obliquely underneath the South American plate (Klotz et al., 2001) at the fastest subduction rate of approximately 54 mm/yr (Mann, 1999; Norabueana et al., 1999) (Fig. 2.1). This collision increased its convergence rate around 26my ago (Wilson, 1996) and is largely responsible for the rise of the Andean Cenozoic orogenic belt and paired foreland basins extending parallel to the long-lived, east-dipping subduction zone.
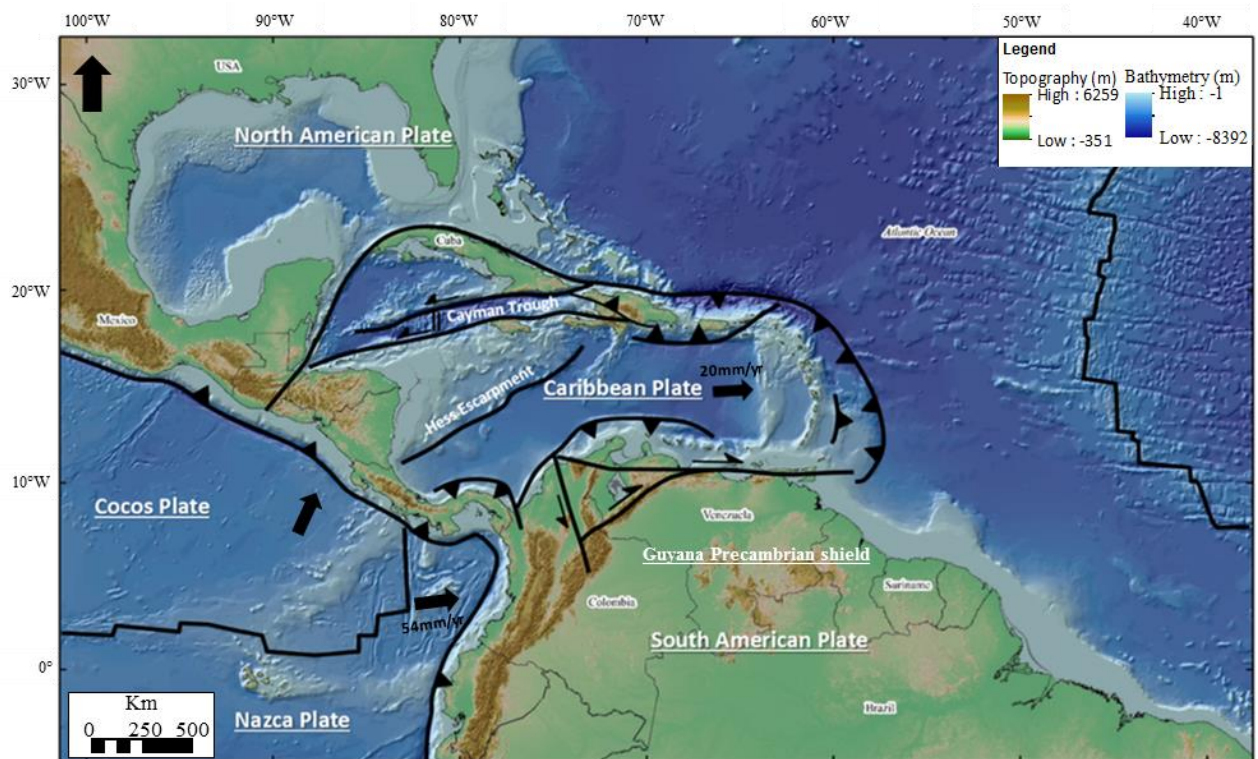


*Fig. 2.1. STRM topography (Jarvis et al., 2008) and GEBCO (2003) bathymetry showing plates boundaries of Caribbean plate. Faults are placed based on published maps of Pindell and Kennan, 2009; Escalona and Mann, 2011.*

The Caribbean plate lies between the North and South American plates and is essentially made of thick basaltic oceanic plateau formed during the Santonian time (Kerr and Tarney, 2005) in the Pacific, which later drifted north-northeast to finally engulf between the Americas. GPS data has shown that the Caribbean plate is moving eastward at a rate of 20 mm/yr. with respect to the South

American plate (Mann, 1999; Weber et al., 2001). This eastward movement began in the Late Eocene and was fully established by the Late Oligocene (Malfait and Dinkelman, 1972; Escalona and Mann, 2011). At present day, strike-slip faults exist along both the north and southeast boundaries of the Caribbean Plate. The northern boundary is left-lateral, while the southern boundary is right-lateral (Mann, 1999), causing eastward movement relative to the South and North American Plates (Fig. 2.1.). The eastwards drift of the Caribbean plate has generated a subduction zone at the leading edge of the Caribbean plate where the oceanic Atlantic crust of North and South American plates is subducted westward beneath the Caribbean plate (Brown and Westbrook, 1987; Deville et al., 2003). This boundary is characterized by the presence of typical convergent margin features such as an accretionary prism, a volcanic island arc, and associated forearc and back arc basin.

## 2.1    THE TOBAGO FOREARC BASIN AND THE BARBADOS ACCRETIONARY PRISM

The Barbados accretionary prism and the forearc Tobago basin constitute the forearc region of the Lesser Antilles arc located at the leading edge of the Caribbean plate in the southeastern Caribbean Sea (Fig. 2.2.).

### 2.1.1.  Geological evolution

The Aves ridge is suggested to be the initial volcanic arc that started during the Late Cretaceous. In front of it, the Grenada and Tobago basin formed a single forearc basin where deep marine, pelagic sedimentation took place over the oceanic plateau of the Caribbean plate during the Late Cretaceous (Aitken et al., 2011). Sedimentation in the Late Cretaceous is proposed to have taken place on top of E-W striking half-grabens present in the basement (Javis et al., 2008).   Paleogene extension due to a slab-roll back and subsequent flexural subsidence of the previous forearc basin caused the basin to be filled with approximately 8 km of marine pelagic sediments and clastic turbidites. Uplift and intrusion of the Neogene Lesser Antilles Island Arc during the Early to Middle Miocene due to eastward migration of volcanism divided the forearc basin into two separate basins (Aitken et al., 2011). The resulting Grenada back-arc basin was virtually underfilled, whereas the Tobago forearc basin was filled with over 12 km of pelagic clays, muds,
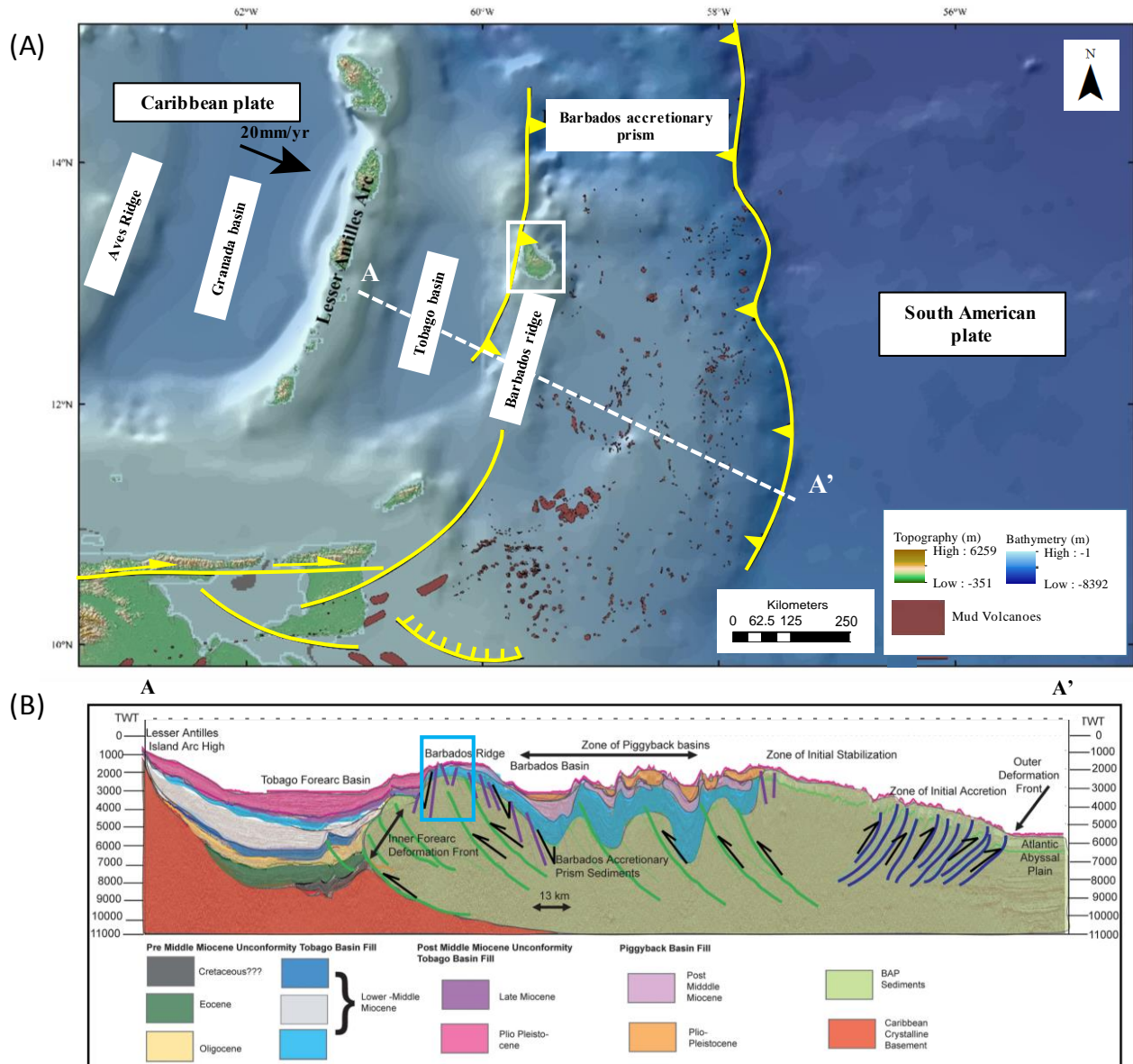
**Fig. 2.2. A.** *Map of southeastern Caribbean region highlighting the main tectonic and geomorphologic features. The study area is outlined;* **B**. *Schematic northwest–southeast cross section of southeastern Caribbean region summarizing the most relevant present-day geological structures and associated megasequences. The study area is outlined. (Chaderton, 2005).*

marls and thin beds of volcanic ash (Speed, 1994) and sediments from the proto Orinoco river (Escalona and Man, 2011). The boundary between the Tobago basin and the adjacent Barbados accretionary prism is a westward, fold and thrust belt active from the Eocene to the present (Chaderton, 2005) called the inner forearc deformation front (IFDF) (Torrini and Speed, 1989; Speed et al., 1991) (Fig. 2.2.).

The Barbados Accretionary Prism (BAP) formed due to off-scraping of predominantly quartz-rich sediments previously brought to the Atlantic abyssal plains by the Orinoco fluvial system and its equivalents since the Eocene (Escalona and Mann, 2011). The accretionary prism is about 300 km wide and about 20 km thick in the south because of the availability of large amount of sediments sourced from the South American continent (Fig. 2.2).

Based on the dominant structural style from east to west the Barbados accretionary prism is subdivided into a zone of initial accretion where the accretionary prism thickens due to incorporation of recent sediments (Fig. 2.2.); A zone of stabilization in which a dynamic balance exists between the processes that tend to widen (offscraping and normal faulting) and processes that tend to thicken (e.g. underplating, thrusting) the prism (Brown and Westbrook, 1987); A zone of supra complex basins characterized by development of piggy back/wedge top basins and minibasins on top of the accretionary complex (Westbrook et al., 1984); and the Barbados ridge uplift which is the oldest, westernmost structural zone of the Barbados accretionary prism characterized by uplift and westward thrusting of the complex over the Tobago forearc basin (Brown and Westbrook, 1987) during the Mid-Miocene time (Chaderton, 2005). Extensive low-angle thrusts generate large anticlinal highs. Gravity collapse of the prism during the Plio-Pleistocene generated a system of ridge-parallel normal faults (Ahmed, 2016; Chaderton, 2005).

A very important aspect of the Barbados accretionary prism is widespread shale tectonics. Mud volcanism and shale diapirs are more important toward the southern part of the prism. The abundance of shale tectonics decreases gradually northward to the extent that no mud volcanism has been reported further of 15° North (Deville et al., 2006; Mudussar, 2016) as shown in Fig. 2.2. Outcrops of fossil mud volcanism are present in the Barbados Island where this unit is called Joe's River Formation (Senn, 1940; Kugler et al., 1984; Gill et al., 2005).
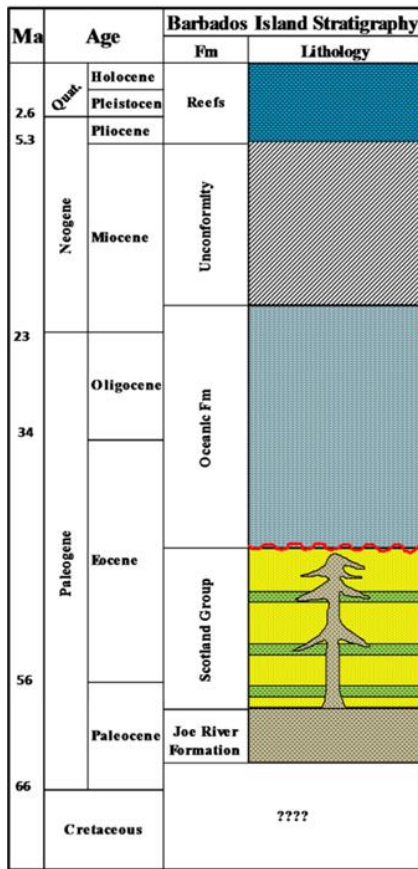
***Fig. 2.3.*** *Generalized stratigraphic column of the Barbados Island. Modified from Mudussar, 2016. Note how the Joes River Formation intrudes the Scotland Group as diapiric shales before the deposition of the Oceanic Formation.*
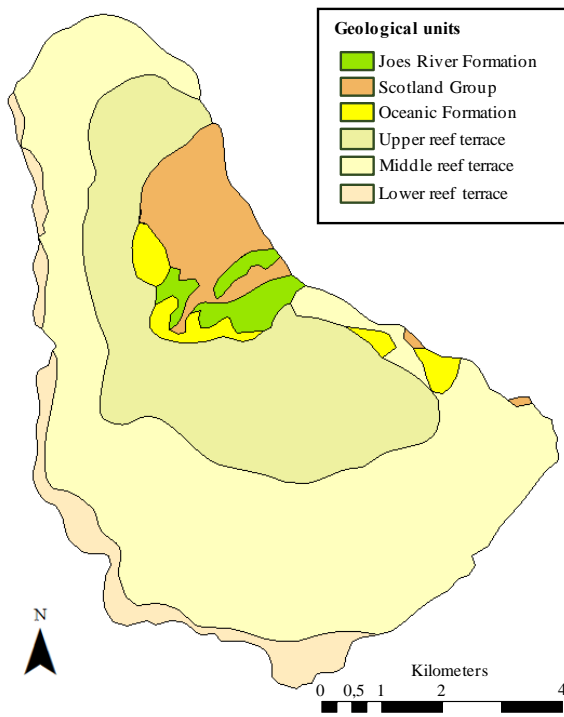


***Fig. 2.4.*** *Map of Barbados showing the different geological units outcropping in the island. Modified from Pool and Barker (1980).*

### 2.1.2  Outcrop stratigraphy onshore Barbados

The Barbados Island is the only subaerially exposed part of the Barbados ridge and rocks outcropping in the Scotland District are inferred to extend into the adjacent deep water areas (Chaderton, 2005). Exposed rocks are divided into four stratigraphic units (Deville and Mascle, 2012) (Fig. 2.3. and 2.4.).

#### 2.1.2.1 Joes River Formation

This Formation consists of a melange of structureless clays, sands, and occasional limestone chunks (Barker and Poole, 1982). Onshore Barbados the Joes River Formation represents isolated paleo-mud volcanoes (Fig. 2.4.). They are interpreted to have intruded the Scotland Group as diapiric shales after the deposition of the Oceanic Formation (Speed et al., 1991) and prior to the localized extensional faulting which characterizes the crest of the Barbados Ridge.

#### 2.1.2.2  The Scotland group

Onshore, these rocks are a thick, (up to 2800 m), succession of interbedded very coarse grained turbidites and leveed channels deposits (Chaderton, 2005). The biostratigraphic age has been found to be Lower Eocene (Deville and Mascle, 2012). These turbidites were initially deposited on the Atlantic abyssal plain and have been subsequently accreted and incorporated into the accretionary prism as vertically stacked trust sheets. This unit outcrops mainly in the northeastern margin of the island (Fig. 2.4.) and serves as the main reservoir at the Woodbourne oil field.

#### 2.1.2.3  The Oceanic Formation

This formation has been interpreted over the area as deep marine pelagic clays and marls interbedded with volcanic ashes (Speed, 1989, 1994), deposited in water depths between 2000 to 4000 m based on foraminiferal data (Saunders, 1984). Onshore units are inferred to be at youngest Middle Miocene in age (Barker and Poole, 1982). The Oceanic Formation on Barbados forms a seal for hydrocarbons trapped in the Mid-Miocene deformed prism (Chaderton, 20045). It is eroded in the northeastern segment of the island where petroleum leakage is found at several locations (Fig. 2.4.).

#### 2.1.2.4  Quaternary limestone

The Quaternary limestone cap covers approximately 80% of the island (Fig. 2.4.) and extends into the adjacent deep water areas where it is contemporaneous with the most recent fill of the Tobago

basin. The limestone records the successive rise of the island in the form of three distinct terraces.

## 2.2    THE SOUTHERN LLANOS BASIN

The southern Llanos Basin, which lies between the Eastern Cordillera and the Guyana Precambrian shield, is the southernmost part of a major Mezo-Cenozoic Andean foreland basin (Fig. 2.5.) that represents the latest stage of a complex Paleozoic-recent multiphase evolution of eastern Colombia (Pindell et al., 1998; Moreno and Pardo, 2003; Escalona and Mann, 2011). Within the foreland, basin, two main stages of deformation since the Late Cretaceous have been recognized: the first stage was triggered by uplift of the Central and Western Cordilleras in the Late Cretaceous–Paleocene (Gomez et al., 2005). The second was caused by inversion of the Eastern Cordillera starting in the Middle Eocene with increasing rates of subsidence from the Oligocene to the Pliocene (Gomez et al., 2003, 2005; Parra et al., 2009, 2010; Horton et al., 2010).

The Llanos basin records sedimentation from the Paleozoic until present day overlaying an igneous-metamorphic, pre-Cambrian basement (Forero-Suarez, 1990) (Fig. 2.6.). Three main sedimentary sequences bounded by major, regionally-extended unconformities have been identified: Paleozoic, Mesozoic, and Cenozoic (Parra et al., 2010).

### 2.2.1    Pre-Cambrian basement

The basement rocks of the Llanos basin have been long defined as a westwards extension of the Paleoproterozoic crystalline rocks of the Guyana shield (Cordani et al., 2010; Tassinari et al., 2000). Recently, geochronological data obtained from several deep oil wells showed evidences of Neoproterozoic rocks buried beneath the Llanos basins (Ibanez-Mejia, 2011a), providing evidence for the existence of a major Neoproterozoic crystalline basement province in eastern Colombia. In the west of the study area, the Paleoproterozoic Crystalline rocks of the Guyana shield are interpreted to be overthrusted by the Neoproterozoic igneous and metamorphic rocks by north–south-oriented thrust faults (Moreno and Escalona, 2015).
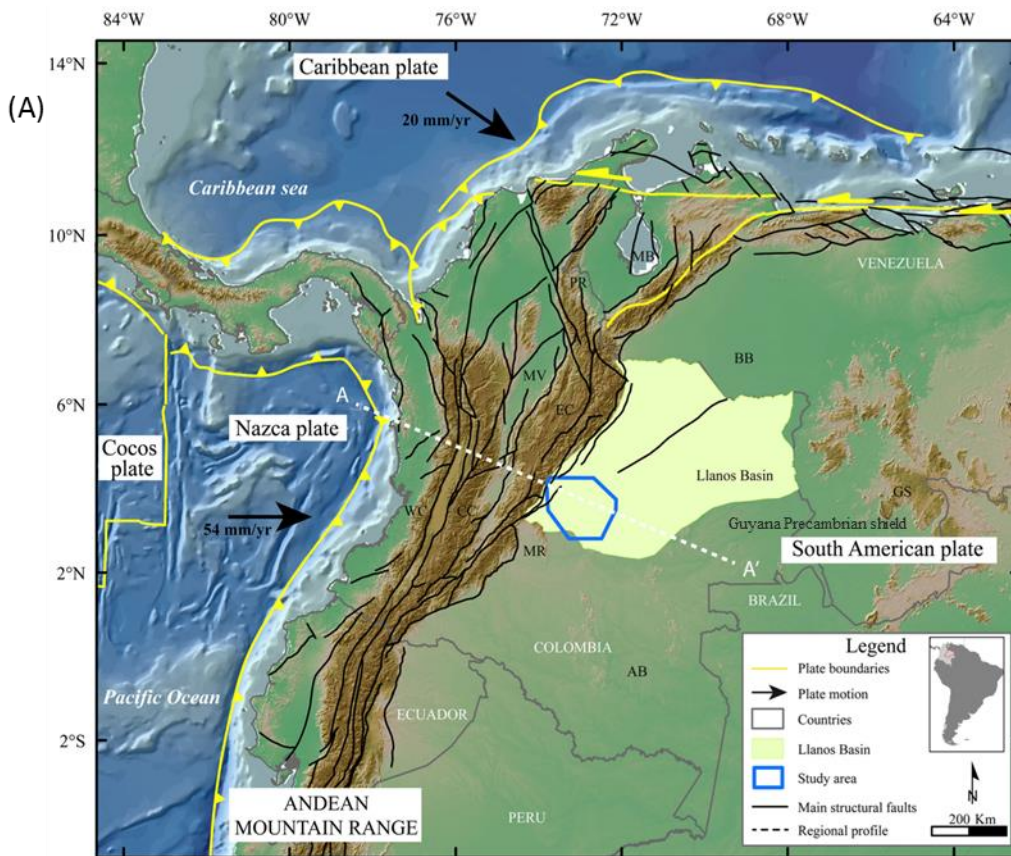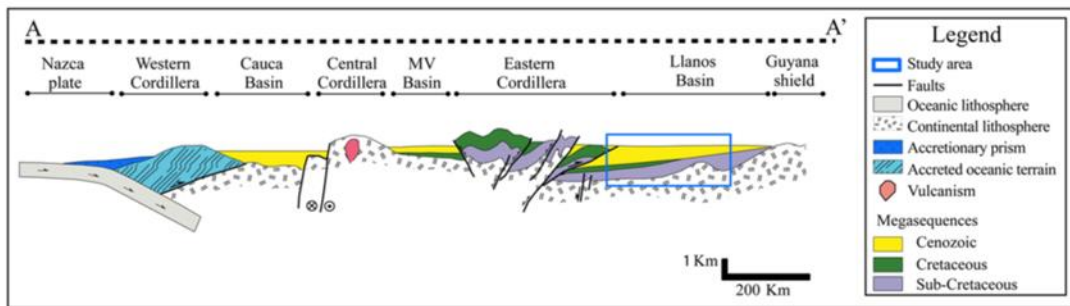
***Fig. 2.5. A.** Map of northwestern South America highlighting the main tectonic and geomorphologic features. WC = Western Cordillera; CC = Central Cordillera; EC = Eastern Cordillera; GS = Guyana shield; BB = Barinas basin; MB = Maracaibo basin; MV = Magdalena Valley basin; PR = Perija Range; MR = Macarena Range; AB = Amazonas basin. The Llanos basin is shown and the study area is outlined. **B.** Schematic northwest–southeast cross section of Colombia summarizing the most relevant present-day geological structures and associated megasequences. The study area is outlined. (Moreno and Escalona, 2015).*

13

### 2.2.2. Paleozoic sequence

The current geological understanding of the Paleozoic units is notoriously limited. Available data from industry seismic datasets, wells, and paleontological data enable recognition of two different sequences: 1. Cambrian? – Ordovician, shallow marine deposits recorded in a generally coarsening coarsening upward sequence consisting from base to top of organic-rich black shales, silty sandstones, shales, and quartz sandstones of the Negritos Formation (Ulloa and Perez, 1982). In the study area, rocks of this age are suggested to be preserved in deep depocenters along inverted Neoproterozoic basement blocks (Moreno and Escalona, 2015). 2. Upper Paleozoic, marginal marine mudstones and sandstones. Palynological assemblages recovered from well samples in the northern Llanos basin suggest a Devonian–Carboniferous age for these rocks in the subsurface (Dueñas and Cesari, 2006). These rocks have not been reported in the study area.

The Llanos basin is inferred to have developed in a back-arc setting behind a rising volcanic arc emplaced to the west of the study area during Ordovician time (Williams, 1995). Stratigraphic, and structural relations in the Eastern Cordillera suggest that an orogenic event occurred near the end of the Ordovician in northern Colombia (Irving, 1975). This event marked the end of the seaway and forced the sea to retreat. During the Late Devonian and Carboniferous sedimentation took place in a continental platform westward and northward to its outer edge (Irving, 1975). At the end of the Paleozoic Era, continent–continent collision between South and North America resulted in the Ouachita–Marathon orogeny during the assemblage of Pangea (Ruiz et al., 1999; Malone et al., 2002) and subjected the region to the most intense orogeny recorded in Phanerozoic rocks of Colombia which triggered reverse faulting and reactivation of older structures (Ceron, 1998; Sarmiento-Rojas et al., 2006).

### 2.2.3 Mesozoic–Cenozoic sequence

The Triassic and Jurassic are characterized by widespread plutonic and volcanic magmatism in northern Colombia. Volcanoclastic Jurassic deposits have been interpreted as terrestrial synrift sediments accumulated in a back-arc setting (Cooper et al., 1995); however, no evidence of Triassic–Jurassic rocks exists in the southern Llanos basin (Cooper et al., 1995), suggesting that the study area was subaerially exposed, and deposition was restricted to basins along the Eastern Cordillera. The back-arc setting continued into the Early Cretaceous and the sea transgressed and

| Age | | | Formation | Thick. m | Lithology |
|---|---|---|---|---|---|
| NEOGENE | Pliocene | | Guayabo | >1250 | |
| | Miocene | | Leon | 350-400 | |
| PALEOGENE | Oligocene | | Carbonera | 1400-2100 | |
| | E | | Mirador | 180-140 | |
| | Paleo- | | Cuervos | 480 240 | |
| | | | Barco | 50-200 | |
| CRETACEOUS | Upper | | Guadalupe | 500-530 | |
| | | | Gacheta | 400-620 | |
| | | | Une | 900-1400 | |
| | Lower | | Fomeque | 700-900 | |
| | | | Juntas | 500-700 | |
| | | | Caqueza | >1500 | |
| LATE PALEOZOIC | Devonian Carboni- | | Unnamed Paleozoic Unit | >1500 | |



retrograded alternating regressive sandstones with organic-rich shales (Cooper et al., 1995). During the Upper Cretaceous the sea gradually spread southward along the seaway and reached its maximum extension in the Turonian and Coniacian time. During this time the organic carbon rich sediments of the Gacheta Formation were deposited (Cooper et al., 1995). As part of the initial convergence of the Caribbean plate with western South America (Moreno and Pardo, 2003), the sea shallowed and eventually withdrew during the Maastrichtian, giving way to an Upper Maastrichtian and Paleocene paralic coal-bearing facies (Irving, 1975).

The Cenozoic in the Llanos basin consists of an upward-coarsening succession of marine to continental strata (Cooper et al., 1995) deposited along the slowly subsiding plains at the base of the Eastern Cordillera. This succession is genetically related to the development of the two foreland basin stages affecting the Llanos basin. Last, Pliocene–Pleistocene fluvial deltaic rocks overfilled the foreland basin (Moreno and Escalona, 2015). These events are related to collision and subduction of arc and oceanic terrenes resulting from the long-term, complex interaction between the Caribbean and South American plate (Pindell et al., 1998; Moreno-Sanchez and Pardo-Trujillo, 2003; Escalona and Mann, 2011).

*Fig. 2.6. Generalized stratigraphic column of the Llanos basin (Moreno and Escalona, 2015).*

## 2.3 UPPER CRETACEOUS ORGANIC-RICH SEDIMENTATION IN NORTHERN SOUTH AMERICA

Upper Cretaceous organic-carbon rich sedimentation extended from the Tempisque basin of Costa Rica through The Venezuelan basin of the central Caribbean Sea, western and eastern Venezuela, Colombia, Trinidad, and the Guyana-Suriname basins (summarized in Erlich et al., 2003) (Fig. 2.7.). Although the lithofacies reported in these units are fairly variable, a general gross pattern is identifiable. Carbonates or biogenic siliceous rocks are the dominant lithology in the northern part of the eastern Venezuelan basin, the Maracaibo basin, the Venezuelan offshore basin, and the Tempisque basin. Siliciclastic rocks are predominant in the Guyana-Suriname basin and Trinidad, the southern part of the Guariaco basin and Maturin sub-basin of eastern Venezuela, the Barinas-Apure basin of western Venezuela, and the Llanos, Magdalena and Eastern Cordillera basins of Colombia.

Profound oceanographic and climatic changes that took place during the Middle to Late Albian played a definitive role in the physical structure of the Tethyan ocean and therefore in marine biodiversity (Erlich et al., 2003). A significant increase in sea-surface temperatures worldwide started during the Middle Aptian and reached its climax in the Middle Albian (Frakes, 1999). The following abrupt drop in sea-surface temperatures during the Early Cenomanian brought about a change from predominantly eutrophic to predominantly oligotrophic conditions in the water column which persisted in the northern South America and Caribbean region. Eutrophic conditions returned to the Atlantic/Tethyan Ocean during the Middle Cenomanian and were later interrupted by several reversals in nutrients content (Premoli Silva and Sliter, 1999).

The combination of elevated eustatic sea level, nutrient flux, and variable sea-surface temperatures in the Cenomanian-Late Turonian resulted in vast deposition of organic-rich sediments (Erlich et al., 2003). The sedimentary record of this period is predominantly dark, laminated, organic-rich shales interbedded with pelagic limestones and marls.

The global Cenomanian-Turonian oceanic anoxic event (OAE) also facilitated the accumulation of organic matter due to a massive burial of organic carbon worldwide (Arthur et al., 1988). According to Frakes (1999), the resulting reduction in $CO_2$ caused the sea-surface temperature to
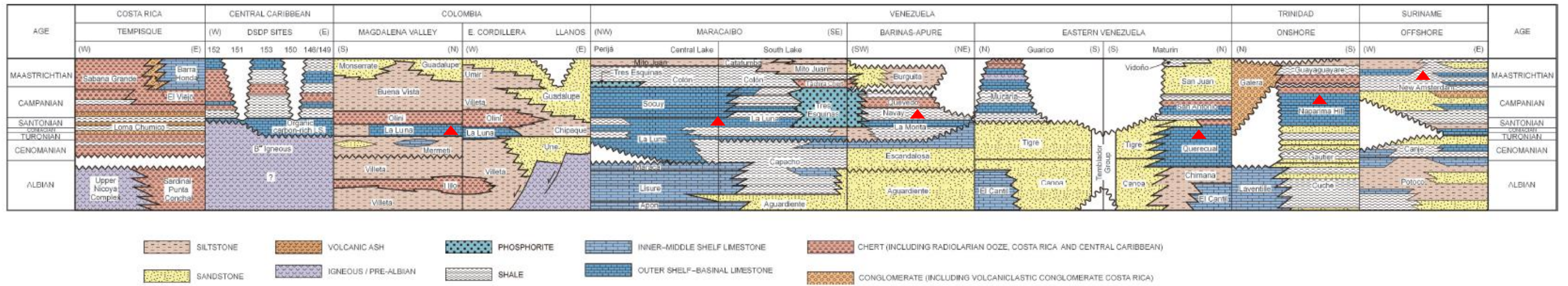
**Fig. 2.7.** *Chrono-lithostratigraphic columns for the Albian-Maastrichtian period for key basins of northern South America and southern Caribbean region. Red triangles represent source rock intervals. (Modified from Erlich et al., 2003).*

drop during the Late Turonian-Coniacian which in turn resulted in seasonal upwelling accompanied by wet/dry cycles and episodic siliciclastic input into slope and deep basinal depositional environments (Barron et al., 1995; Bush and Philander, 1997).

During the Turonian-Santonian period, thin carbon-rich limestones and biogenic siliceous rocks were deposited on the central Caribbean plate (today's Venezuelan basin) as reported by the Central Caribbean Deep Sea Drilling Project (DSDP) sites (Edgar et al., 1973) (Fig. 2.8.B and C). During the earliest Cenomanian to Turonian, a pronounced regional sea level rise allowed deposition of the La Luna Formation and equivalent units over vast areas of Colombia and western Venezuela (Fig. 2.8.B ). This rise in sea level favored deposition and preservation of fine-grained, organic-rich sediments in areas that were earlier dominated by oxic, proximal environments.

In the Late Turonian a rapid low-latitude cooling episode interrupted the hot and arid conditions governing since the Late Cenomanian (Frakes, 1999), and triggered instability in the Maracaibo and Barinas basins. Paleobathymetric highs trapped the local basinal water in the northwestern and eastern Maracaibo basins and permitted only limited surface-water exchange into the Pacific Ocean (Vergara, 1997a; Johnson, 1999). A similar scenario occurred further south of the Maracaibo basin where the proto-Merida Andes permitted only surface-water exchange between the Barinas-Apure and the northern Llanos basins into the Pacific Ocean. Dominant arid conditions and subsequent high evaporation rates in relatively stagnant water masses might have contributed to the formation of saline, oxygen-depleted waters which greatly enhanced the preservation of organic matter (Erlich et al., 2003). The overall primary production was likely low during the Turonian-Coniacian, with bacteria and planktonic foraminifera as the major contributors (Erlich, et al., 1999b). However, Damsté et al., (2004) proposed a rapid rise of the rhizosolenid diatoms during the Upper Turonian (91,5±1.5 million years) that probably resulted from a major reorganization of the nutrient budget in the Mid-Cretaceous oceans brought about by plate tectonics.

Erlich et al., (2003) propose that during the Cenomanian-Turonian the eastern Venezuelan shelf was flooded and extensive organic-carbon rich limestones of the Querecual Formation were deposited (Fig. 2.8.A and B). Dry climatic conditions and seasonal upwelling favored moderate

primary productivity and high preservation of organic matter. During the Late Cenomanian-Middle Coniacian dry conditions were replaced by seasonal wet/dry cycles and episodic fluvial discharge into deep-marine sediments of the basal Naparima Hill Formation in Trinidad (Frakes, 1999) (Fig. 2.8.C). Unclear oceanographic and climatic conditions favored the deposition of organic carbon-rich sediments for more than 13.5 my (Erlich et al., (2003).

Toward the Guyana-Suriname basin the dry/wet climatic cycles were more severe and major submarine fan systems of the Canje and Low Amsterdam Formations were deposited in deep canyons and troughs (Erlich et al., 1999). High TOC contents (as much as 13%) were preserved as oxygenation is unlikely to have occurred during the dry cycles in sediments confined in the deep canyons and troughs (Erlich et al., 2003).
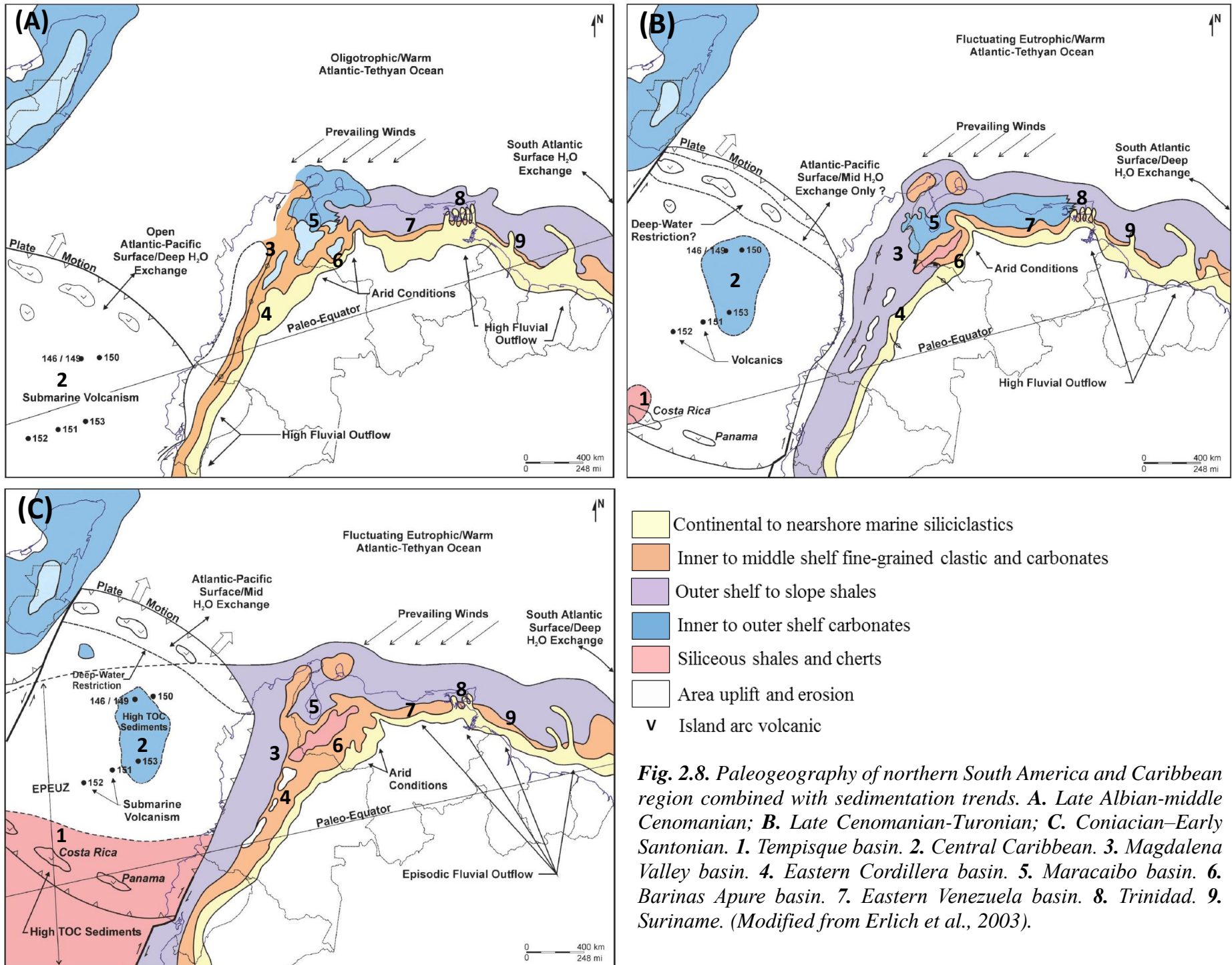
**Fig. 2.8.** *Paleogeography of northern South America and Caribbean region combined with sedimentation trends. A. Late Albian-middle Cenomanian; B. Late Cenomanian-Turonian; C. Coniacian–Early Santonian. 1. Tempisque basin. 2. Central Caribbean. 3. Magdalena Valley basin. 4. Eastern Cordillera basin. 5. Maracaibo basin. 6. Barinas Apure basin. 7. Eastern Venezuela basin. 8. Trinidad. 9. Suriname. (Modified from Erlich et al., 2003).*

20

# 3    DATA SET, AND ANALYTICAL METHODS

## 3.1.    BARBADOS STUDY CASE

### 3.1.1.   Data set

Sample set for Barbados showed in Table 3.1. comprises:

1.      Six crude oils samples from the wellheads of different producing wells at the Woodbourne oil field (WO84, WO88, WO140, WO170, WO196, LG#11). Samples were picked considering different reservoir units, depths, and API degree.

2.      Four oil-saturated sandstones (samples B2, B11, B13, B21) of the Scotland Group. Sample B2 and B11 were collected in the Shale Quarry area (Fig. 3.1.). They were taken from oil-saturated sandstones interbedded with mudstones and siltstones. Particularly, sample B11contains water-escaping structures defined by visible blackish, oil-stained laminations embedded in a brownish-colored, medium-grain sandstone (Fig. 3.2.A). Sample B13 and B21 were collected along the Bath beach and the Berkley Park respectively (Fig. 3.1.). In sample B13 solid bitumen was exclusively present along in centimetric to decimetric fractures within the sandstone beds (Fig. 3.2.A).  Sample B21 was taken from an area in which black solid bitumen was present homogeneously over a big area rather than limited to isolated structures (Fig. 3.2.A).

3.      An active oil seepage (Sample SP) in the Shale Quarry area (Fig. 3.2.A). The sample was collected from the top of a small oil pond. It was taken from what is believed to be the most recently released fluid. The seepage was recovered from severely deformed and loose rock material of the Scotland Group.

4.      Four clay to silt-sized grain samples (Samples B4, B10, B16) from the Paleogene Scotland Group. Samples B4 and B10 were collected in the Shale Quarry area immediately below samples B2 and B11 respectively, whereas samples  B41 and B16 were collected at the Barclay Park (Fig. 3.2.A).

5.      For the regional comparison, published organic geochemical data sets from different studies consists of m/z 191 terpanes fragmetograms along with either m/z 217 or m/z 218 steranes fragmetograms (see Table 6.1 in chapter 6).

**Table 3.1** *Location and description of sample set. Table also includes analyses performed on every sample.*

| SAMPLE | X (m) | Y (m) | Z (m) | Locality | Type | Comment | TOC-Py | GC-MS | δSAT-AR | CSIA |
|---|---|---|---|---|---|---|---|---|---|---|
| B2 | 220339 | 1466586 | 38 | Shale Quarry | OSS | Patches of semi-solid bitumen | | ✓ | ✓ | |
| B4 | 220339 | 1466586 | 38 | Shale Quarry | CL-SL | Dark gray, mud to silt-sized grains | ✓ | ✓ | | |
| B10 | 220403 | 1466467 | 51 | Shale Quarry | CL-SL | Dark gray, mud to silt-sized grains | ✓ | ✓ | | |
| B11 | 220403 | 1466467 | 51 | Shale Quarry | OSS | Solid bitumen in sandstone beds. Water escaping structures | | ✓ | ✓ | |
| B13 | 223838 | 1465386 | 3 | Bath beach | OSS | Solid bitumen in fractures | | ✓ | | |
| B14 | 223998 | 1461451 | 18 | Barclays Park | CL-SL | Blackish, mud to silt-sized grains | ✓ | ✓ | | |
| B16 | 223557 | 1465591 | 52 | Barclays Park | CL-SL | Blackish, mud to silt-sized grains | ✓ | ✓ | | |
| B21 | 223990 | 1464356 | 118 | Barclays Park | OSS | Solid bitumen in fully saturated sandstones | | ✓ | | |
| WO84 | 228508 | 1451067 | -1414 | Woodbourne field | WO | Upper Scotland Basals. Mid-Late Eocene? | | ✓ | ✓ | |
| WO88 | 228314 | 1452095 | -1723 | Woodbourne field | WO | Upper Scotland Basals. Mid-Late Eocene? | | ✓ | | ✓ |
| WO140 | 227453 | 1451686 | -742 | Woodbourne field | WO | Intermediate Unit, Late Olig?-Early Miocene | | ✓ | | |
| WO177 | 224386 | 1451003 | -1226 | Woodbourne field | WO | Lower Scotland, Mid Eocene | | ✓ | | |
| WO196 | 225614 | 1451312 | -1623 | Woodbourne field | WO | Lower Scotland, Mid Eocene | | ✓ | | |
| LG#11 | 225828 | 1450757 | -902 | Woodbourne field | WO | Intermediate Unit, Late Olig?-Early Miocene | | ✓ | | ✓ |
| SP | 220440 | 1466388 | 42 | Shale Quarry | OS | Oil is highly viscous and floating on water | | ✓ | | |

**OSS**. Oil-saturated sandstone; **CL-SL**. Mud to silt-sized grained samples with apparent good source rock potential; **WO**. Whole crude oil collected from the wellheads; **OS**. Oil seepage; **TOC-Py**. TOC and Rock-Eval pyrolysis; **GC-MS**. Gas spectrometry and mass spectrometry; **CSIA**. Compound-specific stable carbon isotope; Z values for the Woodbourne field samples represent the average depth of the main reservoir. See Fig. 3.1. for sample's location.
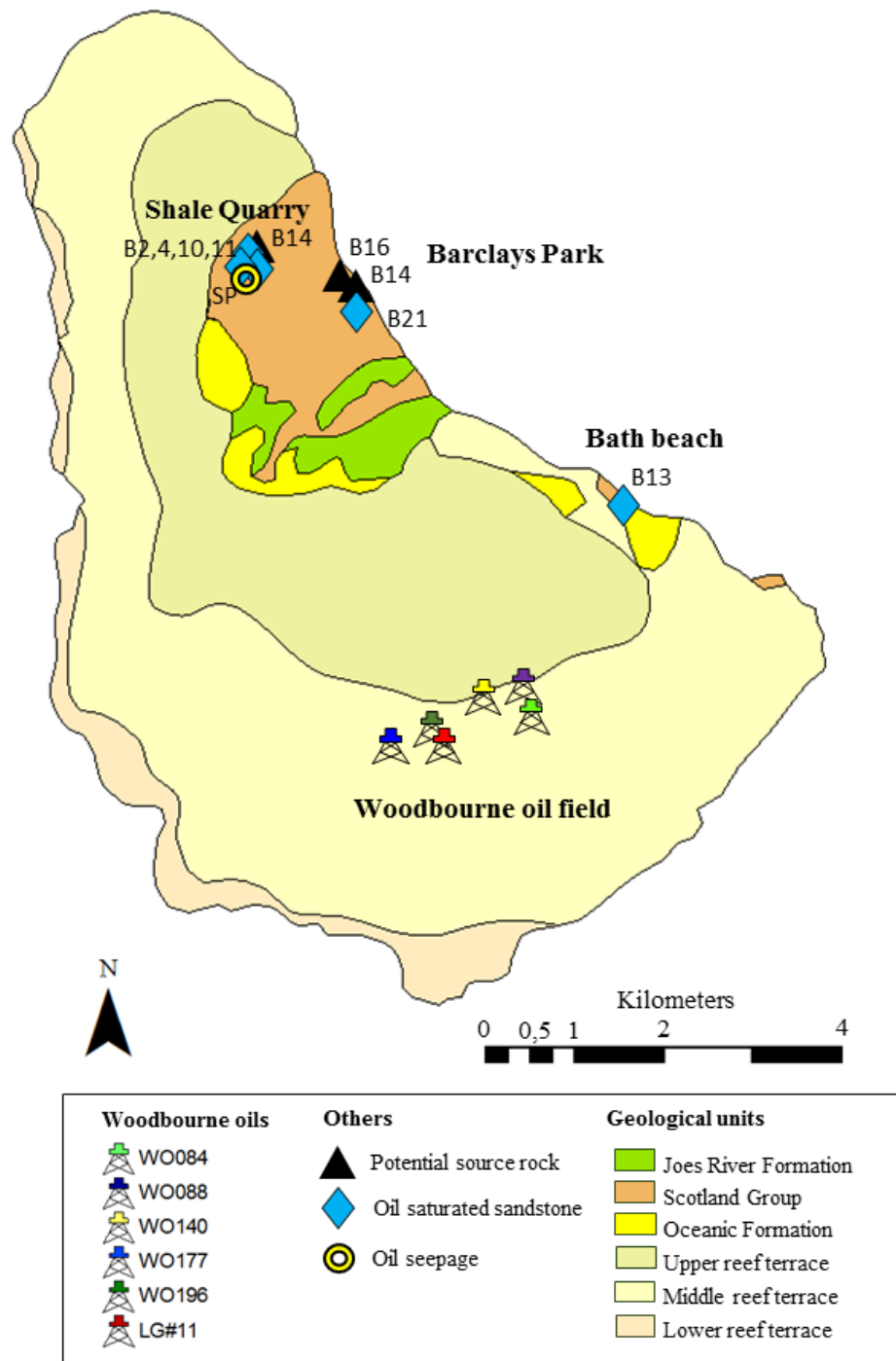
***Fig. 3.1.*** *Map of Barbados Island showing the location of the samples including in this study. Localities are labeled. Geological units outcropping in the island are also displayed. See Table 3.1 for samples description.*

### 3.1.2. Analytical Methods

All the analysis presented in this work were carried out at Applied Petroleum Technology (APT), Kjeller, Norway. The TOC content was determined using a Leco combustion carbon analyzer. Diluted HCl was added to the crushed rock sample to remove carbonate. The samples were then introduced into the Leco combustion oven (Leco SC-632), and the amount of carbon in the samples was measured as carbon dioxide by an IR-detector. A Rock-Eval 6 instrument was used for pyrolysis. Jet-Rock 1 was run every tenth sample and checked against the acceptable range given in NIGOGA (The Norwegian Industry Guide to Organic Geochemical Analyses). The Temperature program started at 300°C and was heated to 650°C at 25 °C/min.

The oil stained samples were crushed into powder before extraction of the organic matter (EOM) fraction. A conventional Soxtec Tecator instrument was used for the extraction. The crushed samples were weighed accurately (10 grams) in the pre-extracted thimbles. They were boiled for 1 hour and rinsed for 2 hours in a solution of approximately 80 cc of dichloromethane (DCM) with 7% (vol/vol) methanol (MeOH) which was heated to 60°C. Copper blades activated in concentrated hydrochloric acid were added to the extraction cups to cause free sulphur to react with the copper. An aliquot of 10% of the extracts was transferred to a pre-weighed bottle and evaporated to dryness. The amount of extractable organic matter was calculated from the weight of this 10% aliquot (Table 3.2). The bulk extracts were separated into saturates, aromatics, polar compounds, and asphaltenes using liquid chromatography on silica gel-coated rods.

A variant capillary gas chromatography-flame ionization detector (GC-FID) model HP7890-A was used, connected to a 30m long CP-Sil-5 CB-MS column which had 0.25 mm inner diameter and a film thickness of 0.25 mm was used for GC-FID of the bulk extracts. The initial column temperature was 50°C and it was heated at a gradient of 4°C/min to 320°C, where it was held 25 min.

As for the GC-FID of the whole oils, a variant Agilent 7890 with a 50m HP-PONA column which had a 0.2 mm inner diameter and a film thickness of 0.5mm was used. Temperature program started at 30 °C (held 10 min.) at a gradient of 2 °C/min to 60 °C (held 10 minutes), and continued to

130°C at a gradient of 2°C/min where it increased the gradient to 4 °C/min to subsequently reach 320°C and held for 25 minutes.

*Table 3.2. Yields and composition (%) for organic matter extracts.*

| Sample | Rock weight (g) | EOM (mg) | EOM (mg/kg Rock) | SAT wt% | ARO wt% | POL wt% | ASP wt% | HC wt% |
|--------|-----------------|----------|------------------|---------|---------|---------|---------|--------|
| B2 | 2.11 | 109 | 51581 | 48.4 | 19.6 | 24.0 | 8.0 | 68.0 |
| B4 | 24.06 | 20.8 | 864 | | | | | |
| B10 | 20.10 | 7.6 | 378 | | | | | |
| B11 | 2.47 | 131.3 | 53182 | 51.9 | 19.9 | 24.8 | 3.4 | 71.8 |
| B13 | 14.22 | 740.4 | 52066 | | | | | |
| B14 | 25.71 | 10.8 | 420 | | | | | |
| B16 | 20.14 | 64.2 | 3188 | | | | | |
| B21 | 8.38 | 899.6 | 107382 | | | | | |
| WO84 | | | | 42.5 | 25.7 | 28.9 | 2.9 | 68.2 |

*SAT, saturate hydrocarbons (%); ARO, aromatic hydrocarbons (%); POL, polar hydrocarbons (%); ASP, asphaltenes (%); HC, total hydrocarbons (%).*

Biomarkers in whole oils and extracts were analyzed using a Thermo Scientific DFS high resolution instrument. The instrument was tuned to a resolution of 3000 and data was acquired in Selected Ion Recording (SIR) mode (GC-MS SIR). The column used was a 60 m CP-Sil-5 CB-MS with a 0.25 mm inner diameter and a film thickness of 0.25 mm. The initial temperature of the column was 50°C and 320°C and held for 20 min. Ions with mass/charge (m/z) 177, 191, 192, 198, 131, 154, 205, 217 and 218 were monitored.

Stable carbon isotope measurements of the C15+ aromatic and saturated hydrocarbon fractions were performed on an isotope ratio mass spectrometers (IRMS) from NU-Instruments.

## 3.2.  SOUTHERN LLANOS BASIN STUDY CASE

### 3.2.1.  Data set

This work performed forward basin modeling on one section from the southern Llanos basin, implements the tectonostratigraphic model proposed by Moreno and Escalona (2015). The main input is a published two dimensional (2D) seismic section perpendicular to the strike direction of

the southern Llanos basin (Moreno and Escalona, (2015). The 2D section has an E-W orientation and a length of about 145km (Fig. 3.2.1).

Geological and geochemical information on the Paleozoic sequence in the southern Llanos basin was limited. Data from three exploration wells adjacent to the section and TD'ed in the top of the Paleozoic sequence were used to constrain and calibrate the model: well 3 at about 25km, well 2 at about 95km, and well 1 at about 125km (Fig 3.2.1 and 3.2.2). Only one out of the three wells (well 2) had a complete maturity record of the Cretaceous-Cenozoic and Paleozoic sequences (Table 3.2.1). Well temperature data for calibration of the model were in general scarce (Table 3.2.2), and therefore temperature data were complemented with information taken from a preliminary geothermal map (Ingeominas-ANH, 2008).

Due to the limited amount of data available for stratigraphic correlation and for depth control of Lower Ordovician rocks, an organic carbon-rich interval observed on top of the metamorphic basement in well 2 was extrapolated and modeled as a potential source rock. A second Upper Cretaceous-Paleogene source interval was also modeled, but was not the main focus of this study. Nevertheless, the modelled temperature and vitrinite values were calibrated utilizing the well data.

### 3.2.2. Analytical Methods

The basin modeling was performed using the TecLink 2D module of PetroMod software 2015 which links structural modeling with petroleum systems modeling by enabling users to integrate the reconstructed paleo sections into 2D PetroMod models. In standard models paleo geometries are created by incorporating depositional/erosional ages and then calculating the compaction/ decompaction of layers. TecLink models, on the other hand, are based on the paleo-stepping approach (PetroMod TecLink 2D reference guide).
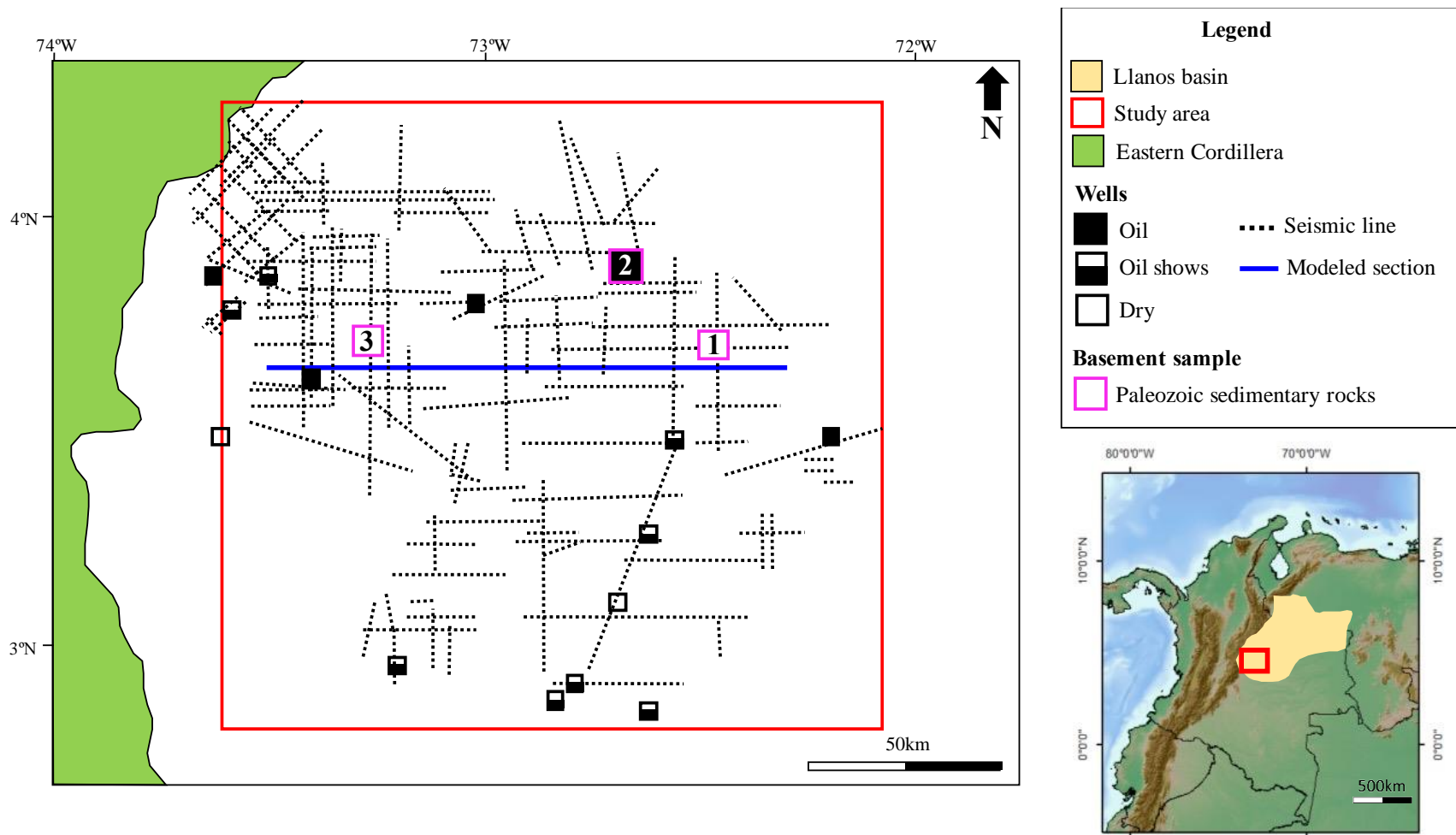
***Fig. 3.2.1.*** *Map showing the data available for the southern Llanos basin area. Numbers 1, 2, and 3 represent the location of the three wells containing geochemical and maturity information used in this study. The modeled section is highlighted in blue. Modified from Moreno and Escalona, (2015).*
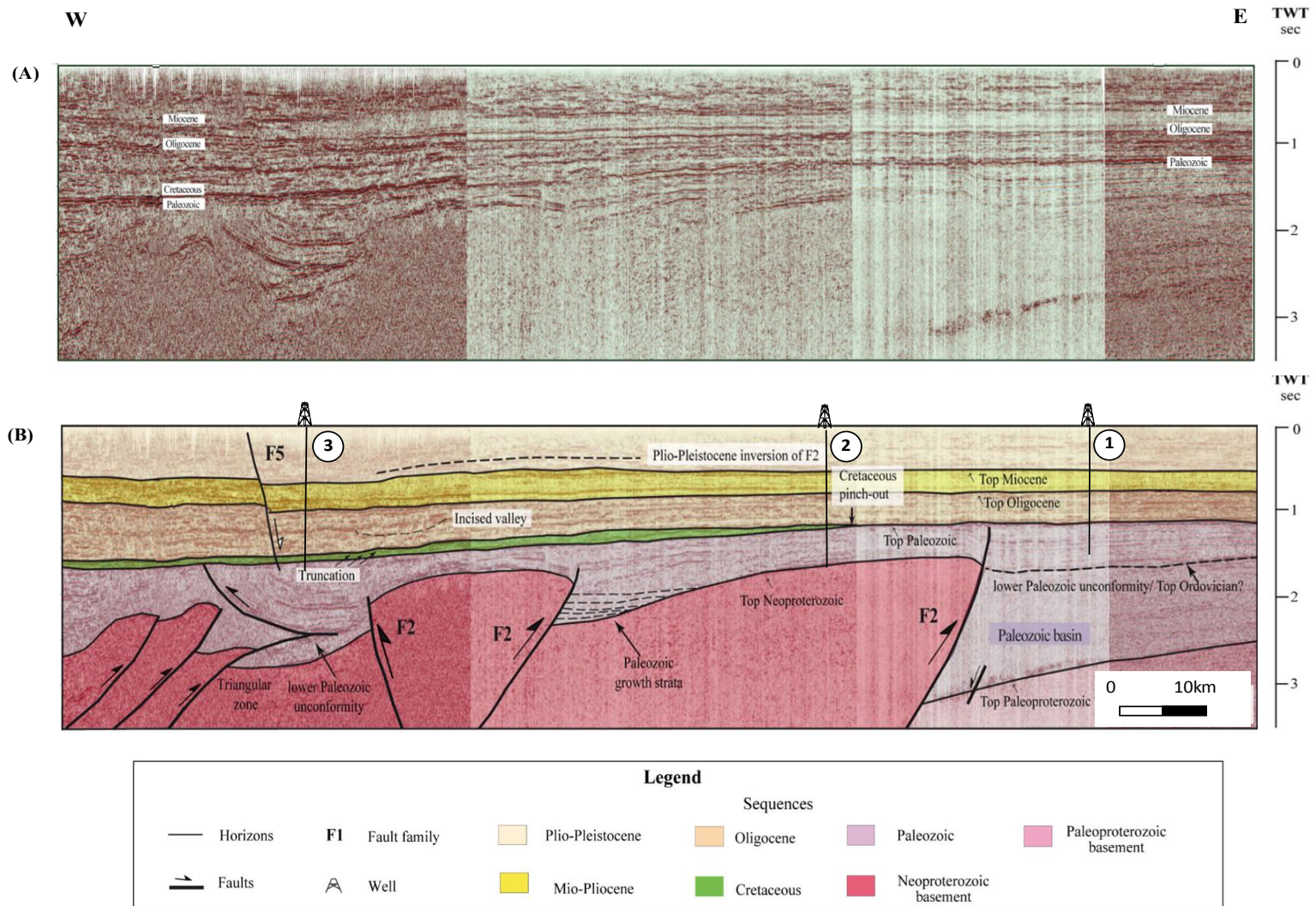
**Fig. 3.2.2. A.** *Uninterpreted two-dimensional (2-D) seismic section;* **B.** *Interpreted 2-D seismic section. TWT = two-way travel time. After Moreno and Escalona, (2015). 1, 2, and 3 represent the location of adjacent explorations wells containing information used for constraining and calibrating the model. Distances are 25km, 95km, and 125km respectively.*

**Table 3.2.1.** *Available vitrine reflectance (%Ro) for the 3 wells. For location of the wells refer to Fig. 3.2.1. * Vitrinite reflectance values within the source rock interval.*

**Well 1 (eastern)**

| Depth (m) | %Ro |
|---|---|
| **Pleistocene** | - |
| **Miocene** | - |
| **Oligocene** | |
| 1152 | 0,40 |
| 1400 | 0,41 |
| **Paleozoic** | |
| 1629 | 0,47 |
| 1796 | 0.45 |

**Well 2 (Central)**

| Depth (m) | %Ro |
|---|---|
| **Pleistocene** | - |
| **Miocene** | |
| 762 | 0.29 |
| 944.88 | 0.3 |
| 1066.8 | 0.35 |
| **Oligocene** | |
| 1143 | 0.35 |
| 1173.48 | 0.39 |
| 1234.44 | 0.35 |
| 1264.92 | 0.36 |
| 1325.88 | 0.37 |
| 1356.36 | 0.35 |
| 1417.32 | 0.4 |
| 1508.76 | 0.36 |
| 1562.11 | 0.39 |
| 1569.72 | 0.41 |
| **Cretaceous** | |
| 1615.44 | 0.41 |
| 1684.02 | 0.42 |
| **Paleozoic** | |
| 1722.12 | 0.85 |
| 1813.56 | 1 |
| 1874.52 | 1.04 |
| 1935.48 | 1.02 |
| 1972.06* | 1.03 |
| 2023.87* | 0.96 |
| 2046.73* | 1.06 |
| 2072.64* | 1.04 |
| 2101.57* | 1.05 |

**Well 3 (western)**

| Depth (m) | %Ro |
|---|---|
| **Pleistocene** | - |
| **Miocene** | - |
| **Oligocene** | |
| 1790m | 0,38 |
| 1921m | 0,37 |
| 2035m | 0,40 |
| **Cretaceous** | |
| 2124m | 0,39 |
| 2245m | 0,41 |
| **Paleozoic** | |
| 2685m | 0,68 |
| 2707m | 0,73 |

In order to simulate the basin's geometry through time, a reconstruction was done in Move software. Unfolding, unfaulting, and decompaction were carried out in a process in which the layers and main structures were removed one by one and corrections were made for the present-day compacted thickness. The grain density and lithological parameters used are shown in Table 3.2.3. The reconstruction used Simple Shear for high-angle, planar faults and Fault Parallel Flow for no planar faults.

***Table 3.2.2.*** *Available well temperature data in°C for the 3 wells.*

| Depth/Well | 3(western) | 2(central) | 1 (eastern) |
|---|---|---|---|
| 1005m | | 60° | |
| 1115m | 53° | | |
| 1330m | | 64° | |
| 1680m | | | 97° |
| 1705m | 66° | | |
| 1876m | | 80° | |
| 1981m | | | 106° |
| 2290m | 79° | | |

***Table 3.2.3.*** *Lithological and rheological properties used for performing reconstruction of the basin history.*

| Rock Type | Rock Group | Sandstone(%) | Shale(%) | Limestone(%) | Porosity | Depth Coefficient | Vshale | Grain Size | Density | Young Modulus | Poisson Ratio |
|---|---|---|---|---|---|---|---|---|---|---|---|
| Pleistocene | Silt | 30 | 70 | 0 | 0.59 | 0.44 | 0.7 | 0.01 | 2699.00 | 27250.00 | 0.30 |
| Miocene | Sand | 75 | 25 | 0 | 0.53 | 0.33 | 0.25 | 0.03 | 2667.50 | 19375.00 | 0.30 |
| Oligocene | Silt | 35 | 65 | 0 | 0.58 | 0.43 | 0.65 | 0.02 | 2695.50 | 26375.00 | 0.30 |
| Cretaceous-Paleocene | Shale | 20 | 70 | 10 | 0.58 | 0.45 | 0.7 | 0.01 | 2705.00 | 30250.00 | 0.29 |
| Upper Ordovician | Sand | 70 | 30 | 0 | 0.53 | 0.34 | 0.3 | 0.03 | 2671.00 | 20250.00 | 0.30 |
| Lower Ordovician | Shale | 30 | 70 | 0 | 0.59 | 0.44 | 0.7 | 0.01 | 2699.00 | 27250.00 | 0.30 |
| Basament | Basement | | | | | | | | | | |

The geological model was summarized in seven key paleo sections: A. Late Ordovician-Silurian; B. Early Permian; C. Late Permian-Triassic; D. Late Cretaceous-Paleocene; E. Oligocene; F. Miocene; G. Present day (Fig. 3.2.3). Key times are those that represent time of deposition, non-deposition (hiatus), erosion, and tectonic uplift.

The paleo sections, together with their geological ages, were the basis for forward modeling using the PetroMod Block Concept. In each section, independent blocks were created (Fig. 3.2.4A) and parent and child blocks were established to enable the software to re-build the paleo relationships between blocks (PetroMod TecLink 2D reference guide). The software was also provided with the order in which it should assemble the blocks within each paleo section. This information was given by the block order in which each block was assigned a number (Fig. 3.2.4B).

The thermal evolution of the basin was calculated using a variable heat flow that includes the four major thermal stages. Lithological properties and surface temperature through time were also
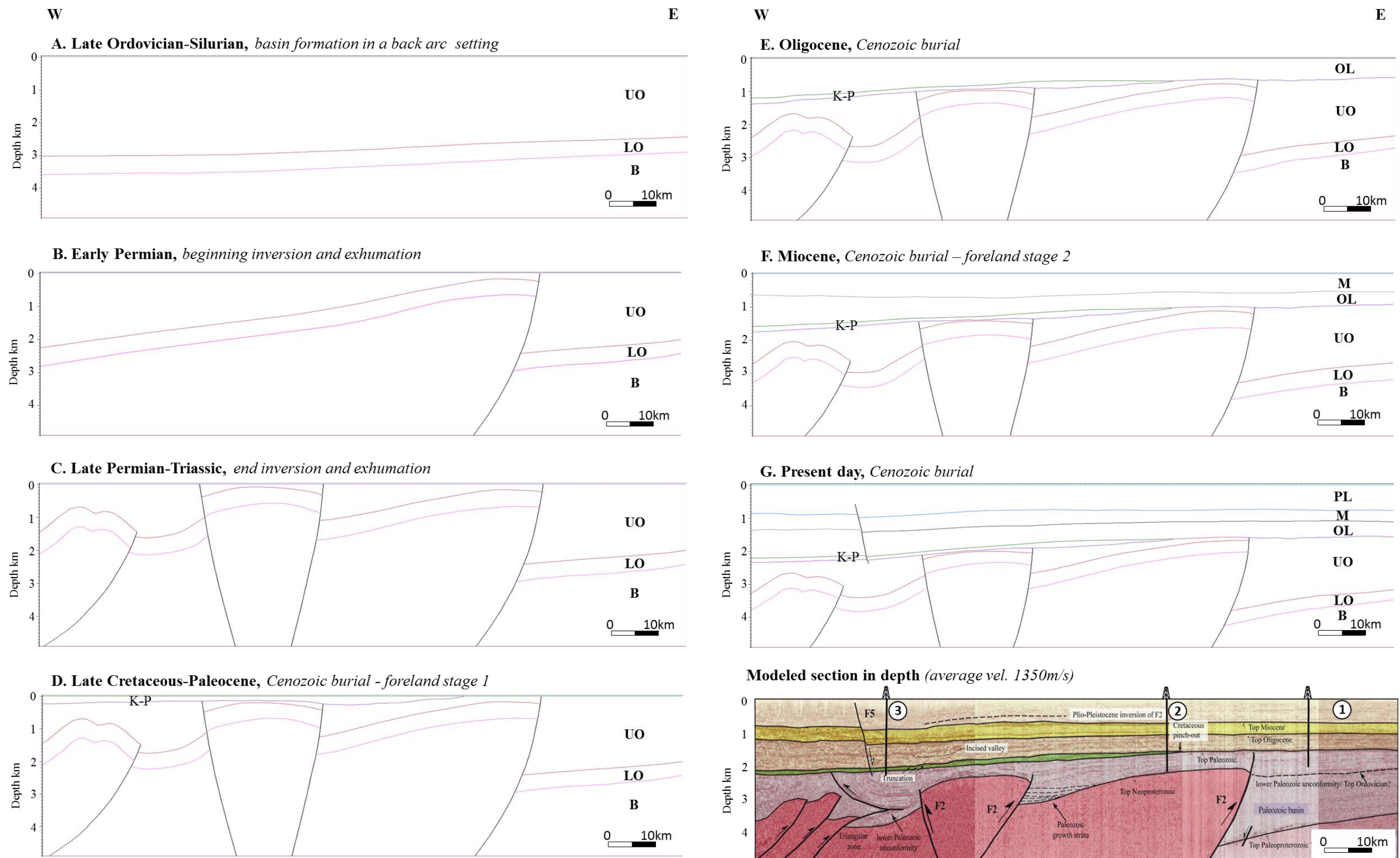
**Fig. 3.2.3.** *Seven key paleo sections used for forward basin modeling are shown. Horizons and faults for every section are displayed. Additionally, the adopted model by Moreno and Escalon, (2015) used for basin modeling is shown. Location of the wells containing input information are indicated by numbers 1, 2, and 3. B: Basement; LO: Lower Ordovician; UO: Upper Ordovician; K-P: Upper Cretaceous-Paleocene; OL: Oligocene; Mi: Miocene; Pl: Pleistocene.*

| Name | Color | Parent Block | Block Order |
|---|---|---|---|
| Master | | | 1 |
| A | | Master | 5 |
| B | | Master | 10 |
| C | | B | 15 |
| D | | B | 20 |
| E | | B | 25 |
| F | | F | 30 |
| G | | G | 35 |
| H | | H | 40 |
| I | | I | 45 |
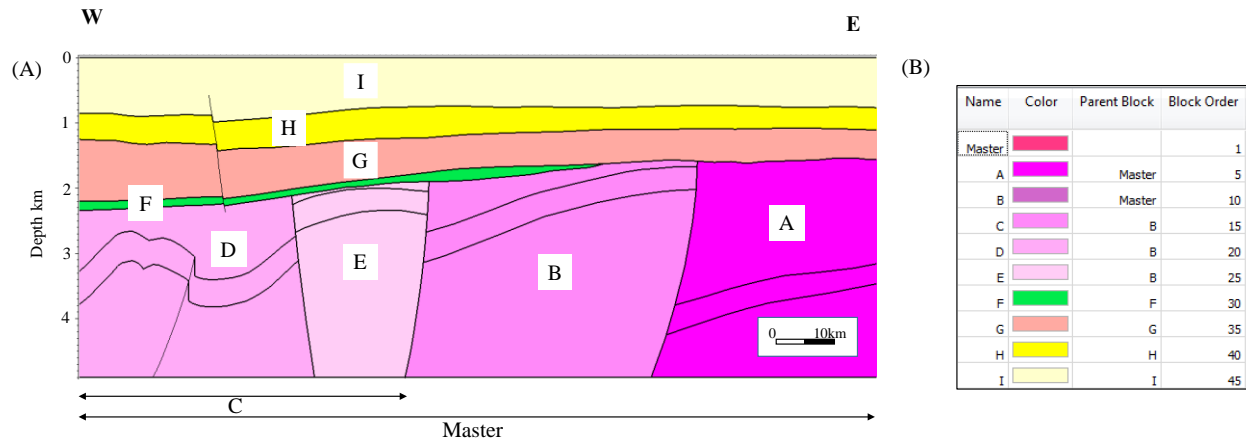
***Fig. 3.2.4 A.*** *Present-day section showing all the assigned blocks;* ***B.*** *Table shows the assigned blocks with corresponding Parent Blocks and values for Block Order.*

considered. The kerogen maturation models were based on first-order kinetics applicable to decomposition reactions (Behar et al., 1997).

The basin modeling simulated temperature, maturity, and transformation ratio for the two source rock intervals from the Ordovician to present. Additionally, this study evaluated the ideal time-temperature window for hydrocarbon preservation in reservoirs (Nadeau et al., 2005) and the relationship with source rock maturation trough time in order to develop a better understanding of a potential petroleum system.

# 4. GEOCHEMICAL CHARACTERIZATION

## 4.1. SOURCE ROCK ANALYSIS

As an attempt to assess the generation potential of Paleogene units outcropping in the northeastern margin of the island (Fig. 3.1.), four fine-grained samples were analyzed.

In hand specimen, all the samples are dark-gray to black in color. They consist of silt to mud-sized particles. They were collected from parallel-laminated beds that do not typically exceed 40cm in thickness and do not show any evident oil stains.

The total organic carbon (TOC) content obtained for the samples ranges between 0.25% and 3.02 % (Table 4.1.1). In the histogram presented in Fig. 4.1.1.A, two of the samples (B4 and B10) are classified as poor source rocks, one is classified as a fair source rock, and one as a good source rock for hydrocarbon generation in terms of TOC content.

All samples have very low to low Rock-Eval $S_1$ signal and the $T_{max}$ values range between 319°C and 426°C (Fig. 4.1.2. and Table 4.1.1.). This suggests that the samples are immature for thermal hydrocarbon generation. The hydrogen index (HI) yields values ranging between 80 and 121, which indicates Kerogen type III to IV for all the samples in the pseudo-Van Krevelen diagram shown in Fig. 4.1.1.B. The analyzed Paleogene samples show low potential for petroleum generation. In a more distal depositional setting the Paleogene rocks may have generation potential.

**Table 4.1.1** *TOC and Rock-Eval Pyrolysis data for the Barbados sample set.*

| Sample | TOC (%) | S1 (mg/g) | S2 (mg/g) | S3 (mg/g) | PI (wt ratio) | HI (mg HC/g TOC) | OI (mg CO2/g TOC) | Tmax (°C) |
|--------|---------|-----------|-----------|-----------|---------------|------------------|-------------------|-----------|
| B4 | 0.25 | 0.05 | 0.2 | 0.16 | 0.2 | 80 | 64 | 319 |
| B10 | 0.25 | 0.02 | 0.14 | 0.33 | 0.13 | 56 | 131 | 413 |
| B14 | 1.06 | 0.02 | 0.82 | 3.65 | 0.02 | 77 | 300 | 437 |
| B16 | 3.02 | 0.17 | 3.65 | 0.95 | 0.04 | 121 | 31 | 426 |
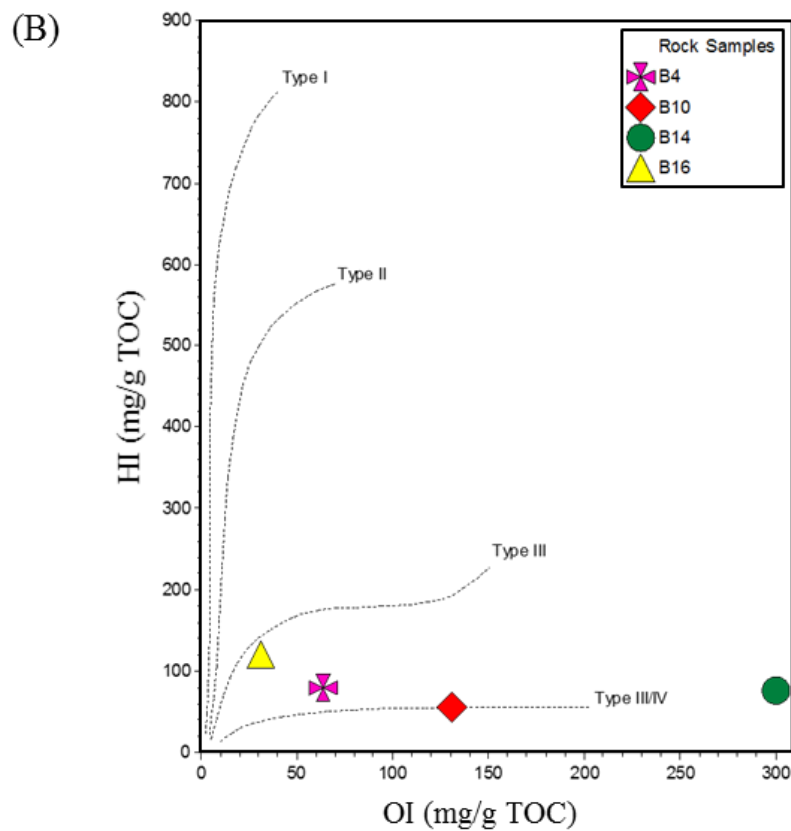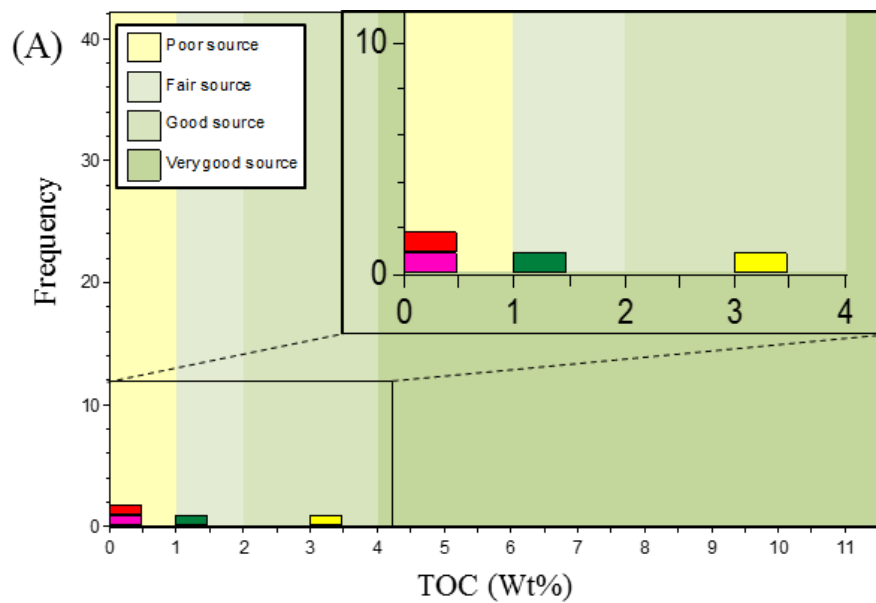
***Fig. 4.1.1. A***. *Histogram classifying the source rock potential of the Barbados samples. A zoomed portion of the figure details the distribution of the samples;* ***B.*** *Pseudo-Van Krevelen diagram showing type III and IV kerogen for the analyzed sample set.*
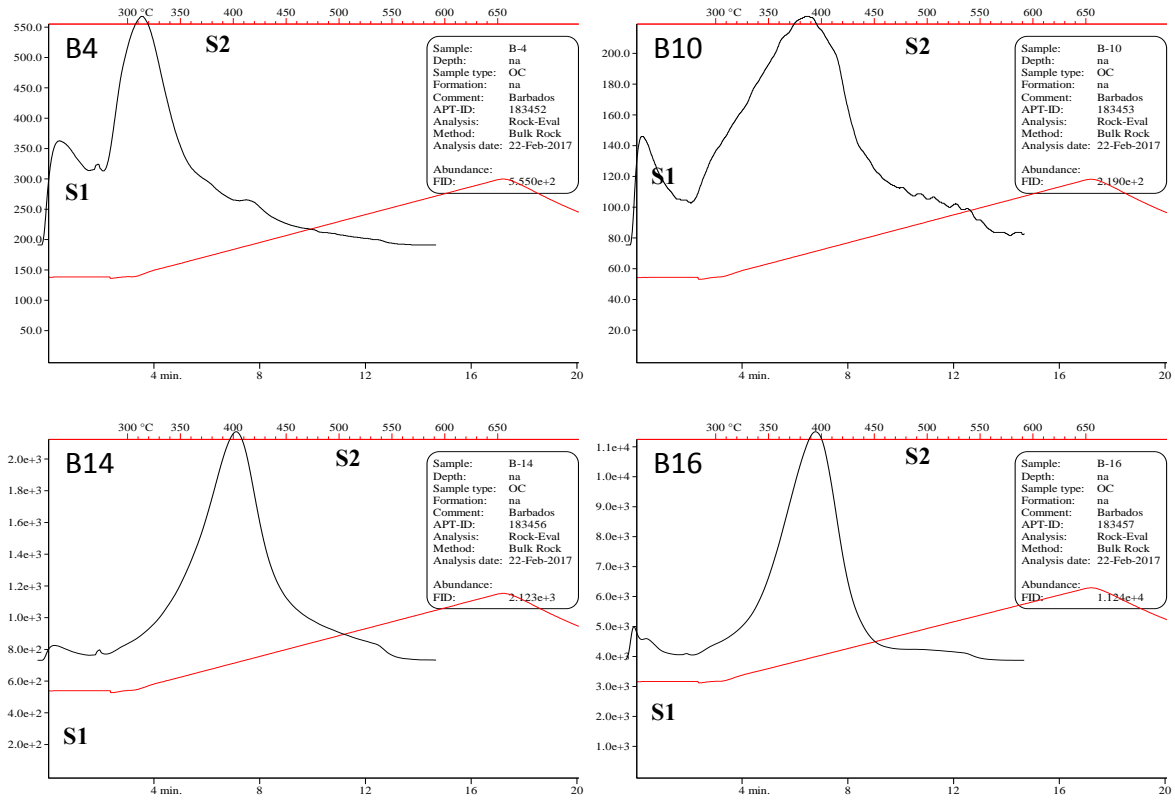
**Fig. 4.1.2** *Pyrograms showing dominant S2 peaks in all the analyzed samples.*

## 4.2. PETROLEUM ANALYSIS

### 4.2.1. Biodegradation assessment

Source and thermal maturity assessment of organic matter in oils can be significantly hampered by biodegradation.

Crude oil samples WO84, WO88, WO177 and WO196 from the Woodbourne field sampled below 1000 meter depth show n-alkane profiles from n-C$_3$ extending up to n-C$_{36}$ with no sign of extensive biodegradation (Fig. 4.2.1.). However, slight biodegradation might explain the lower concentration in the front end n-alkanes in the oils WO177 and WO 196. Low isoprenoids to n-alkane ratios for these four samples also suggest that they are nearly pristine oils (Peters et al., 2005) (Table 4.2.1). By contrast, the depletion of n-alkanes in GC-FID chromatograms (Fig. 4.2.2.) of the crude oils from the Woodbourne field sampled above 1000 meter depth (WO140 and LG#11) clearly demonstrate that these oils are biodegraded. The oil seepage (SP) and all the extracts are severely biodegraded as indicated by the total or partial lack of n-alkanes, pronounced unresolved complex mixture (UCM) humps, and the ubiquitous presence of solid and semi-solid bitumen.

The partial or total absence of n-alkanes in extracts from samples B4, B10, B11, and B13 (Fig. 4.2.2.) ranks them at level 2 and 3 for biodegradation (Peters et al., 2005). For samples WO140, LG#11, and SP biodegradation is ranked at level 5, defined by the total absence of acyclic isoprenoids. In sample B21, regular steranes and hopanes (Fig. 4.2.3. and 4.2.4.) are slightly depleted indicating biodegradation degree 6-7. In addition, sample B13 shows evidence of extensive biodegradation of steranes and hopanes (7-8 biodegradation degree). Finally, aromatic steroids appear intact in all samples (Fig. 4.2.5.), which suggests that none of them reach degree 10, making them the most reliable parameter for geochemical characterization.
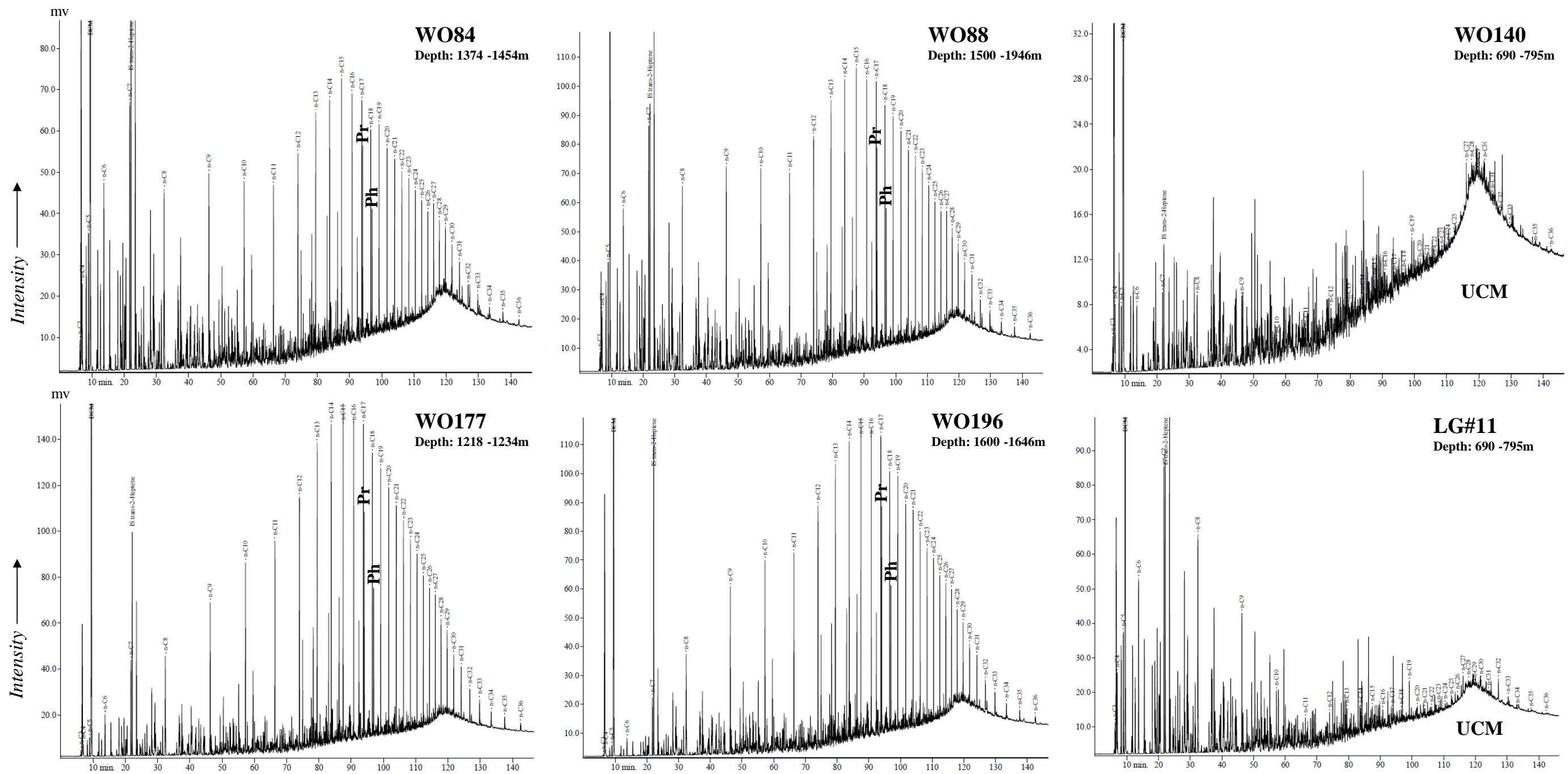
**Fig. 4.2.1.** *GC-FID chromatographs of whole oils from the Woodbourne field. Samples WO140 and LG#11 show biodegraded profiles in the n-alkanes > $C_{11}$ with a well-preserved light fraction and UCM bumps. UCM: unresolved complex mixture. Normal n-alkanes and isoprenoids (Pr= Pristane; Ph=Phytane) are labeled and the corresponding depth or location is shown.*
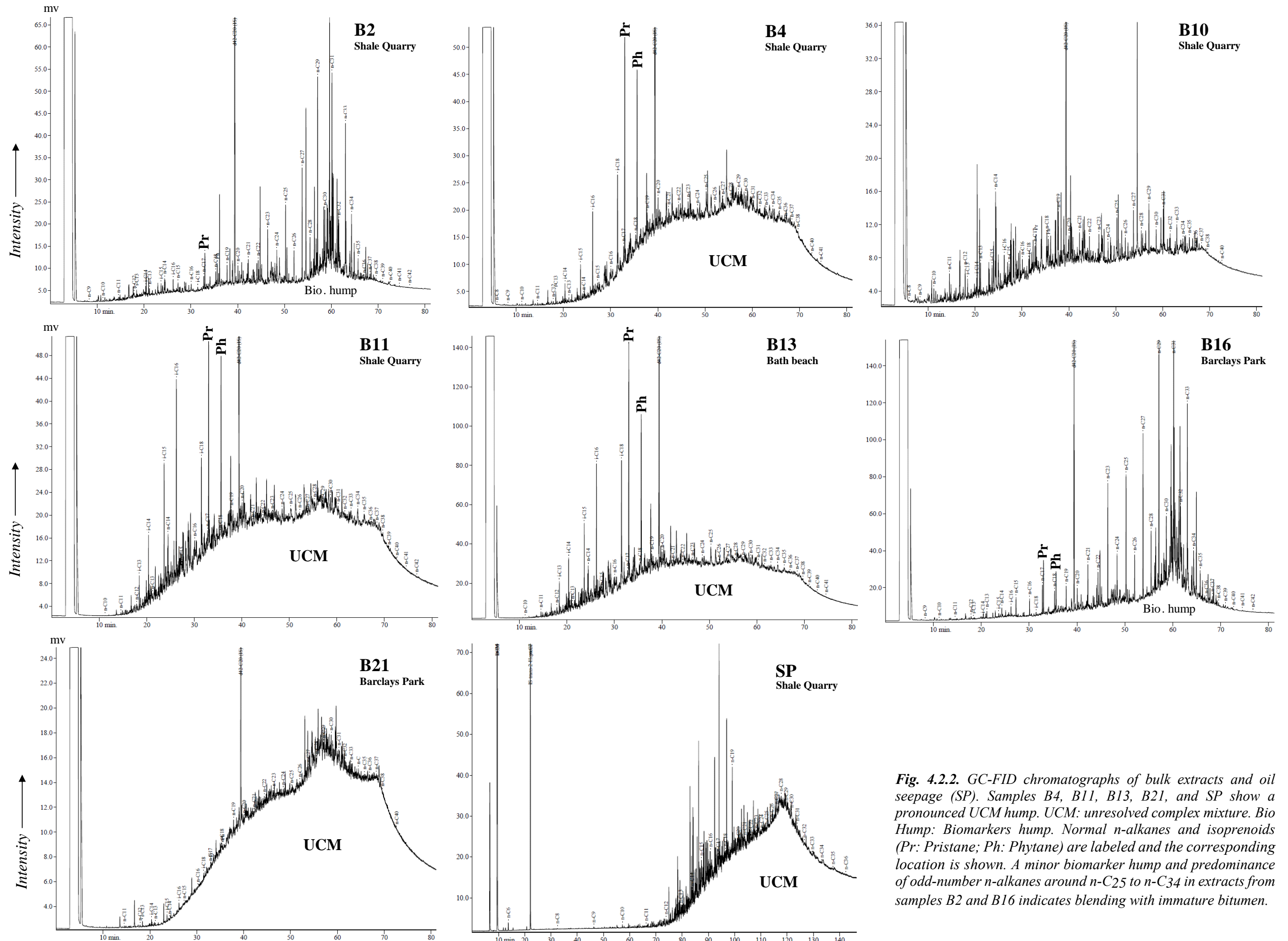
**Fig. 4.2.2.** GC-FID chromatographs of bulk extracts and oil seepage (SP). Samples B4, B11, B13, B21, and SP show a pronounced UCM hump. UCM: unresolved complex mixture. Bio Hump: Biomarkers hump. Normal n-alkanes and isoprenoids (Pr: Pristane; Ph: Phytane) are labeled and the corresponding location is shown. A minor biomarker hump and predominance of odd-number n-alkanes around n-C25 to n-C34 in extracts from samples B2 and B16 indicates blending with immature bitumen.

*Table 4.2.1. Description of the preservation levels for the analyzed biomarker families and biodegradation degrees in accordance with Peters et al., (2005). – No evident biodegradation. * Biodegradation levels inferred for the initial oil prior to blending with immature bitumen.*

| Sample | n-Alkanes | Isoprenoids | Steranes | Hopanes | Biode. degree |
|--------|-----------|-------------|----------|---------|---------------|
| WO84 | Intact | Intact | Intact | Intact | - |
| WO88 | Intact | Intact | Intact | Intact | - |
| WO140 | Scarce | Removed | Intact | Intact | 0-5 |
| WO170 | Intact | Intact | Intact | Intact | - |
| WO196 | Intact | Intact | Intact | Intact | - |
| LG#11 | Very scarce | Removed | Intact | Intact | 0-5 |
| B2 | Scarce | Very depleted | Intact | Intact | 4-5* |
| B4 | Very scarce | Nearly intact | Intact | Intact | 2-3 |
| B10 | Scarce | Very depleted | Immature | Immature | |
| B11 | Very scarce | Nearly intact | Intact | Intact | 2-3 |
| B13 | Absent | Nearly intact | Affected | Nearly removed | 3-4-8 |
| B16 | Scarce | Low | Immature | Immature | |
| B21 | Absent | Removed | Affected | Nearly intact | 6-7 |
| SP | Absent | Removed | Intact | Intact | 5 |

However, it should be noted in Table 4.2.1 that some of the samples show simultaneously non-correlative and very distinctive degrees of biodegradation. For example, crude oils WO144 and LG-11 have scarce and very scarce amounts of n-alkanes and acyclic isoprenoids (degree 5) with the anomalous presence of a well-preserved light fraction (n-$C_3$ to n-$C_9$). It is consistent with the presence in the reservoir of a mixture of a degraded oil and a later charge of very light oils. Biodegradation at the Woodbourne field appears to increase dramatically above 1000m as manifested by the substantial change in biodegradation between oil samples below 1000 meter (WO84, WO 88, WO177, WO196) and above1000 meter (WO144 and LG#11) (Table 3.1). Similarly, sample B13 has experienced extensive biodegradation as demonstrated by depleted $C_{29}$ regular steranes and hopanes (degree 8), but preserves acyclic isoprenoids typical of biodegradation degree 3 to 4. This heterogeneous degree of biodegradation suggests the dilution of a crude oil severely degraded near the surface with a second, less degraded oil.

In extracts from the oil-stained sample B2 and from the fine-grained sample B16, n-alkanes from $C_{23}$ to $C_{35}$ appear intact, displaying clear predominance of odd-number over even-number n-

alkanes. Such predominance is typically observed in immature bitumen. In contrast to the relatively pronounced UCM humps in the other samples which are interpreted as severe biodegradation, B2 and B16 sample extracts exhibit only a minor biomarker hump around $C_{28}$ to $C_{35}$ (Fig. 4.2.2.), which is also indicative of immature to very low mature bitumen. However, these three samples, as will be discussed in the maturity assessment section, show high maturity levels based on aromatic parameters. Although other explanations cannot be discarded to account for this anomalous pattern, the most probable explanation consists of a blend of an initial degraded crude oil with immature bitumen, or alternatively with a fresh immature oil.

It is likely that the immature fraction in samples B10 and B16 represents in-situ, immature bitumen contained in the hosting rocks which correspond to clay to silt-sized grained samples. In Table 4.1.1 these two samples show TOC value of 0.25% and 3.15% and $T_{max}$ of 413 and 425 respectively, suggesting they may have released some immature bitumen later mixed with the allochthonus aromatic fraction.
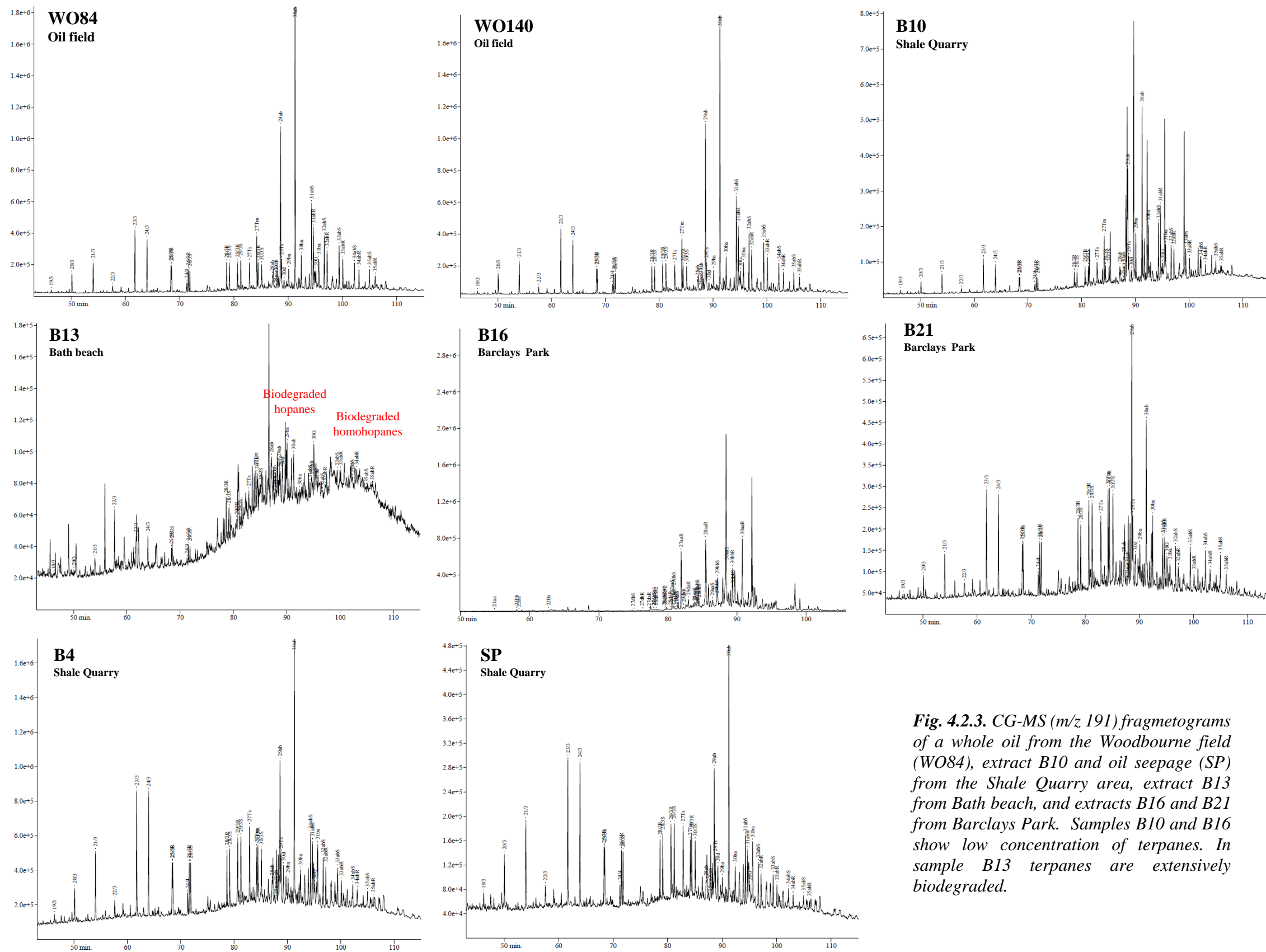
**Fig. 4.2.3.** *CG-MS (m/z 191) fragmetograms of a whole oil from the Woodbourne field (WO84), extract B10 and oil seepage (SP) from the Shale Quarry area, extract B13 from Bath beach, and extracts B16 and B21 from Barclays Park. Samples B10 and B16 show low concentration of terpanes. In sample B13 terpanes are extensively biodegraded.*
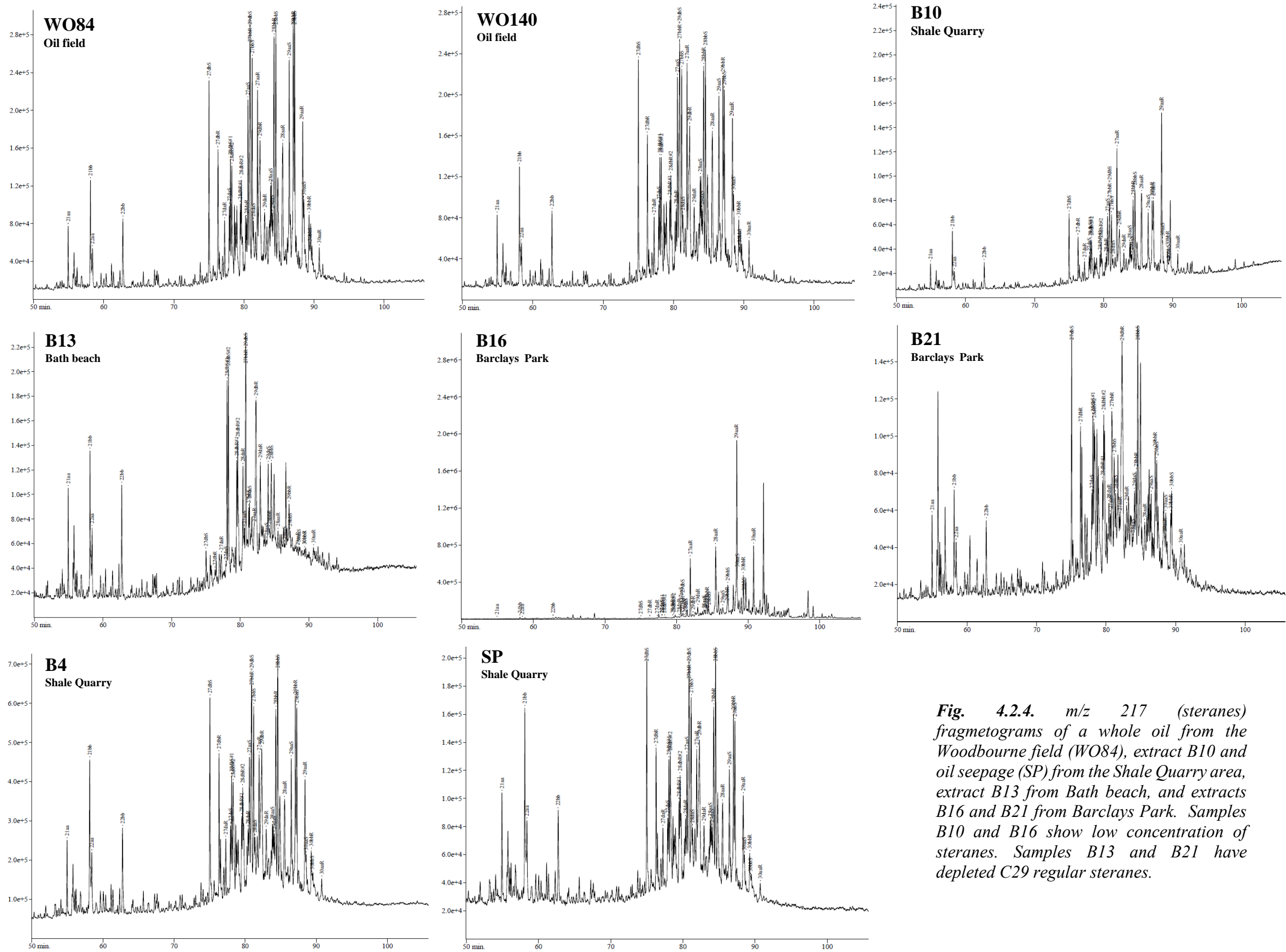
**Fig. 4.2.4.** *m/z 217 (steranes) fragmetograms of a whole oil from the Woodbourne field (WO84), extract B10 and oil seepage (SP) from the Shale Quarry area, extract B13 from Bath beach, and extracts B16 and B21 from Barclays Park. Samples B10 and B16 show low concentration of steranes. Samples B13 and B21 have depleted C29 regular steranes.*
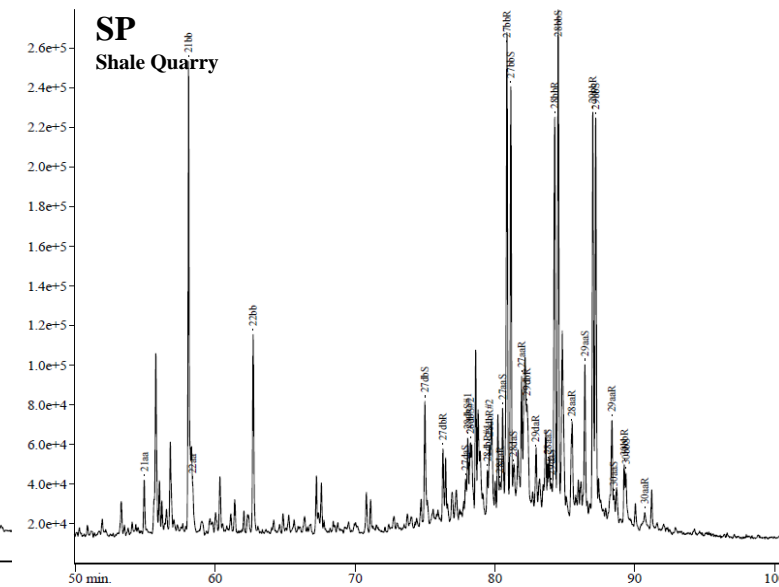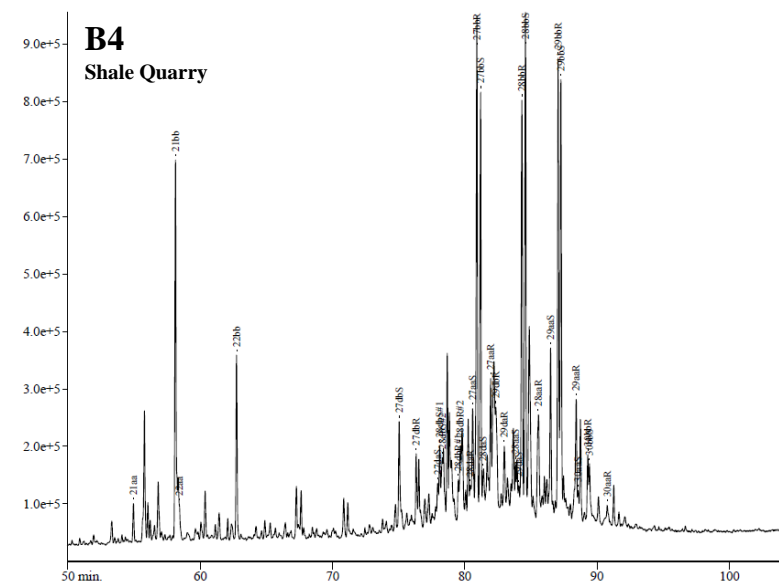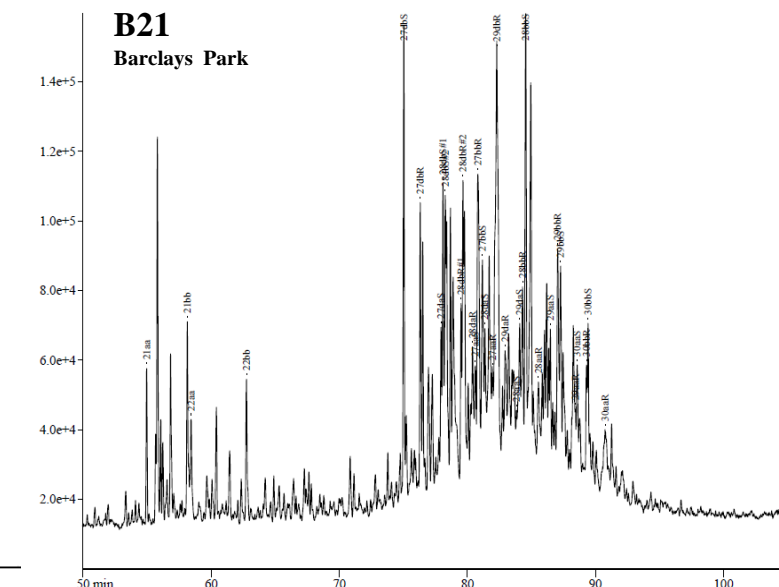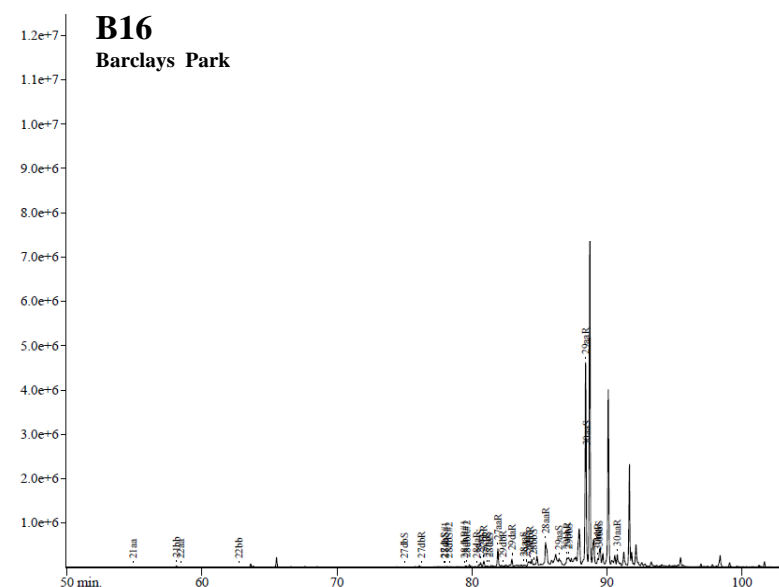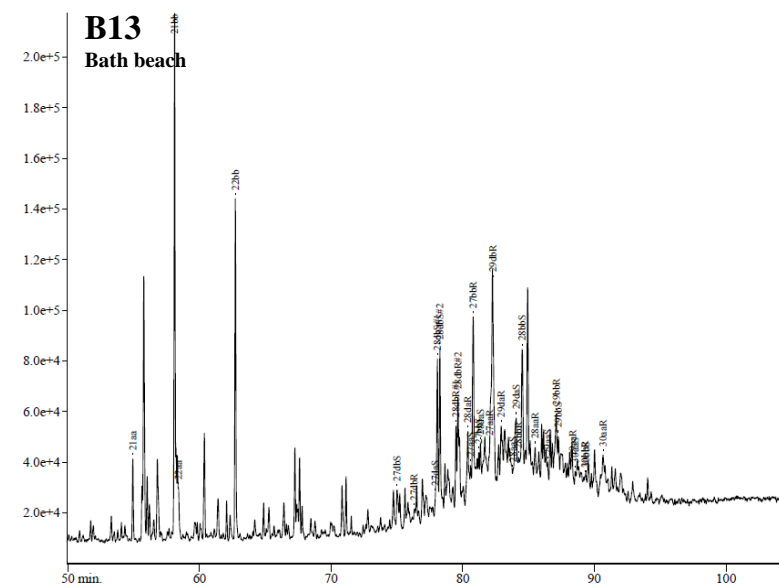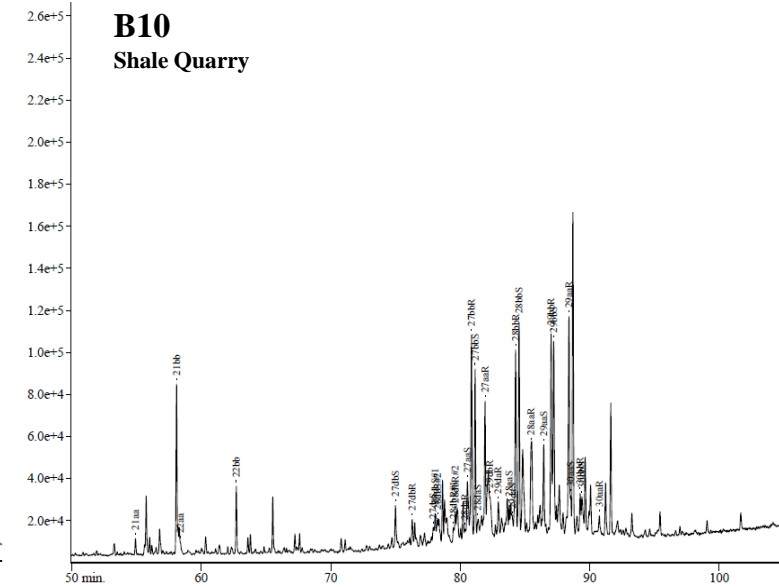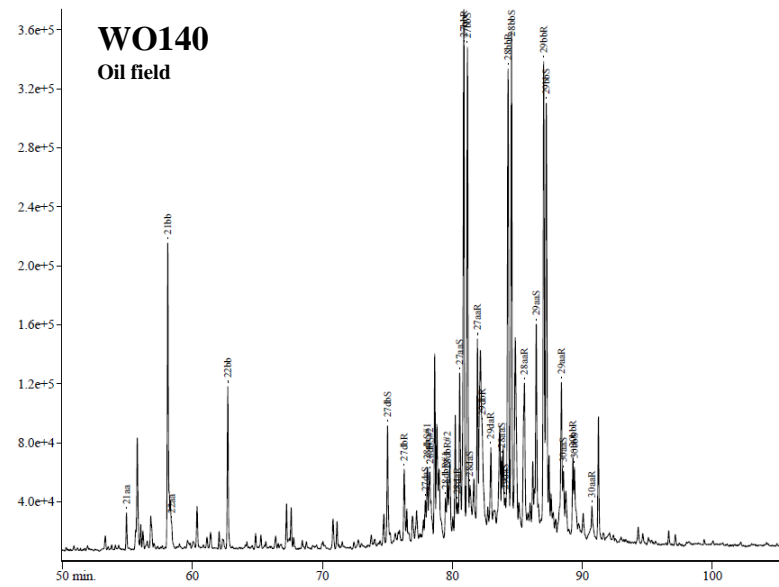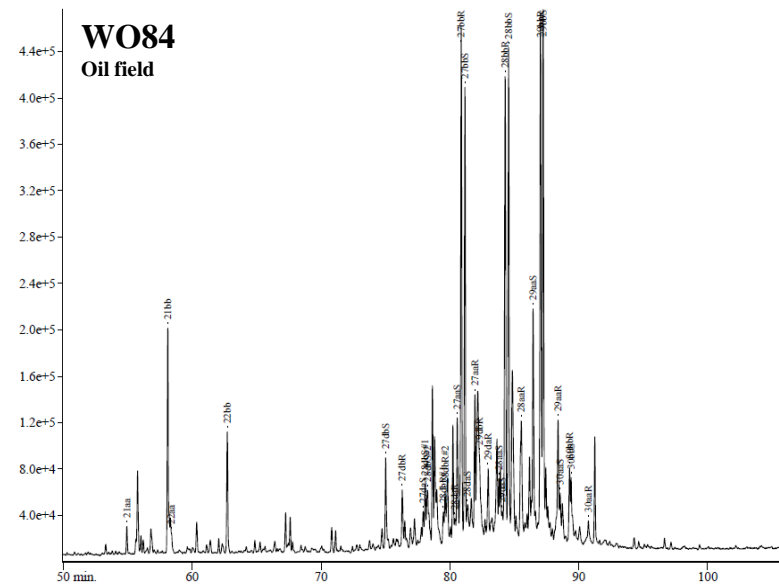
**Fig. 4.2.5.** *m/z 218 (ββ steranes) fragmetograms of a whole oil from the Woodbourne field (WO84), extract B10 and oil seepage (SP) from the Shale Quarry area, extract B13 from Bath beach, and extracts B16 and B21 from Barclays Park. Samples B10 and B16 show low concentration of steranes. Samples B13 and B21 have depleted profiles.*

WO84
Oil field

m/z 192

m/z 198

m/z 231

WO140
Oil field

B10
Shale Quarry

B13
Bath beach

44
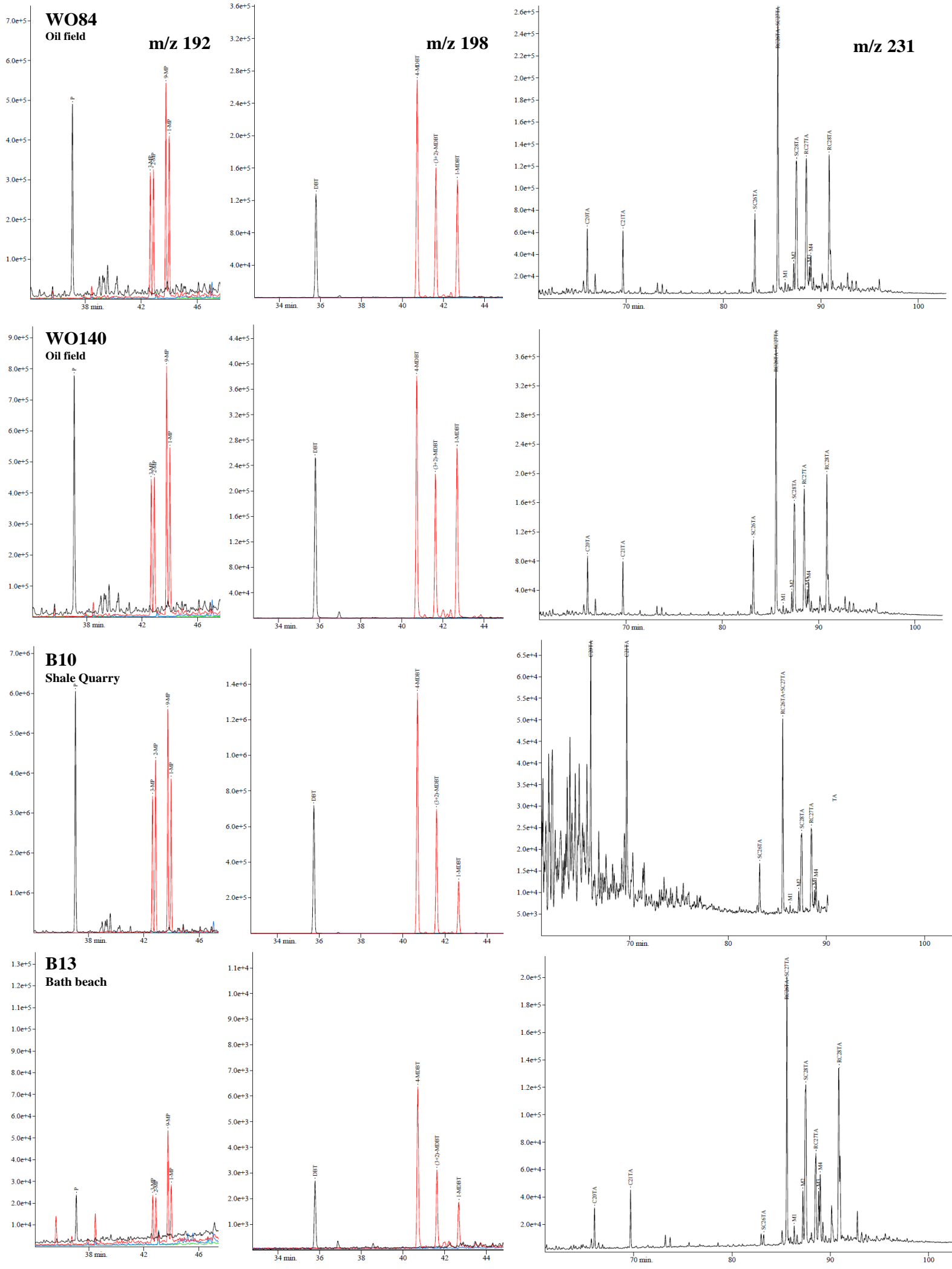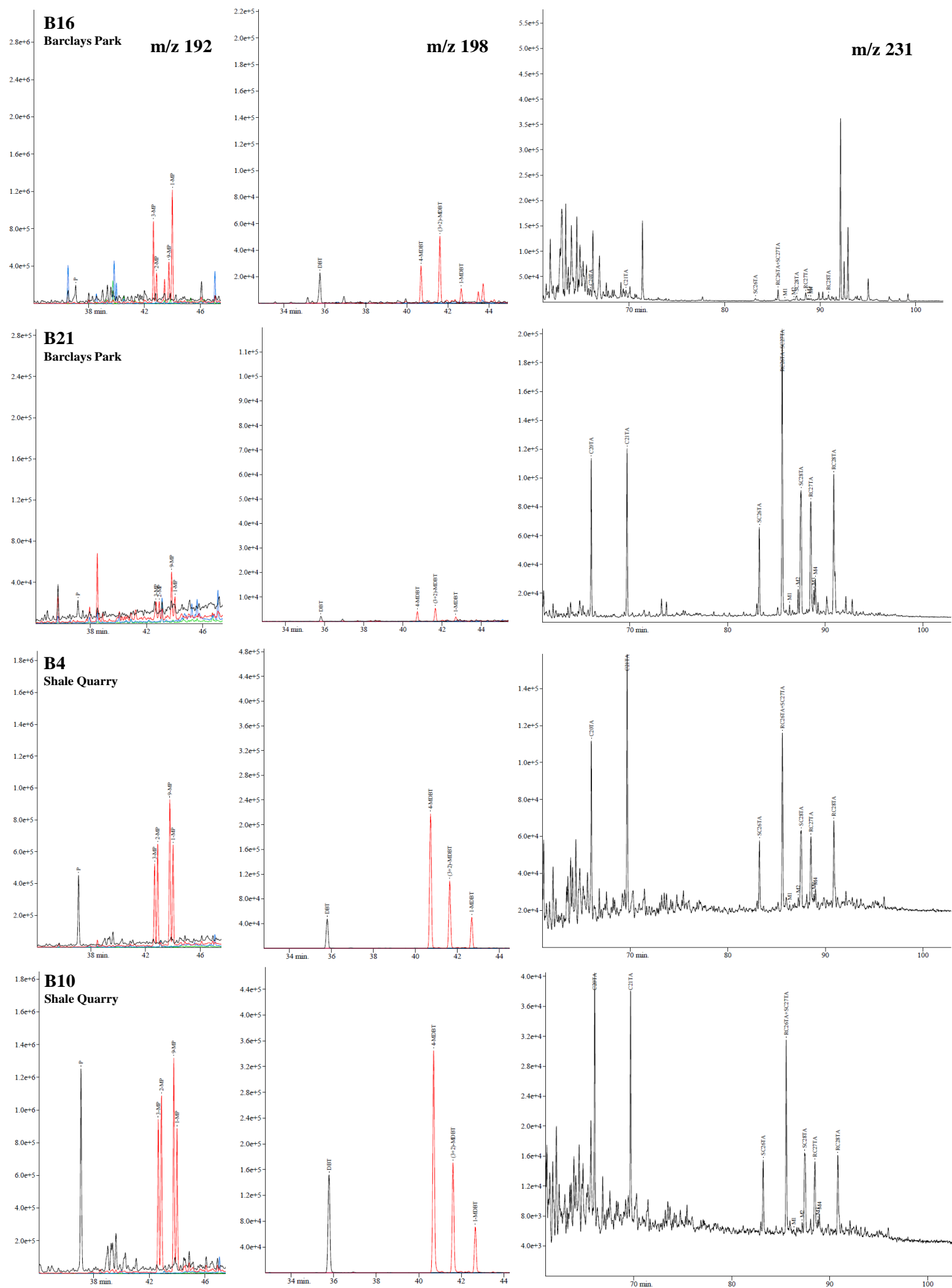
**Fig. 4.2.6**. *Mass chromatograms of methyl-phenanthrenes (m/z 192), methyl-dibenzothiophenes (m/z 198), and triaromatic steroids (m/z 231) for a whole oil from the Woodbourne field (WO84), bulk extracts (B4, B10, B13) and oils seepage (SP) from the Shale Quarry area, and extracts B13, B16 and B21 from the east coast of the Barbados island.*

45

### 4.2.2. Thermal maturity assessment

Maturity estimates in this study are based first on aromatic maturity parameters and their calculated vitrinite reflectance ($R_c$), as these are the most reliable markers at relatively advanced biodegradation levels. However, variations in the type of organic matter and lithology in the source rock can affect methylphenanthrene ratios. Indeed, Cassani et al., (1988b) reported that high MPI-1 resulted from the high carbonate content of La Luna Formation. Thus, they need to be interpreted with caution.

Oils samples from the Woodbourne field and the extract from sample B13 exhibit comparatively higher concentration of long ($C_{26}$-$C_{28}$) over short ($C_{20}$-$C_{21}$) chain triaromatic (TA) steroids ($m/z$ 231 in Fig. 4.2.6.). By contrast, the remaining extracts and the seepage (SP) are dominated by short-chain $C_{20}$ and $C_{21}$ triaromatic steroids. Extract from sample B16 contains extremely low concentration of these compounds. Mackenzie et al., (1981) found that the relative concentration of these compounds can be used to evaluate maturity in the range 0.3-1.5%$R_o$.

The $C_{20}/(C_{20}+C_{28})$ ratios of the triaromatic (TA) steroids for the Woodbourne crude oils and extract from sample B13 range between 0.19 and 0.36 (Table 4.2.2), indicating generation at the early mid-oil window. The extracts from samples B16 and B21 have $C_{20}/(C_{20}+C_{28})$ TA steroids ratios of 0.52 and 0.53 respectively, suggesting generation at about the mid-oil window. The same parameter for samples B2, B4, B10, B11, and the seepage (SP) yields values between 0.68 to 0.76, indicating generation at peak of the mid-oil window. Note that the seepage has the highest values of maturity in the sample set (0.76). Although TA steroid ratios for samples B16 and B21 (0.52 and 0.53) suggest higher maturity than those of samples from the Woodbourne crude oils and the extract from sample B13 (0.3-0.36), calculated vitrinite reflectance from medium range aromatics suggest that all these samples have the same maturity.

Relative peak heights of medium range aromatics compounds such us methyl-phenanthrene (MP) and methyl-dibenzothiophene (MDBT) may be used to determine maturation levels. This is demonstrated by the height of 3-MP and 2-MP compared to 9-MP and 1-MP in the $m/z$ 192 fragmetograms, and similarly 4-MDBT compared to 1-MDBT in the $m/z$ 198 fragmetograms. Radke, (1988) noted an increase in the relative amounts of 3-MP and 2-MP compared to 9-MP and

1-MP with increasing burial depths and temperatures. The concentration of methyl-phenanthrene and methyl-dibenzothiophene isomers are present in considerable proportions in all the samples (*m/z* 192 and 198 Fig. 4.2.6.), except for the extracts from samples B16 and B21 which have very low concentrations, but overall the aromatic maturity parameters calculated for these samples are still consistent. In the *m/z* 198 fragmetograms (Fig. 4.2.6.), the 1-MDBT concentration for the Woodbourne oils is higher than its equivalent for the extracts (B2, B4, B10) and the seepage (SP). This suggests that the oils from the Woodbourne field are less mature than the extracts and the oil seepage from the Shale Quarry (Table 4.2.2).

**Table 4.2.2.** *Aromatic and biomarker parameters used to assess thermal maturity of analyzed samples.*

| Sample | %Rc -MPR | %Rc- MPI I | %Rc- MPDF | %Rc -MDR | %Rc -Ave | $C_{20}$ /$(C_{20}+C_{28})$ | Ts /(Ts+Tm) | $C_{29}\alpha\alpha S$ /$(\alpha\alpha S+\alpha\alpha R)$ | $C29\beta\beta$ /$(\beta\beta+\alpha\alpha)$ |
|---|---|---|---|---|---|---|---|---|---|
| SP | 1.05 | 0.93 | 0.91 | 0.87 | 0.94 | 0.77 | 0.59 | 0.54 | 0.73 |
| B11 | 1.00 | 0.94 | 0.87 | 0.83 | 0.91 | 0.68 | 0.58 | 0.52 | 0.72 |
| B10 | 1.01 | 0.85 | 0.84 | 0.85 | 0.89 | 0.74 | 0.32 | 0.26 | 0.51 |
| B4 | 0.96 | 0.92 | 0.79 | 0.83 | 0.87 | 0.68 | 0.57 | 0.53 | 0.72 |
| B2 | 0.97 | 0.92 | 0.80 | 0.78 | 0.87 | 0.72 | 0.40 | 0.53 | 0.73 |
| WOI77 | 0.88 | 0.80 | 0.76 | 0.65 | 0.77 | 0.36 | 0.24 | 0.55 | 0.68 |
| B13 | 0.84 | 0.79 | 0.63 | 0.70 | 0.74 | 0.19 | 0.43 | 0.65 | 0.78 |
| WO088 | 0.88 | 0.80 | 0.74 | 0.62 | 0.76 | 0.32 | 0.34 | 0.52 | 0.65 |
| WO84 | 0.84 | 0.80 | 0.74 | 0.65 | 0.76 | 0.32 | 0.33 | 0.58 | 0.71 |
| WO140 | 0.86 | 0.78 | 0.73 | 0.61 | 0.74 | 0.30 | 0.34 | 0.51 | 0.65 |
| WO96 | 0.87 | 0.72 | 0.69 | 0.66 | 0.74 | 0.35 | 0.39 | 0.52 | 0.65 |
| B21 | 0.85 | 0.77 | 0.61 | 0.67 | 0.73 | 0.53 | 0.42 | 0.60 | 0.66 |
| LG#11 | 0.83 | 0.76 | 0.68 | 0.62 | 0.72 | 0.36 | 0.38 | 0.52 | 0.68 |
| B16 | 0.32 | 0.99 | 0.78 | 0.70 | 0.70 | 0.52 | 0.55 | 0.04 | 0.14 |

**%Rc-MPR** = 1.1 x log10 MPR + 0.95 (Radke, 1988), where methylphenanthrene ratio, MPR = 2-MP/1-MP.
**%Rc-MPI 1** = 0.60 x MPI1 + 0.40 (Radke, 1988), where methylphenanthrene index 1, MPI 1 = 1.5 x (3-MP + 2-MP)/(P + 9-MP + 1-MP).
**%Rc-MPDF** = 2.242 x MPDF - 0.166 (Kvalheim *et al*., 1987), where methylphenanthrene distribution fraction, MPDF = (3-MP + 2-MP)/ (3-MP + 2-MP + 1-MP + 9-MP).
**%Rc-MDR =** 0.073 x MDR + 0.51 (Radke, 1988), where methyldibenzothiophene ratio, MDR = 4-MDBT/1-MDBT.
**%Rc-Ave:** average of the four calculated vitrinite reflectance values.

Four different vitrinite reflectance values are calculated from the methyl-phenanthrene ratio (MPR), methyl-phenanthrene distribution factor (MPDF), methyl-phenanthrene index (MPI), and methyl-dibenzothiophene ratio (MDR) (kvalheim et al., 1987; Radke, 1988). In addition, an average vitrinite reflectance value (%$R_c$–Ave) is computed (Table 4.2.2). Fig. 4.2.7. A and B, are cross-plots of the calculated vitrinite reflectances displaying two well-separated maturity levels. The crude oils from the Woodbourne oil field and the extract from samples B13 and B21 plot at low maturation levels (low maturity group), whereas extracts from samples B2, B4, B10, and B11, together with the seepage (SP) plot at higher maturity level (high maturity group). Sample B16 plots as an outlier in Fig. 4.2.7.A and plots close to the high maturity group in Fig. 4.2.7.B.

Average vitrinite reflectance values (%$R_c$–Ave) ranging between 0.70% and 0.77% estimated for samples in the low maturity group (red symbols on Fig 4.2.7) represent migrated oil expelled at about early to mid-oil window; the corresponding values for the samples in the high maturity group (blue symbols) ranging between 0.87% to 0.94% correspond to oil expelled at peak of the oil window, with the highest value representing the oil seepage. The reduced amount of the aromatic fraction in sample B16 hinders an accurate assessment of its maturity level.

The m/z 191 fragmetograms (Fig. 4.2.3.) show relatively higher concentration of tricyclic terpanes compared to hopanes in the extracts B4 and B10 the oil seepage (SP) from the Shale Quarry than in the Woodbourne oils due to the higher thermal stability of tricyclic terpanes compared to pentacyclic terpanes (van Grass, 1990). This suggests that the extracts and the seepage are more mature than the crude oils produced from the Woodbourne field. Alternatively, fractionation during migration could lead to the observed distribution.

The applicability of maturity parameters such as the steranes isomerization ratio $C_{29}$ $\alpha\alpha S/(\alpha\alpha S+ \alpha\alpha R)$ and the steranes ratio $C_{29}$ $\beta\beta/(\beta\beta+\alpha\alpha)$ is limited to a range between the onset of the oil generation window (0.6%$R_o$) and the early stages of the main oil generation window (0.9%$R_o$). The sterane ratio C29 $\alpha\alpha S/(\alpha\alpha S+\alpha\alpha R)$ reaches equilibrium at values of 0.52 to 0.55 (Seifert and Moldovan, 1986), corresponding to maturities of 0,8 %Ro to 0.9 %Ro. The sterane ratio C29 $\beta\beta/(\beta\beta+\alpha\alpha)$ reaches equilibrium at values of 0.68 to 0.71 (Seifert and Moldovan, 1986), equivalent to a maturity of about 0.9%$R_o$. Based on previously calculated vitrinite reflectance values, some of
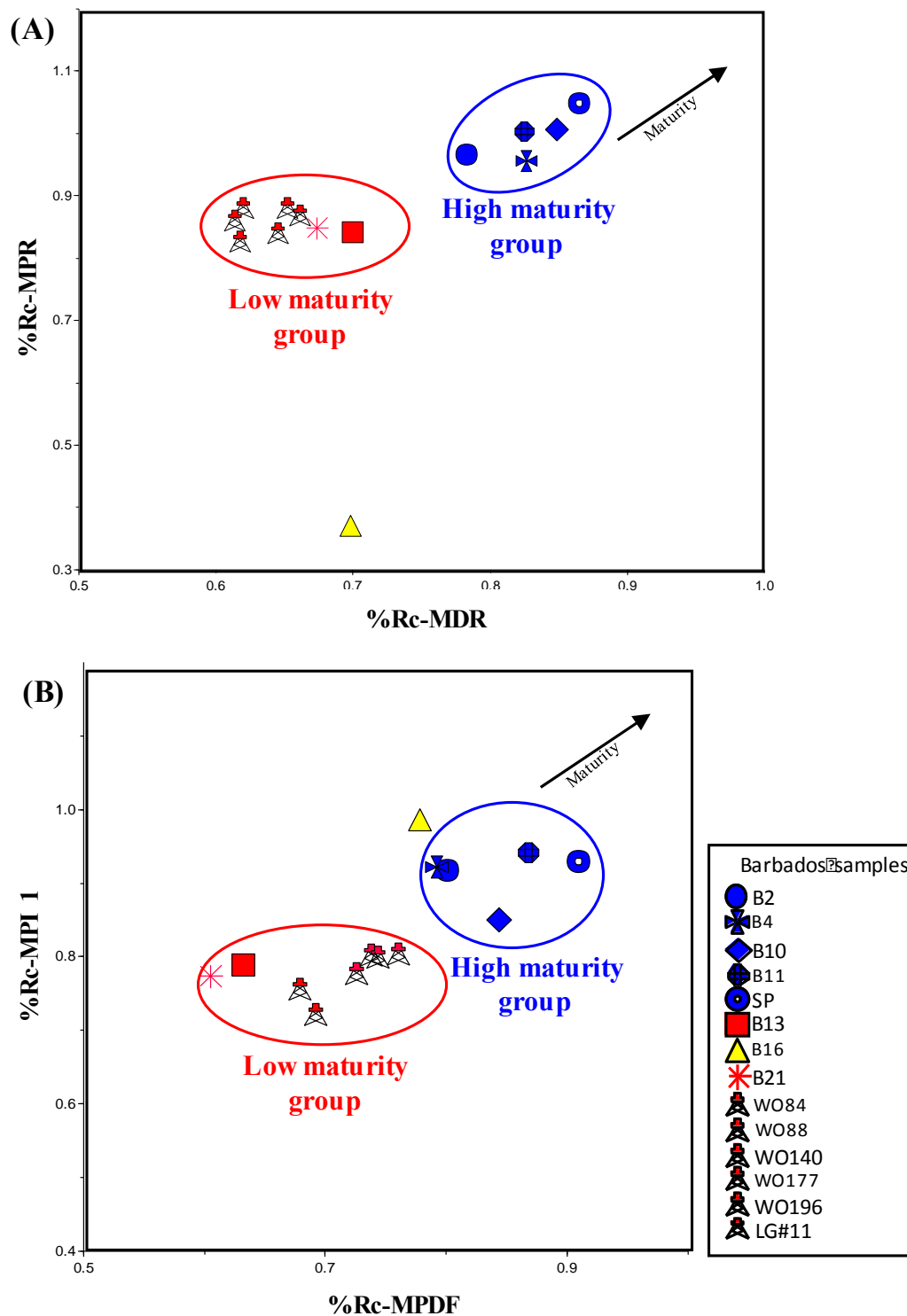
**Fig. 4.2.7.** *Cross plots of maturity parameters using calculated vitrinite reflectances from medium range aromatics.* **A.** *%Rc (MDR) versus %Rc (MPR);* **B.** *%Rc (MPDF) versus %Rc (MPI 1). See Table 4.2.2 for calculated aromatic parameters. Samples plot in two different maturities groups:* **Low maturity group** *= Woodbourne oils, and extracts B13 and B21;* **High maturity group** *= extracts B2, B4, B10, B11, and oil seepage SP. Sample B16 plots as an outlier.*

the samples in this study exceed slightly the equilibrium for sterane isomerization parameters. However, the above mentioned parameters are applied to the studied samples, and the evaluation is complemented with the application of another maturity parameter which extends until the end of the oil window (1.3%$R_o$) such as the Ts/(Ts+Tm) ratio.

Fig. 4.2.8.A is a cross-plot of $C_{29}\beta\beta/(\beta\beta+aa)$ versus $C_{29}\alpha\alpha S/(\alpha\alpha S+\alpha\alpha R)$ ratios. Extracts from samples in the Shale Quarry area (B2, B4, B11) and the oil seepage (SP) plot slightly above the equilibrium area for the $C_{29}$ $\beta\beta/(\beta\beta+\alpha\alpha)$ ratio with average values of 0.72 (maximum 0.73 and minimum 0.71) (Table 4.2.2). The average $C_{29}\alpha\alpha S/(\alpha\alpha S+\alpha\alpha R)$ isomer ratio of the same samples is 0.53 (maximum 0.54 and minimum 0.52). The Woodbourne crude oils have average $C_{29}$ $\beta\beta/($ $\beta\beta$ +aa) and $C_{29}\alpha\alpha S/(\alpha\alpha S+\alpha\alpha R)$ ratios of 0.67 (maximum 0.71 and minimum 0.65) and 0.53 (maximum 0.58 and minimum 0.51) respectively and plotting mainly in the equilibrium zone. Samples B10 and B16 plot as immature. This opposes the average vitrinite reflectance values earlier calculated from aromatic parameters (0.89%$R_o$ and 0.70%$R_o$ respectively). Extract from sample B13 plots far out of the equilibrium zone for both maturity parameters. Similarly, extract from sample B21 plots above the equilibrium zone for the $C_{29}$ $\alpha\alpha S/(\alpha\alpha S+\alpha\alpha R)$ ratio. The most likely explanation for this significant deviation from the maturity trend of samples B13 and B21 is biodegradation of steranes isomers. Preferential biodegradation of $C_{29}$ $\alpha\alpha R$ steranes as observed in (Fig. 4.2.4.) may cause the $\alpha\alpha$ S/($\alpha\alpha S+\alpha\alpha R$) ratios to increase above 0.55 (Peters et al., 2005).

On Fig. 4.2.8.B there is a good correlation between Ts/(Ts+Tm) hopanes and the average calculated vitrinite reflectance values for all the samples except for samples B10 and B16, confirming lower maturity based on biomarkers for these two samples. Thus, samples B10 and B16 are of high maturity similar to those extracts and seepage of the Shale Quarry area (B2, B4, SP) and the Woodbourne field based on triaromatic (TA) steroids and calculated vitrinite reflectances, but of low maturity and immature based on steranes and hopanes maturity ratios. These anomalous variations in maturity estimates between aromatic parameters and biomarkers may be explained by a mixture of mature petroleum with immature bitumen. The *m/z* 217 and 218 fragmetograms (Fig. 4.2.4. and 4.2.5.) for samples B10 and B16 show low and very low concentration of steranes respectively, and the biologically-derived $C_{29}\alpha\alpha R$ isomer is the dominant peak. These pattern is characteristic of immature to very low mature source rocks with low degree
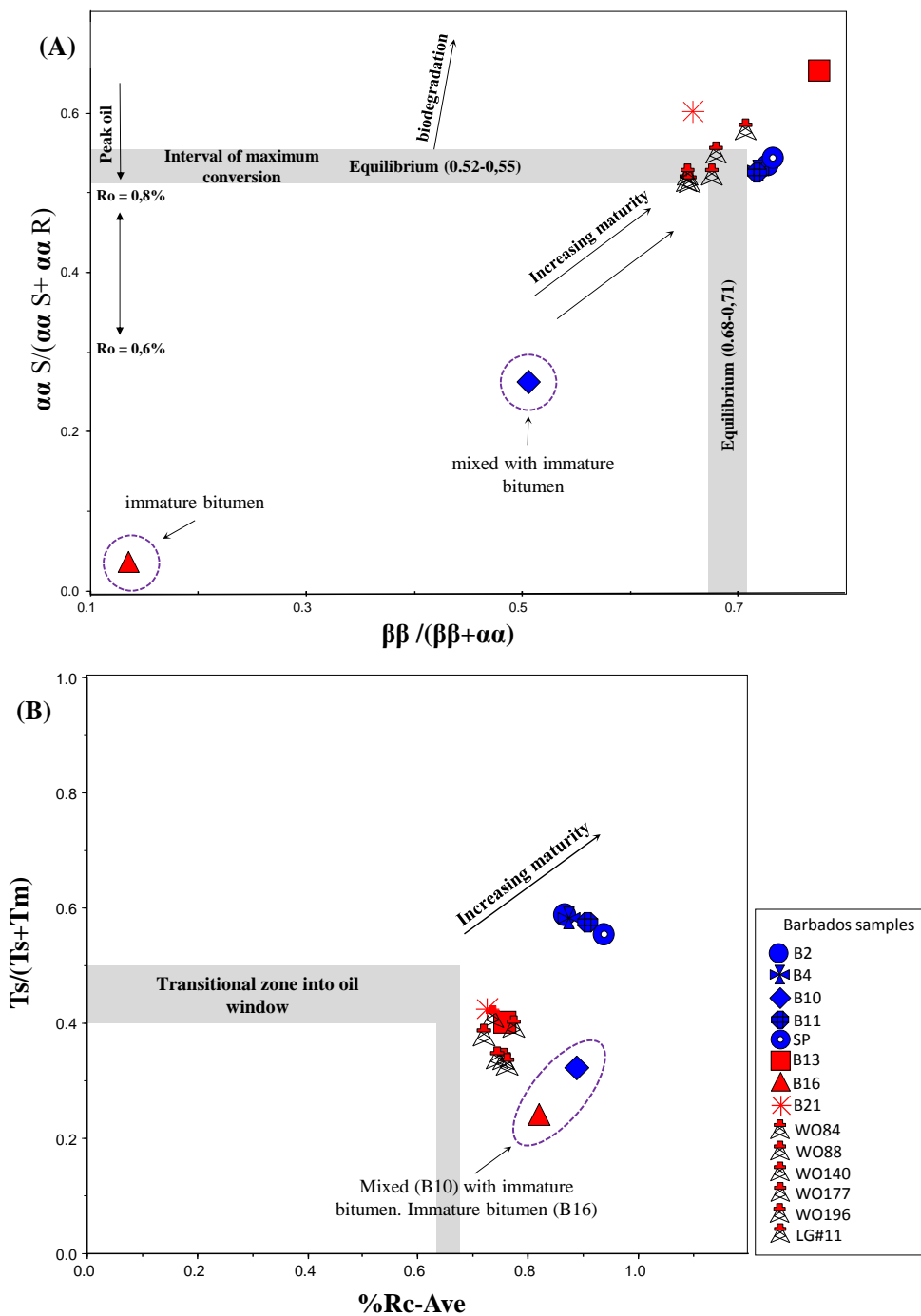
***Fig. 4.2.8.*** *Cross plots of maturity parameters using biomarkers and average vitrinite reflectances calculated from medium range aromatics showing the maturity variations of the analyzed samples.* ***A.*** *ββ/(ββαα) versus aaS/(ααS+αα R) C₂₉ steranes. The intervals of maximum conversion and equilibrium are indicated in accordance to Seifert and Moldovan, (1986).* ***B.*** *%Rc-Av versus Ts/(Ts+Tm) hopanes. The transition zone into the oil window is indicated. The low biomarker ratios for samples B10 and B16 are probably a result of mixing with immature bitumen. See Table 4.2.2 for aromatic and biomarker maturity parameters.*

**Table 4.2.3.** *GC-MS parameters used to determine the depositional environment, organofacies, and lithofacies of the analyzed samples.*

| Sample | Pr/n-C17 | Ph/n-C18 | Pr/Ph | Diast/Ster | C27–C28–C29 Steranes 27ββ % | 28ββ % | 29ββ % | C28/C29 | C30 Ster | 22/21 TT | 19/23 TT | 21/23 TT | 24/23 TT | C29/C30 | Tr/(Tr+C30) Hop | C35/C34 | Gam Ind. | MDBT conc. | 3-MP/4-MDBT |
|---|---|---|---|---|---|---|---|---|---|---|---|---|---|---|---|---|---|---|---|
| B2 | 2.82 | 1.97 | 1.54 | 0.76 | 34.46 | 32.64 | 32.90 | 0.90 | Yes | 0.24 | 0.09 | 0.58 | 0.96 | 0.49 | 0.75 | 0.61 | 0.08 | 2340837 | 2.51 |
| B4 | 11.59 | 16.38 | 1.28 | 0.75 | 33.17 | 33.65 | 33.18 | 0.90 | Yes | 0.27 | 0.08 | 0.54 | 0.98 | 0,54 | 0.76 | 0.55 | 0.08 | 1849969 | 2.37 |
| B10 | 10.97 | 15.06 | 1.15 | 0.50 | 32.23 | 33.92 | 33.86 | 0.71 | Yes | 0.23 | 0.11 | 0.57 | 0.83 | 0,65 | 0.57 | 0.68 | 0.10 | 1525556 | 2.53 |
| B11 | 1.73 | 0.88 | 1.51 | 0.76 | 33.32 | 34.42 | 32.26 | 0.95 | Yes | 0.27 | 0.10 | 0.58 | 1.05 | 0.49 | 0.76 | 0.55 | 0.08 | 586041 | 2.70 |
| SP | 7.09 | 9.79 | 1.56 | 0.79 | 34.53 | 34.58 | 30.89 | 1.01 | Yes | 0.25 | 0.12 | 0.60 | 0.97 | 0.52 | 0.79 | 0.62 | 0.08 | 376497 | 2.72 |
| B13 | 23.36 | 16.41 | 1.46 | 0.26 | 43.30 | 31.50 | 25.20 | 1.43 | No | 3.50 | 0.13 | 0.55 | 1.02 | 0.90 | 0.88 | 0.53 | 1.13 | 11073 | 3.49 |
| B16 | 1.95 | 2.09 | 1.20 | 0.02 | 23.57 | 23.24 | 53.20 | 0.38 | No | 0.15 | 0.31 | 1.63 | 1.07 | 0.35 | 0.09 | 1.52 | 0.09 | 89314 | 31.14 |
| B21 | 1.17 | 1.08 | 0.76 | 2.39 | 32.86 | 39.66 | 27.47 | 1.38 | Yes | 0.32 | 0.05 | 0.42 | 0.95 | 1.56 | 0.83 | 0.43 | 0.21 | 11140 | 4.45 |
| WO84 | 1.05 | 0.79 | 1.52 | 0.57 | 32.62 | 31.89 | 35.50 | 0.78 | Yes | 0.23 | 0.05 | 0.48 | 0.85 | 0.57 | 0.58 | 0.57 | 0.07 | 573739 | 1.17 |
| WO88 | 0.99 | 0.76 | 1.48 | 0.57 | 35.70 | 35.49 | 28.81 | 0.97 | Yes | 0.21 | 0.05 | 0.53 | 0.80 | 0.63 | 0.61 | 0.66 | 0.08 | 668376 | 1.31 |
| WO140 | 0.93 | 0.48 | 2.02 | 0.61 | 35.23 | 33.52 | 31.25 | 0.91 | Yes | 0.23 | 0.05 | 0.51 | 0.83 | 0.60 | 0.58 | 0.61 | 0.07 | 873603 | 1.15 |
| WO177 | 0.92 | 0.66 | 1.55 | 0.75 | 31.80 | 35.06 | 33.14 | 0.88 | Yes | 0.21 | 0.07 | 0.48 | 0.86 | 0.57 | 0.60 | 0.56 | 0.07 | 419246 | 1.46 |
| WO196 | 0.97 | 0.77 | 1.51 | 0.57 | 34.48 | 34.99 | 30.53 | 0.91 | Yes | 0.26 | 0.08 | 0.54 | 0.89 | 0.52 | 0.59 | 0.61 | 0.07 | 491441 | 1.35 |
| LG#11 | 3.40 | 4.59 | 1.32 | 0.61 | 34.94 | 34.02 | 31.03 | 0.91 | Yes | 0.24 | 0.06 | 0.54 | 0.87 | 0.59 | 0.60 | 0.62 | 0.07 | 909805 | 1.16 |

**Pr/n-C17:** pristane/n-heptadecane; **Ph/n-C18:** phytane/n-octadecane

**Pr/Ph:** pristane/phytane

**Diast./Ster**: diasteranes/(diasteranes + regular steranes);

**%27bbS** = 100 x $C_{27}\beta\beta S$ /($C_{27}\beta\beta S$ + $C_{28}\beta\beta S$ + $C_{29}\beta\beta S$); **%28bbS** = 100 x $C_{28}\beta\beta S$ / ($C_{27}\beta\beta S$ + $C_{28}\beta\beta S$ + $C_{29}\beta\beta S$)

**%29bbS** = 100 x $C_{29}\beta\beta S$ / ($C_{27}\beta\beta S$ + $C_{28}\beta\beta S$ + $C_{29}\beta\beta S$)

**$C_{28}/C_{29}$** = $C_{28}/C_{29}$ regular steranes

**C30:** C30 regular sterane

**23/21Tr**, **19/23 Tr**, **21/23Tr**, **24/23 Tr**; where Tr stands for tricyclic terpane

**$C_{29}/C_{30}$**: $C_{29}$ norhopane / C30 Hopane

**Tr/(Tr+$C_{30}$ Hop**: $C_{23}$-$C_{29}$Tr/($C_{23}$-$C_{29}$Tr+C30hop); where Tr stands for tricyclic terpane

**$C_{35}/C_{34}$**: $C_{35}$S/(S + R)/ $C_{34}$ +$C_{34}$ S/(S + R) homohopane

**Gam Ind.**: gammacerane/Hopane

**MDBT Conc.**: sum of 1, 2, 3, and 4 methyldibenzothiophenes

**3-MP/4-MDBT**: 3- methylphenanthrenes/4-methyldibenzothiophenes

of isomerization, supporting blending of immature bitumen with variables amounts of aromatic hydrocarbons.

Regarding maturity, the analyzed samples are classified into two groups. The first group comprises all the crude oils from the Woodbourne field and the extract from samples B13 (Bath beach), B16, and B21 (Barclays Park) with vitrinite reflectances (0.70% to 0.77%) corresponding to the early to mid-oil window. The second group includes the oil seepage (SP) and all the remaining extracts (B2, B4, B10) at the Shale Quarry having vitrinite reflectance values (0.87% to 0.94%) consistent with the peak of the oil window.

### 4.2.3. Organic facies assessment

The presence of C30 steranes is unequivocal evidence that the source rock contained marine algal organic matter (Moldowan, 1984) (Table 4.2.3). However, Pr/Ph ratios greater than one and the presence of n-alkanes above $C_{21}$ in the undegraded samples indicates a contribution of continental organic matter. The percentage of $C_{27}$, $C_{28}$, and $C_{29}$ regular steranes were calculated from peaks height of the m/z 218 GC-MS chromatographs (Fig. 4.2.5.) and their distribution is illustrated on a ternary plot (Fig. 4.2.9.A). The steranes distribution suggests that oils originated from a rock deposited in an environment with a mixture of marine planktonic and land-plant derived organic matter. Values slightly deviating for samples B13 and B21 are believed to be the consequence of severe biodegradation as previously discussed in this work. B16 plots as an outlier most probably due to the low maturity determined for this sample.

A closer examination of other biomarker parameters shows slight differences between the Woodbourne oils and the samples from the Shale Quarry area.

**C27, C28, and C29 regular steranes**

The average content of C27, C28, and C29 regular steranes for the Woodbourne oils are 34.60%, 34.16%, and 31.24% respectively and those of the Shale Quarry samples are 33.25%, 33.84%, and 32.91% respectively. Higher percentages of C27 over C29 steranes suggests predominant marine-derived organic matter for the Woodbourne oils. By contrast, the nearly
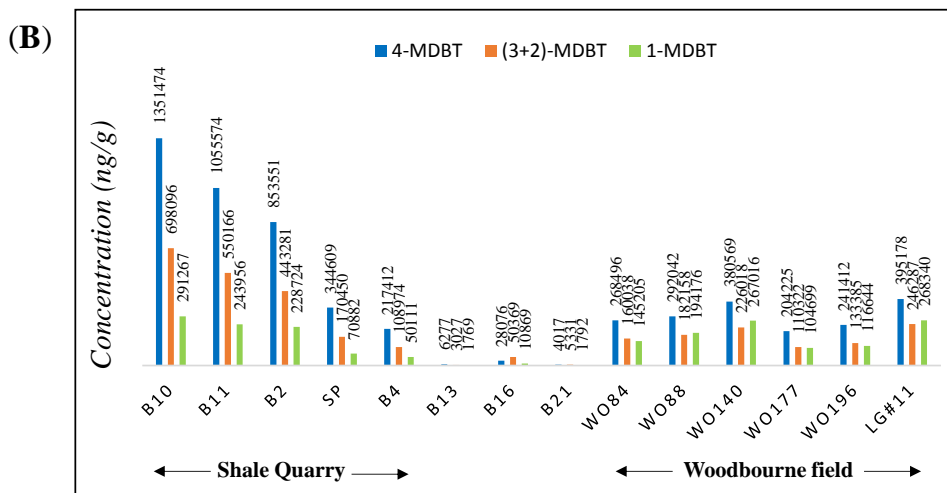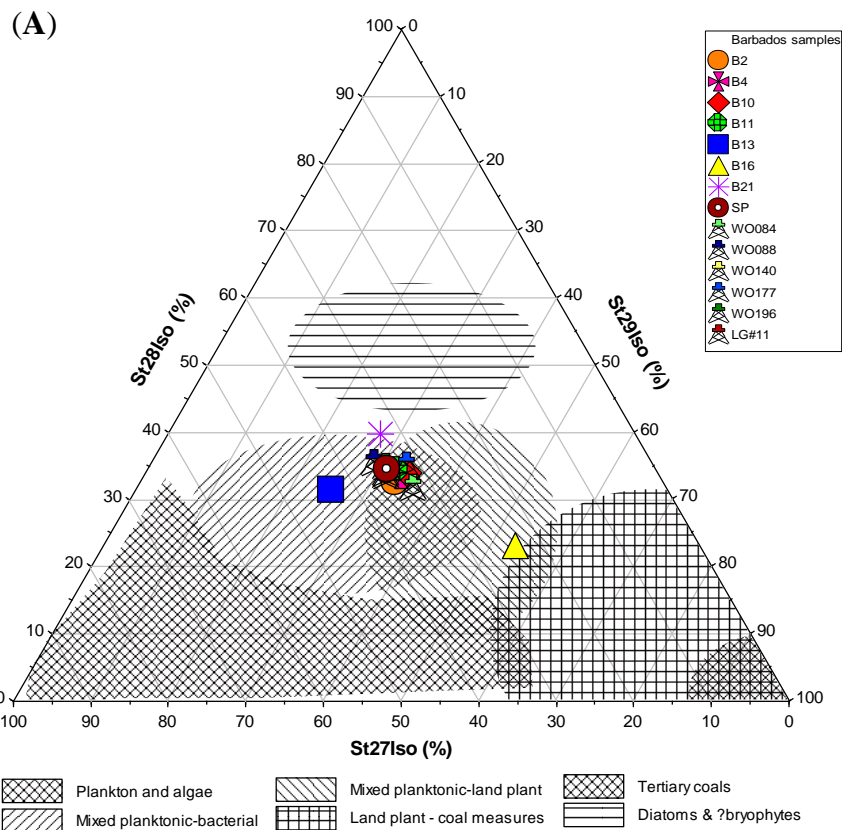
***Fig. 4.2.9. A.*** *Ternary plot of the C₂₇, C₂₈, and C₂₉ regular steranes from the 218m/z GC-MS fragmetograms showing organofacies of the Barbados samples; **B.** Histograms show the concentration of methyldibenzothiophene (MDBT) in the Barbados data set. Number represent the concentration of every compound measured in the 198 m/z fragmetograms. Samples from the Shale Quarry area have higher concentration of methyldibenzothiophenes indicating possible differences in the organic matter composition.*

54

identical percentages of C27, C28, and C29 steranes suggests an equal contribution of marine and land plant-derived organic matter for the extracts and the oil seepage from the Shale Quarry.

## $C_{19}/C_{23}$ tricyclic terpanes (TT)

The C23 tricyclic terpane is predominantly derived from algal and bacterial organic matter, while the C19 and C20 tricyclic diterpanes derive mainly from higher plants with C19 as the predominant compound (Simoneit, 1977; Alberdi et al., 2001). Therefore, oils generated from source rocks containing significant amounts of land plants-derived organic matter show high C19/C23 tricyclic terpane ratios. By contrast, oils derived from algal organic matter show low C19/C23 tricyclic terpane ratios. The C19/C23 ratio ranges between 0.05 and 0.08 for the oils from the Woodbourne oil field, while the corresponding ratio for the extracts and oil seepage from the Shale Quarry area range between 0.08 and 0.12 (Table 4.2.3). This difference in the C19/C23 supports slightly higher content of higher plants-derived organic matter in the rock sourcing the oils from the Shale Quarry area.

## C23-C29Tr/(C23-C29Tr+C30hop)

The C23-C29Tr/(C23-C29Tr+C30hop) ratio is used to differentiate oils over a wide range of maturities due to the high thermal stability and resistance to biodegradation of the tricyclic terpanes (Peters and Moldovan, 1993). The C23-C29Tr/(C23-C29Tr+C30hop) ratio for the Woodbourne oils ranges between 0.58 and 0.61, and between 0.75 and 0.79 for the Shale Quarry extracts and oil seepage (Table 4.2.3). This difference is also believed to result from variations in the organic matter sourcing the Shale Quarry oils. Corresponding ratios for extracts from samples B10, B13, B16, and B21 are not considered due to either mixing with immature bitumen (B10 and B16) or biodegradation (B13 and B21).

## Methyldibenzothiophenes (MDBT's) concentration

Thermal maturity is believed to cause redistribution of these compounds, namely, the relative concentration of 4-MDBT increases with higher maturity, while the concentration of 1-MDBT decreases (Radke, 1988). Regardless of the thermal effects, the total concentration of

MDBT's is higher in the extracts from the Shale Quarry area (Table 4.2.3. and Fig 4.2.9.B) which may imply origin from a source rock that allows more sulfur rich molecules to be expelled. Biodegradation is also known to increase the relative concentration of sulfur in degraded oils. Extracts from the Shale Quarry seem to have experienced similar levels of degradation as the WO140 and LG#11F oils from the Woodbourne field, which are therefore expected to have high MDBT's. However, concentration of these compounds in the two degraded oils is still low and similar to those concentrations in the undegraded oils (Fig 4.2.9.B). Thus, biodegradation may be ruled out as a possible reason for increased sulfur content in the Barbados oils. These observations indicate that higher MDBT's concentration in the Shale Quarry extracts may certainly represent differences in the source rock.

**3-MP/4-MDBT**

The relative proportion of 3-MP to 4-MDBT varies from 2.37 to 2.72 for extracts and oil seepage from the Shale Quarry area and between 1.15 and 1.86 for oils from the Woodbourne oil field (Table 4.2.3.). These facts may also suggest variations in the organic matter composition of the rock sourcing these two areas. Alternatively, fractionation during migration and thermal stress could lead to the observed differences in the concentration of medium range aromatics.

### 4.2.4. Depositional environment assessment

There is an appreciable higher abundance of $C_{23}$ and $C_{24}$ tricyclic terpanes (TT) compared to other tricyclic homologs in the m/z 191 fragmetograms (Fig. 4.2.3.); thus, the $C_{24}/ C_{23}$ TT ratios show values (0.80 to 1.07) indicative of oils derived from organic matter accumulated in a shale-rich environment (Waples and Machihara, 1991). The $C_{29}$ hopane abundance is about half that of $C_{30}$ hopane yielding $C_{29}/C_{30}$ ratios of 0.49 to 0.63, which are typical values of shale-sourced oils (Peters and Moldowan, 1993). Sample B13 and B21 show deviating values of 0,9 and 1,56 respectively, suggesting hopanes biodegradation. Finally, the shale source interpretation is supported by $C_{22}/C_{21}$ tricyclic terpane ratios of about 0.15 to 0.31for all samples. Zumberge (1984), noted that the $C_{22}/C_{21}$ tricyclic terpane ratios for oils generated from shaly facies is commonly less than 0.5,

while for oils generated from carbonate facies the $C_{22}/C_{21}$ ratio is 0.5 or greater. Table 4.2.3 summarizes the above listed parameters.

Diasteranes/steranes ratios are amply used to distinguish petroleum derived from carbonate or clastic source rocks (Mello et al., 1988b). High diasteranes/steranes ratios are typical of petroleum derived from clay-rich source rocks (Rubinstein et al., 1975; Sieskind et al., 1979), whereas low diasteranes/steranes ratios are indicative of petroleum derived from a clay-poor source rock (Hughes, 1984; Mello et al., 1988a,b). Alternatively, oxic (High Eh) and acidic (Low Ph) conditions favor diasteranes formation during diagenesis (Moldowan et al., 1986; Brincant and Abbott, 2001). Although it is also clear that maturation effects may enrich the disteranes compared to regular steranes (Moldovan et al., 1986) in the higher mature extracts and oil seepage from the Shale Quarry, source rocks effects cannot be ruled out. The diasteranes/steranes ratios for the Barbados data set varies from to 0.50 to 0.76, typical values for petroleum derived from siliciclastic sediments deposited in oxic and acidic environments.

Despite the microbial degradation of some crude oils, the seepage and the extracts, it is still possible to calculate the most common acyclic isoprenoid parameter (Pr/Ph) used for organofacies assessment. Pr/Ph ratios between 0.75 and 2, together with very low MDBTs/MPs (0.09 to 0.36) ratios plotted in Fig. 4.2.10.A indicate that the organic matter was accumulated in a marine oxic setting (Hughes et al., 1995).

Gammacerane is interpreted to indicate stratification of the water column, commonly resulting from hypersalinity at depth (Damste et al., 1995). Additionally, high concentrations of this compound are indicative of highly reducing, hypersaline conditions during source rock sedimentation (Moldowan et al., 1985). The gammacerane index of the analyzed samples is low (0.07 to 0.1; Table 4.2.3), suggesting normal salinity conditions during the deposition of the shale lithofacies. Biodegradation is believed to account for the increased gammacerane index in samples B21 and B13 (0.2 and 1.12 respectively), and therefore these two values are not an indicator of hypersalinity.

The C35/C34 homohopane ratio can be used to define the redox potential of source facies of oils. Values of $C_{35}/C_{34}$ ratio lower than 1 are interpreted to indicate deposition under oxic to dysoxic conditions, while $C_{35}/C_{34}$ ratios greater than 1 are distinctive of source rock deposition under
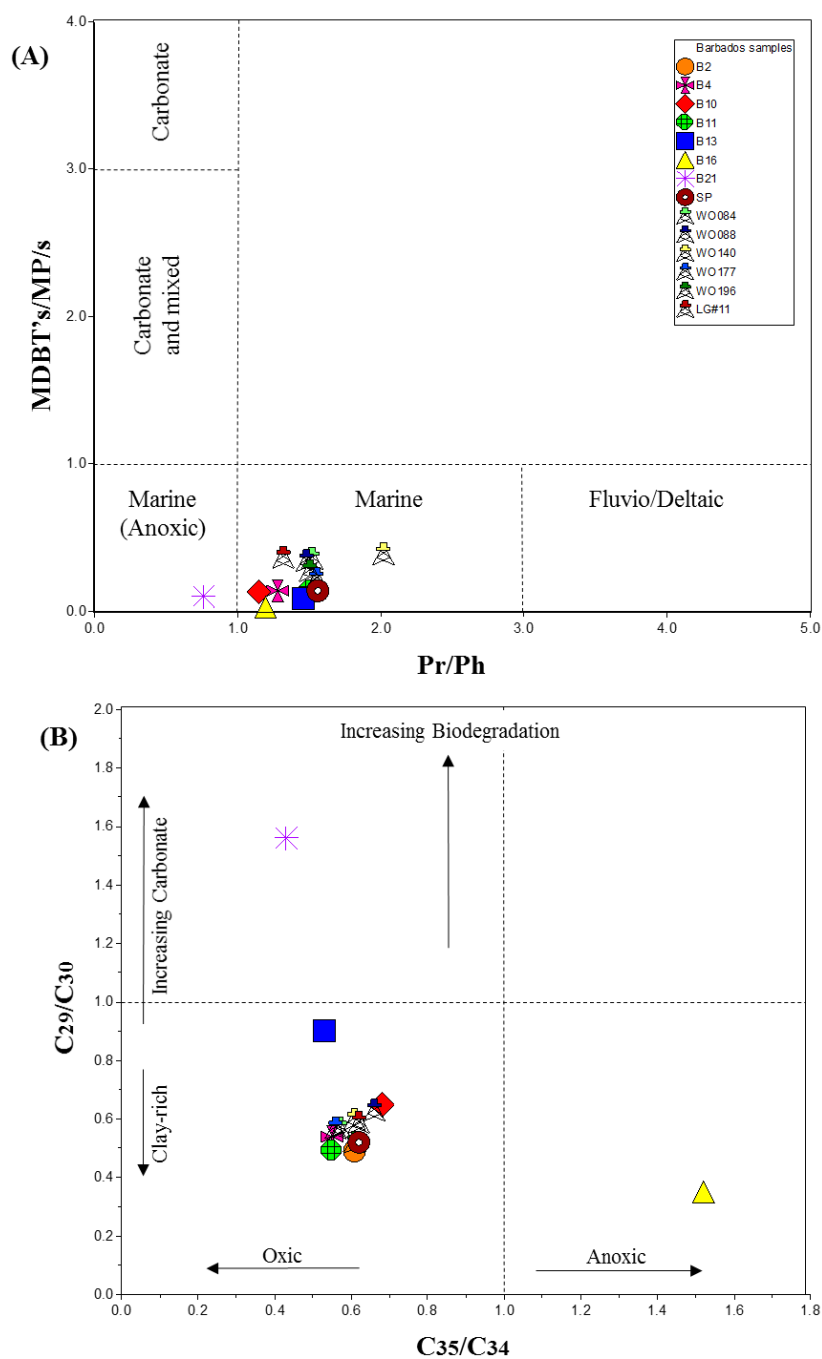
***Fig. 4.2.10.*** *Cross-plots of facies parameters.* ***A.*** *Plot of pristane/phytane (Pr/Ph) versus the ratio of the sum of methyl-dibenzothiophenes to the sum of methyl-phenanthrenes (MDBT/MP) (modified from Hughes et al., 1995);* ***B.*** *$C_{35}/C_{34}$ hopane ratio versus $C_{29}/C_{30}$ hopane ratio for the Barbados samples set. The $C_{35}/C_{34}$ hopane ratio of 1 for distinguishing between dysoxic and anoxic conditions is proposed by Peters and Moldowan, (1991). The $C_{29}/C_{30}$ hopane ratio of 1 for distinguishing between clay-rich and carbonate lithologies is after (Peters and Moldowan, 1993). See Table 4.2.3 for CG-MS calculated parameters used in this plot.*

anoxic conditions (Peters and Moldowan, 1991). The $C_{35}/C_{34}$ homohopane ratio for all the Barbados samples ranges between 0.43 and 0.66 (Table 4.2.3), indicating oxic to dysoxic conditions for the source rock facies generating these oils. The deviating value of 1.54 for sample B16 may be related to the low maturity of this sample. Fig. 4.2.10.B cross-plots red-ox conditions versus lithofacies for the sample set. It supports that the source rock generating the Barbados oils is a shale-rich unit deposited under oxic to dysoxic conditions.

In summary, it is reasonable to assume that all the petroleum in the analyzed samples was sourced by marine shale lithofacies deposited within a paleo-environment dominated by oxic-to-dysoxic, acidic, and normal salinity conditions, in which marine algal and planktonic organic matter dominate with varying contribution of land plants-derived organic matter. The suggested environment corresponds to an outer shelf setting, in which slight variations in distal/proximal locations and proximity to paleo-river input, controls variations in oxygen content and the amount of marine relative to continental-derived organic matter.

The majority of parameters used in these sections appear to be outliers for the extract from sample B16, which is most likely caused by the dominant presence of immature bitumen in the extractable organic matter (EOM). The Rock-Eval pyrolysis data indicates this sample contains terrestrial-derived type III kerogen with fairly low hydrogen index (HI) of 121(mg HC/g TOC) (Fig. 4.1.1.) at a $T_{max}$ of 426. The interpreted organofacies are consistent with continental-derived organic matter brought to deep marine environments by turbiditic currents as proposed by Chaderton, (2005) for the blackish, fine-grained beds of the Scotland group, where sample B16 was collected.

**Table 4.2.4.** *Transformation (TR) and correlation (C) ratios for the Woodbourne oil samples as defined by Halpern (1995).*

| Sample | Tr1 | Tr2 | Tr3 | Tr4 | Tr5 | Tr6 | Tr7 | C1 | C2 | C3 | C4 | C5 |
|--------|-----|-----|-----|-----|-----|-----|-----|-----|-----|-----|-----|-----|
| WO84 | 0.33 | 8.77 | 4.37 | 3.25 | 7.62 | 2.19 | 2.74 | 0.06 | 0.56 | 0.19 | 0.05 | 0.14 |
| WO88 | 2.33 | 10.06 | 4.76 | 3.68 | 8.43 | 2.25 | 2.95 | 0.07 | 0.55 | 0.19 | 0.06 | 0.13 |
| WO140 | 1.51 | 2.45 | 3.55 | 1.58 | 5.12 | 0.86 | 1.34 | 0.05 | 0.56 | 0.16 | 0.04 | 0.18 |
| WO177 | 3.92 | 10.73 | 4.48 | 3.49 | 7.97 | 1.92 | 2.93 | 0.07 | 0.55 | 0.18 | 0.07 | 0.12 |
| WO196 | 4.61 | 12.18 | 4.39 | 3.07 | 7.46 | 2.23 | 3.13 | 0.05 | 0.59 | 0.16 | 0.05 | 0.15 |
| LG#11 | 2.67 | 10.25 | 4.69 | 3.47 | 8.17 | 2.17 | 2.79 | 0.06 | 0.57 | 0.19 | 0.05 | 0.14 |
| SP | 2.15 | 8925,40 | 5.72 | 2.9 | 8.63 | 1.21 | 0.13 | 0.96 | 0.02 | 0 | 0 | 0.01 |

**Tr1:** Toluene/1,1-dimethylcyclopentane; **Tr2:** n-C7/1,1-dimethylcyclopentane; **Tr3:** 3-methylhexane/1,1-dimethylcyclopentane; **Tr4:** 2-methylhexane/1,1-dimethylcyclopentane; **Tr5:** P2*/1,1-dimethylcyclopentane; **Tr6:** 1-t-3-dimethylcyclopentane/1,1-dimethylcyclopentane; **Tr7:** P2/P3**; **C1:** 2,2-dimethylpentane/P3; **C2:** 2,3-dimethylpentane/P3; **C3:** 2,4-dimethylpentane/P3; **C4:** 3,3-dimethylpentane/P3; **C5:** 3-ethylpentane/P3. * P2 = 2-methylhexane + 3-methylhexane; ** P3 = 2,2-dimethylpentane + 2,3-dimethylpentane + 2,4-dimethylpentane + 3,3-dimethylpentane + 3-ethylpentane.

**Table 4.2.5.** *Calculated gasoline compositional ratios for the Woodbourne oil samples as defined by Thompson (1983).*

| Sample | A | B | X | W | C | I | F | H | U | R | S |
|--------|---|---|---|---|---|---|---|---|---|---|---|
| WO84 | 0.08 | 0.04 | 0.31 | 1.53 | 1.01 | 0.91 | 0.71 | 21.49 | 0.74 | 2.7 | 39.69 |
| WO88 | 0.11 | 0.23 | 0.44 | 1.82 | 0.93 | 0.96 | 0.68 | 21.49 | 0.82 | 2.74 | 40.43 |
| WO140 | 0.27 | 0.62 | 0.44 | 17.35 | 3.61 | 2.32 | 2.49 | 16.22 | 0.61 | 1.55 | 27.79 |
| WO177 | 0.14 | 0.37 | 0.56 | 1.65 | 0.71 | 1.06 | 0.59 | 21.8 | 1.1 | 3.08 | 30.92 |
| WO196 | 0.09 | 0.38 | 0.44 | 1.24 | 0.74 | 0.86 | 0.63 | 23.91 | 0.9 | 3.97 | 99.75 |
| LG#11 | 0.07 | 0.26 | 0.34 | 1.4 | 1.08 | 0.94 | 0.79 | 23.5 | 0.74 | 2.95 | 47.14 |
| SP | 0 | 0.87 | 0.34 | 302.4 | 1.91 | 459.15 | 99.52 | 0.17 | 3074.0 | 0 | 0 |

**A:** Benz/n-C6; **B:** Tol/n-C7; **X:** m+p-Xyl/n-C8; **W:** Benz*10/CyC6; **C:** (n-C6+n-C7)/(CyC6+MCyC6); **I:** (Isoheptane value) (2-MC6+3-MC6)/(c1,3-DMCyC5+t1,3-DMCyC5+t1,2-DMCyC5); **F:** n-C7/MCyC6; **H:** (Isoheptane value) n-C7*100/(CyC6+2-MC6+3-MC6+c1,3-DMCyC5+t1,3-DMCyC5+t1,2-DMCyC5+n-C7+MCyC6); **U:** CyC6/MCyC5; **R:** n-C7/2-MC6; **S:** n-C6/2,2-DMC4.

### 4.2.5. Light fraction

#### 4.2.5.1. Water washing

An essential aspect of the Woodbourne produced oils is the relatively low concentration of toluene, which together with moderately low benzene and xylene and low concentration of aromatics in the $C_{10+}$ fraction, suggests partial removal of aromatic hydrocarbons due to water washing. Fig. 4.2.11. presents a cross-plot of Benz/CyC6 versus Tol/MCyC6 confirming significant water washing in samples WO84, WO88, WO170, WO196, and LG#11 from the Woodbourne field and the oil seepage (SP). Oppositely, sample WO140 plots in the upper right corner as a heavily biodegraded oil. Additionally, the C7 transformation star diagram (C7-OTSD) (Fig. 4.2.12.) shows that all the Woodbourne oils and the oil seepage have reduced Tr1 (toluene/1,1-dimethylcyclopentane ratio) (Table 4.2.4) which further suggests water washing as toluene is the most water-soluble $C_7$ compound (Halpern, 1995).
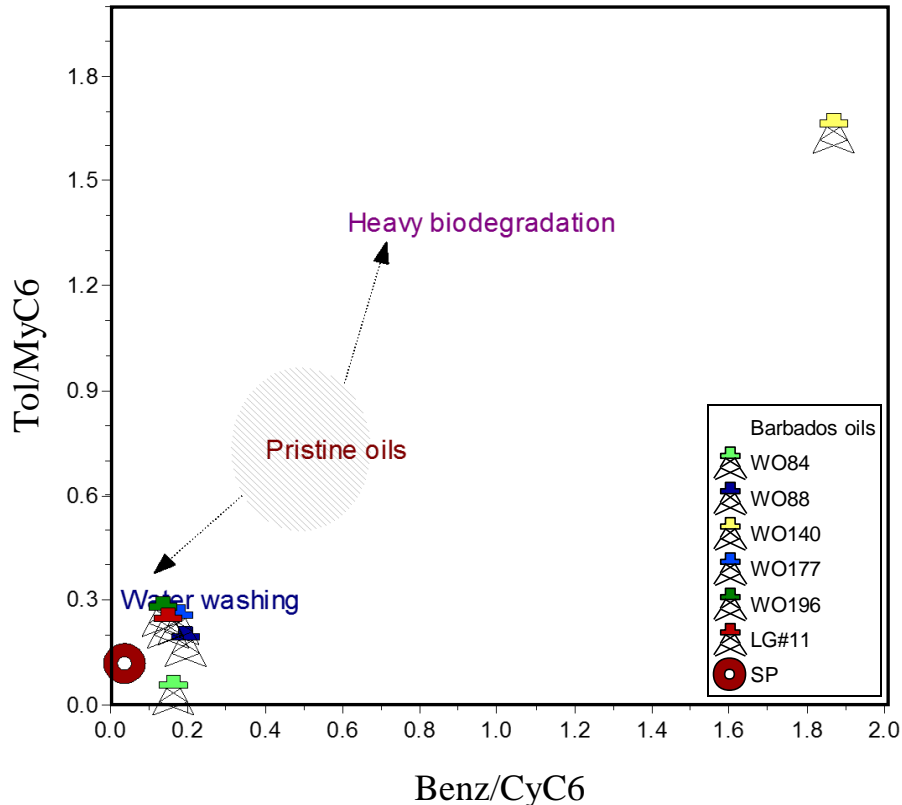


***Fig. 4.2.11.** Benzene/Cyclohexene versus Toluene/Methyl cyclohexene cross-plot indicating water washing effects for samples WO84, WO88, WO177, WO196, LG#11, and oil seepage (SP), and heavy biodegradation for the oil sample WO140.*

On the C7 transformation star diagram (C7-OTSD) (Fig. 4.2.12.) all the Barbados oils show approximately the same degree of transformation, except for sample WO140 which has undergone higher transformation. In addition, the seepage (SP) shows evidence of dramatic transformation particularly manifested by an utterly high value of Tr2 value of 8925,40 (Table 4.2.4). The moderately low contents of aromatic hydrocarbons due to water washing seems to confirm that biodegradation of the light fraction in the Woodbourne oil field is associated to circulation of superficial, meteoric waters.

### 4.2.5.2. Maturity and facies assessment

The n-Hep/mcHX and n-Hep ratios were proposed to assess paraffinicity properties as indicators of increasing maturity (Thompson, 1983). The cross-plot of n-Hep/mcHX (F) versus n-Hep (H) ratios (Fig. 4.2.13.A) shows that five out of the six oils from the Woodbourne field are classified as Normal oils in terms of maturity having average values of 0.6 and 21 respectively (Table 4.2.5). The determined maturity is equivalent to vitrinite reflectance levels of approximately 0.86-1.05 (Thompson, 1983). The WO140 sample plot as an outlier and is believed to be due to biodegradation of this sample.

Thompson (1983), also suggested the use of n-Heptane (H) together with the Isoheptane (I) ratio to evaluate source rock types. The calculated concentrations of these two parameters are cross-plotted in Fig. 4.2.13.B indicating an aliphatic, type II kerogen source rock for five of the samples. The oil sample WO140 has a much higher Isoheptane (I) ratio compared to the other samples and plots as an aromatic type III kerogen. However, the C7 correlation star diagram (C7-OCSD) (Fig. 4.2.14.) clearly shows that the samples are nearly identical, supporting that all the light fractions are sourced from the same organofacies. It is however important to highlight that the seepage (SP) is not plotted along with the other samples in Fig. 4.2.14. due to the previously stablished transformation and the total absence of correlation parameters C3 and C4 (Table 4.2.4.).
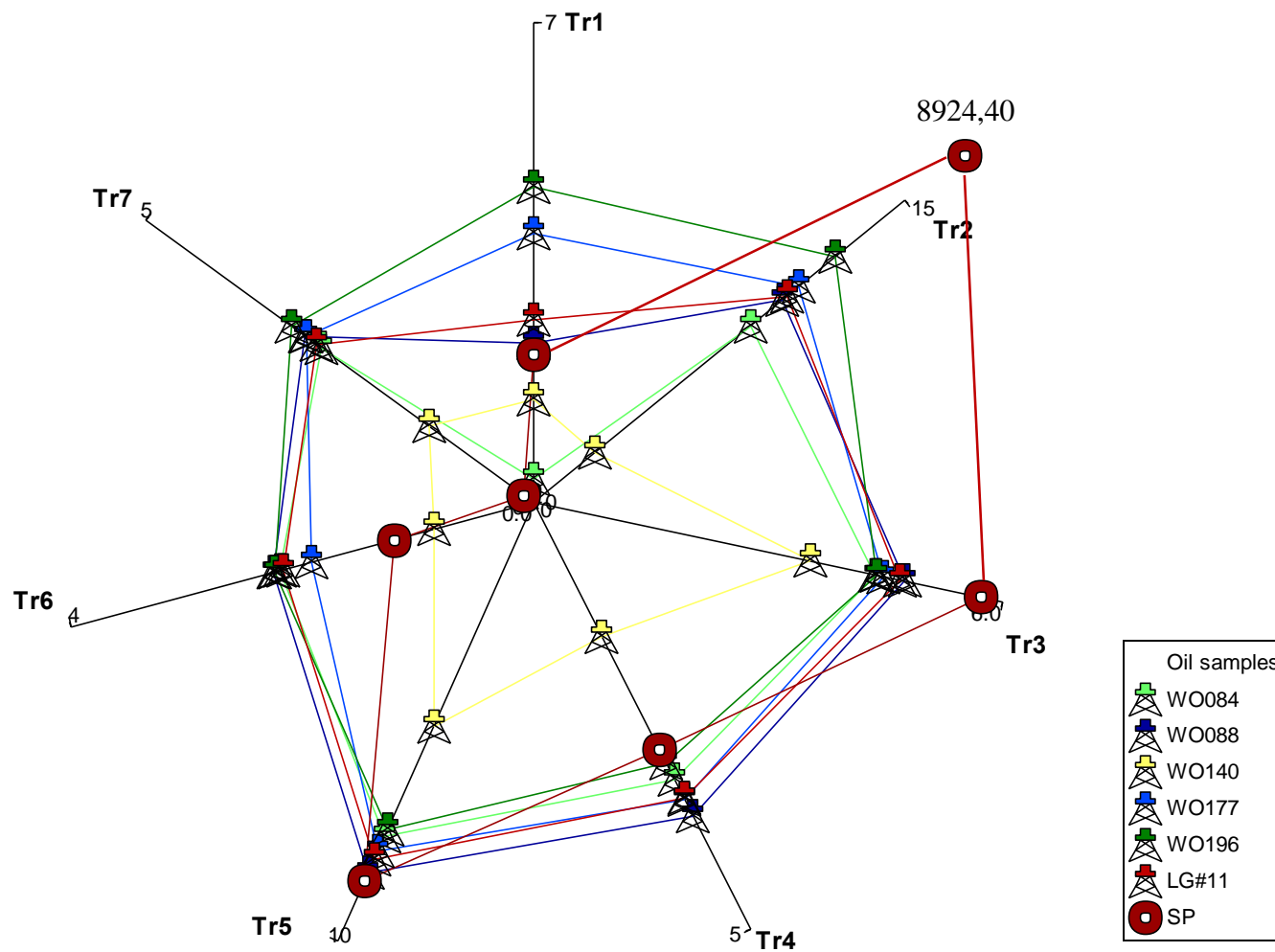
**Fig. 4.2.12.** *Halpern transformation star diagram for oil samples from the Woodbourne oil field and the oil seepage (SP) from the Shale Quarry. Samples WO84, WO88, WO177, WO196, LG#11 show nearly identical pattern suggesting that they have experiences similar degrees of alteration, if any. Samples WO140 and SP are outliers and are interpreted to have undergone severe alteration (water washing and biodegradation). See Table 4.2.4 for plotted values.*

63
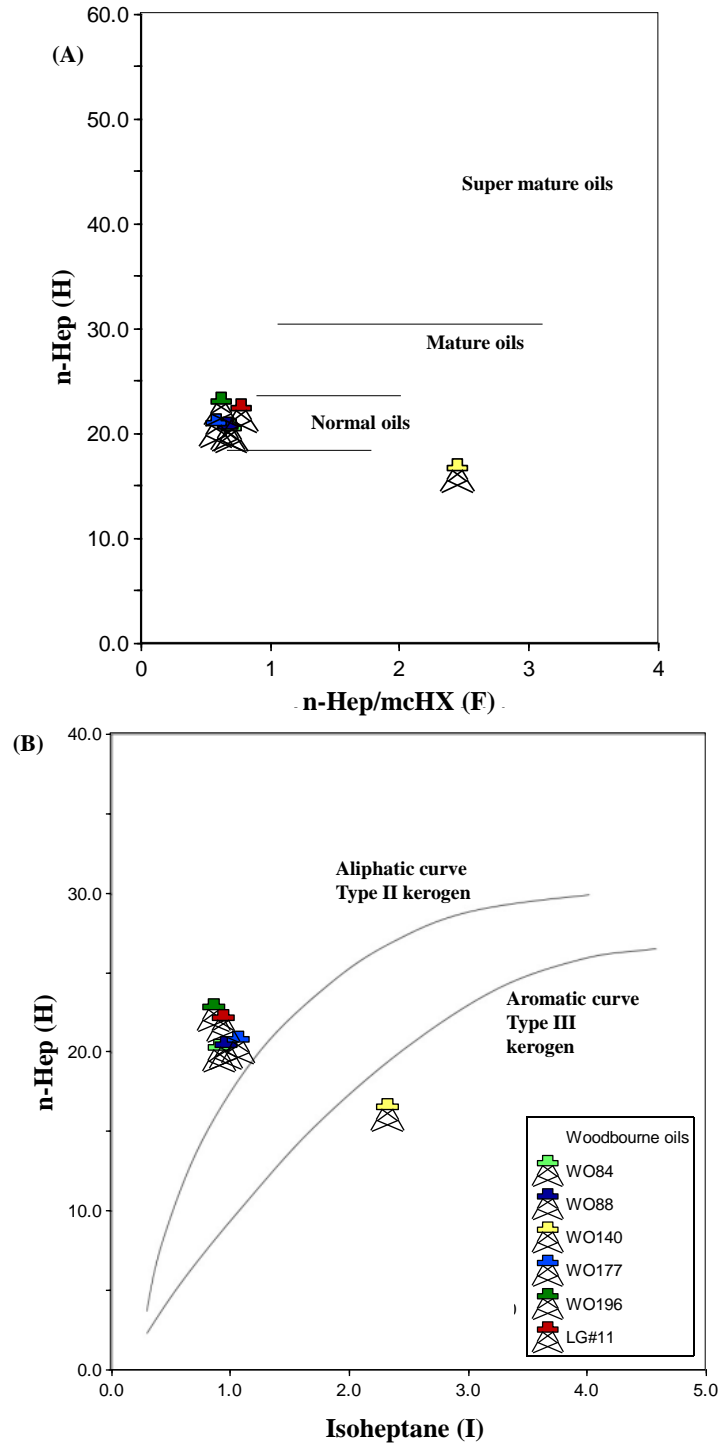
***Fig. 4.2.13.*** *Determination of oil maturity and kerogen type contained in the rock sourcing the Woodbourne oils based on Thomson parameters (Thomson, 1983).* ***A.*** *n-Hep/mcHX (F) versus n-Hep (H) for assessing oil maturity;* ***B.*** *Isoheptane (I) versus n-Hep (H) for determining kerogen type. The oil seepage sample (SP) is not plotted due to heavy transformation of this sample. See Table 4.2.5 for plotted values.*
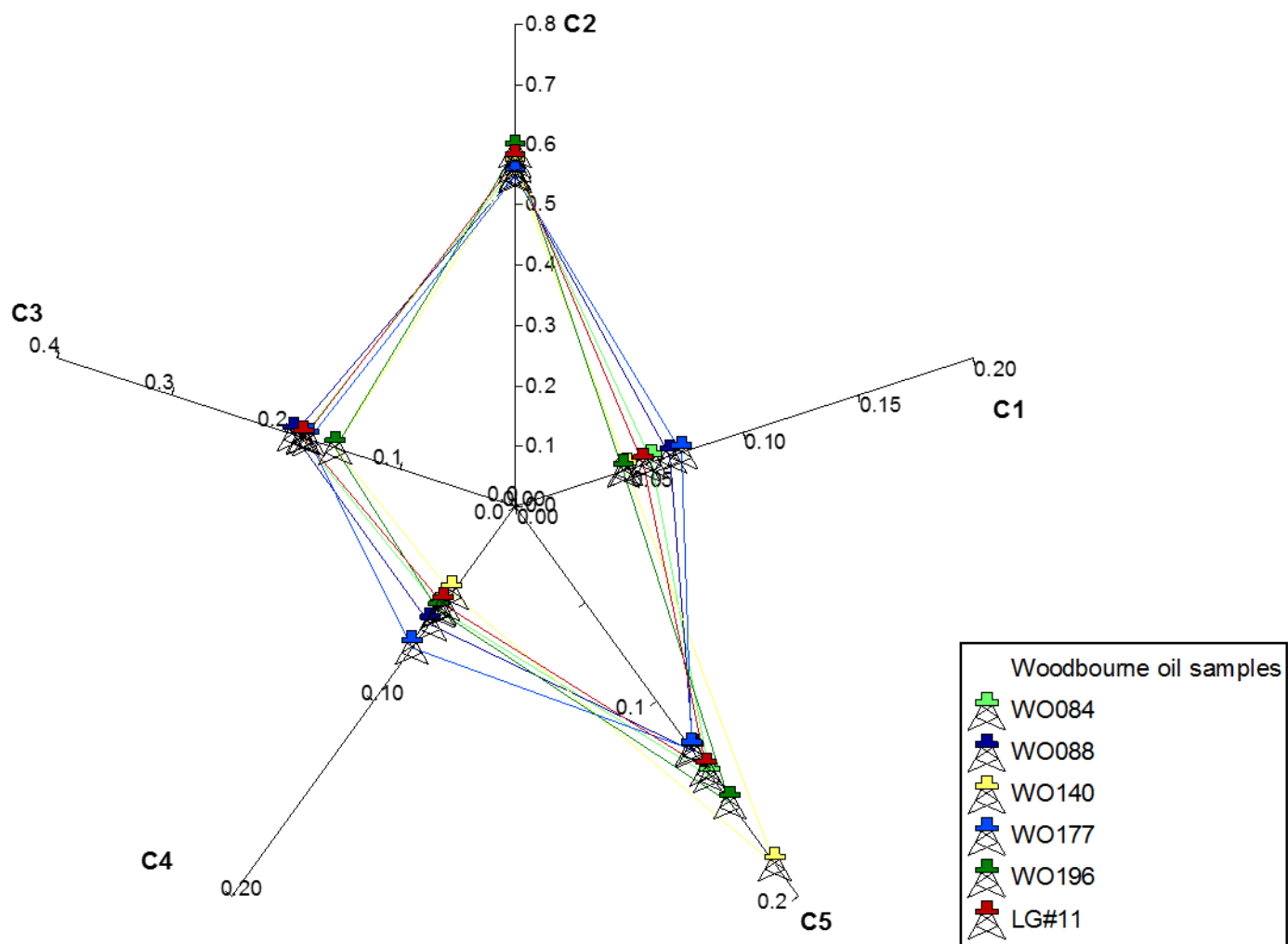
***Fig. 4.2.14.*** *Halpern correlation star diagram for oil samples from the Woodbourne oil field showing nearly identical pattern for all samples, suggesting that all the light fractions are sourced from the same organofacies. See Table 4.2.4 for plotted values.*

### 4.2.5.3.  Correlation

It is unclear whether the light fraction in the undegraded oils below 1000 meters (WO84, WO88, WO177, WO196) is 1- preserved from the first charging event or 2- represents a later charge event as occurs in oils above 1000 meter (WO144 and LG#11). 3- An alternative scenario considers a mixture of light fractions partially preserved from the initial oil blended with a second pulse of very light, fresh hydrocarbons.
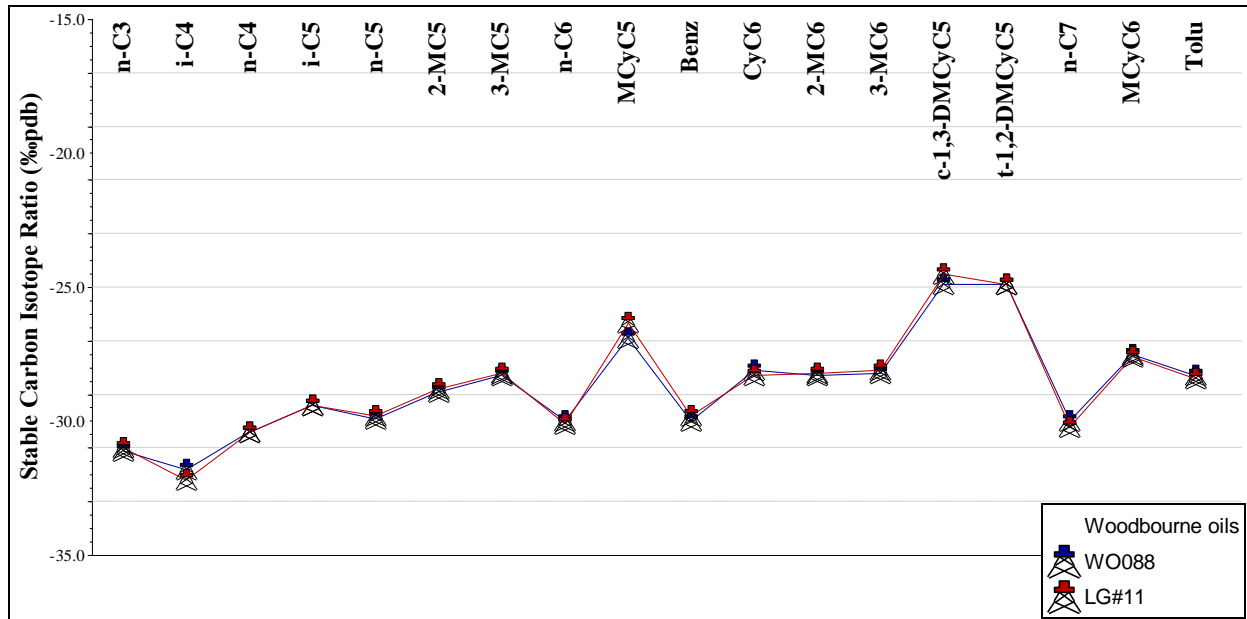


***Fig. 4.2.15****. Compound specific isotope profile for a representative fresh oil (WO88) and a degraded oil (LG#11) from the Woodbourne oil field. Similar isotopic distribution profiles suggest that the light fractions are similar and have the same origin.*

Compound specific isotope analysis of the light fraction from a fresh oil (WO88; undegraded >1000m) and from a degraded oil (LG#11; degraded <1000m) (Fig.4.2.1) are presented in Fig. 4.2.15. The d13C are seen to be nearly identical between the two samples. This suggests that there is a present ongoing charge of the light fraction to the shallower and biodegraded Woodbourne oils. The similar maturity of the light fraction and the heavier (Fig. 4.2.13A and 4.2.8) suggests that they have the same origin, and support that the light charge to the Woodbourne oils is a result of leakage from deeper reservoirs. This also hints on a deeper buried oil accumulation below 1800 meters.

### 4.2.6. Age of the source rock

The sterane distribution from Barbados oils was used to determine the source rock age (Fig. 4.2.16.). Grantham and Wakefield (1988) showed that the $C_{28}/C_{29}$ sterane ratio of organic matter increased as a function of decreasing geologic age. They reported values of <0.5 for oils of Early Paleozoic and older ages; 0.4-0.7 for Late Paleozoic to Early Jurassic oils; and values of >0.7 for Late Jurassic to Miocene oils. The $C_{28}/C_{29}$ sterane ratios for the Barbados oils, oil seepage, and extracts that are not affected by severe biodegradation range between 0.87 and 1.13, and are interpreted to have been sourced by an Upper Cretaceous-aged source (Fig. 4.2.16.).
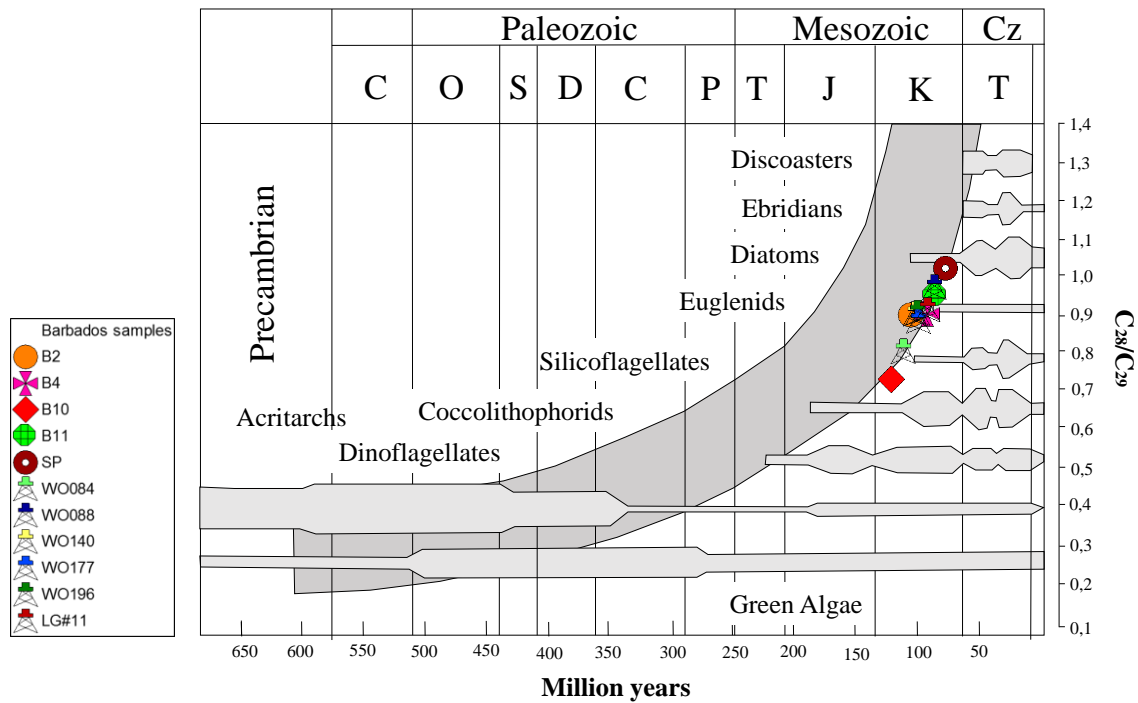


*Fig. 4.2.16. Determination of source rock age based on $C_{28}/C_{29}$ steranes (Grantham and Wakefield, 1988) indicating Cretaceous age for the Barbados samples. Samples B13 and B21, and B16 are not plotted due to biodegradation of steranes or low isomerization values respectively.*
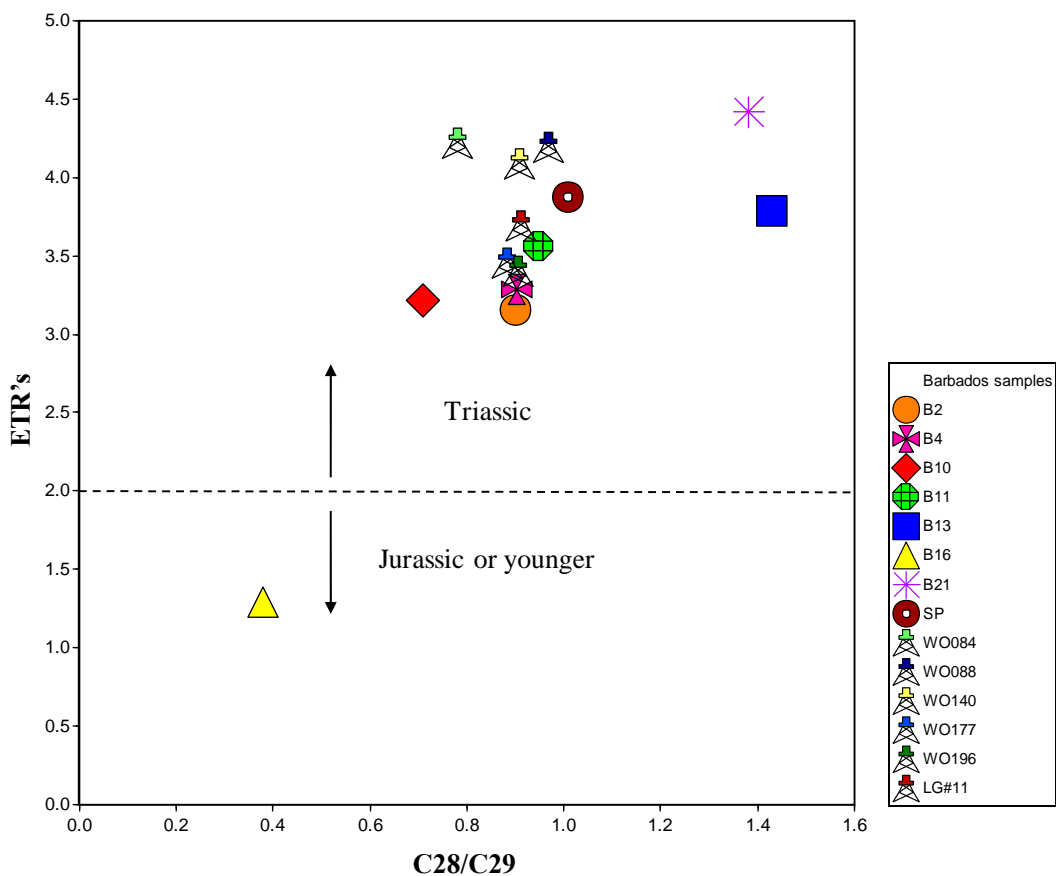
***Fig. 4.2.17.*** *Determination of source rock age based on extended tricyclic triterpanes (ETR's) (Holba et al., 2001) indicating Triassic or older age for the Barbados data set. The extract from Sample B16 plots as a Jurassic or younger source. This is consistent with the Paleogene age of the rock sample, but may be also a result of the immaturity of this sample.*

Extended tricyclic terpane ratios (ETR's) ($C_{28}+C_{29}$ tricyclic/Ts) have been described to differentiate between Triassic (>2) and Jurassic or younger (< 2) source rocks (Holba et al., 2001). Holba linked the increased value to diatom bloom in connection to upwelling in the Triassic. The elevated ETR's (>2) for the Barbados oils suggest a Triassic or older aged source rock

The current geological knowledge of the Caribbean region, however, does not refer to any sedimentary rock of Triassic or older age that could account for those oils. This anomalously high ETR's may instead be related to a diatom (rhizosolenid) bloom which occurred in the Caribbean region at about 91.5±1.5 million years during the Upper Turonian. This event may have had an impact on the biological sources of terpanes (Damsté et al., 2004). The extract from Sample B16 plots anomalously to the rest of the data set with lower RTR's. This is an organic rich sample shale sample (Table 4.1.1) of Paleogene age.

### 4.2.7. Identification of petroleum groups

In summary, all the petroleum in the analyzed samples was sourced by Upper Cretaceous, marine shale lithofacies deposited within a paleo-environment dominated by oxic to dysoxic, acidic, and normal salinity conditions. However, this petroleum can be subdivided into two groups based on subtle heterogeneities in organic facies and maturity: Group A (Woodbourne oils) and Group B (Shale Quarry) (Fig. 4.2.18.). A third group (Group C) consists of samples that are extensively biodegraded or mixed with immature bitumen, and therefore petroleum in those samples cannot be classified in any of the other groups. Table 4.2.6 summarizes the parameters used to distinguish between these three groups.

*Table 4.2.6. Ranges of organofacies-related parameters, maturity, and biodegradation used for identifying different petroleum groups.*

| Parameter | Group A | | Group B | | Group C | |
|---|---|---|---|---|---|---|
| | Min | Max | Min | Max | Min | Max |
| $\%C_{27}$ | 31.8 | 35.7 | 33.17 | 34.3 | 23.57 | 43.30 |
| $\%C_{28}$ | 31.89 | 35.06 | 32.64 | 34.58 | 23.24 | 53.20 |
| $\%C_{29}$ | 28.81 | 35.5 | 30.89 | 33.86 | 25.20 | 53.20 |
| $C_{19}/C_{23}$ Tr | 0.05 | 0.08 | 0.08 | 0.12 | 0.05 | 0.31 |
| $C_{23}$-$C_{29}$Tr/($C_{23}$-$C_{29}$Tr/C30hop) | 0.58 | 0.61 | 0.75 | 0.79 | 0.09 | 0.83 |
| MDBT's height | Low | Low | High | High | - | - |
| 3-MP/4-MDTB | 1.15 | 1.86 | 2.37 | 2.72 | 3.49 | 31.14 |
| %Rc-Ave | 0.72 | 0.77 | 0.87 | 0.94 | 0.7 | 0.74 |
| Biodegradation (PM scale) | 0 | 5 | 2 | 5 | 6 | 8 |

PM= Peter and Moldowan biodegradation scale (Peters et al., 2005). Note the comparatively higher biodegradation level for samples included in Group C.

**Group A petroleum**

Group A petroleum includes all the crude oils from the Woodbourne oil field (WO84, WO88, WO140, WO177, WO196, LG#11). Petroleum in this group have relatively low ratios of $C_{19}/C_{23}$ tricyclic terpanes, tricyclic terpanes/$C_{30}$ hopanes, 3-MP/4-MDTB, and low MDBT's abundance (Table 4.2.6). There is also a slight dominance of $C_{27}$ over $C_{29}$ regular steranes. Expulsion of these petroleum took place at the early to mid-oil window (0.72-0.77 %$R_c$) based on medium range aromatic parameters.
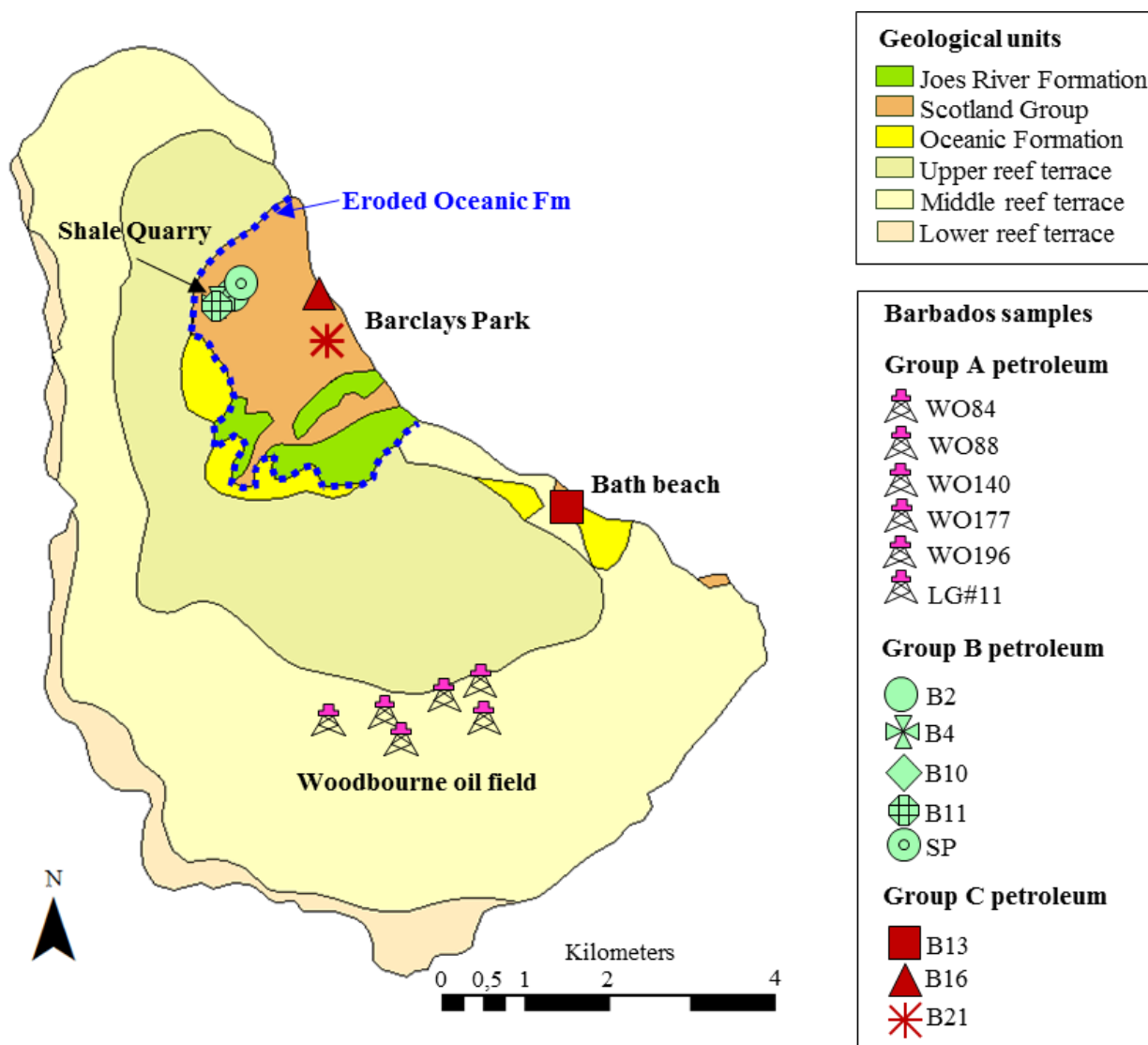
***Fig. 4.2.18.*** *The map illustrates the distribution of Group A (pink), B (green), and C (dark red) petroleum in the Barbados Island. Geological units are displayed. The area where the Oceanic Formation has been eroded is outlined in blue.*

### Group B petroleum

Group B petroleum consists of all the extracts (B2, B4, B10, B11) and the oil seepage (SP) from the Shale Quarry area. The petroleum in these extracts have comparatively high ratios of $C_{19}/C_{23}$ tricyclic terpanes, tricyclic terpanes/$C_{30}$ hopanes, 3-MP/4-MDTB, and high MDBT's abundance (Table 4.2.6). They also show fairly similar $C_{27}$, $C_{28}$, and $C_{29}$ regular sterane distribution. The $C_{29}$ sterols were probably derived from higher plants that were transported into a deep marine depositional environment (Volkmann, 1988), but they may also have been derived

from bacteria and planktonic algae (Tissot and Welte, 1984).

The maturity of the samples in this group is inferred to be that of the peak oil window (0.87 to 0.94 %$R_c$ = high maturity group in the maturity assessment section). They have the highest maturity in the dataset.

**Group C petroleum**

This group includes the heavily biodegraded B13 (Bath beach) and B21 (Barclays Park) samples (Table 4.2.6). Likewise, it includes the extract from sample B16 which was determined to be mainly composed of immature bitumen mixed with small amounts of allochthonus aromatics. Therefore, biomarker-based parameters cannot be used for classifying petroleum in this samples. Maturity parameters in this group appear to be consistent and correspond to expulsion at the early oil window. This may suggest correlation with the Woodbourne oils (Group A).
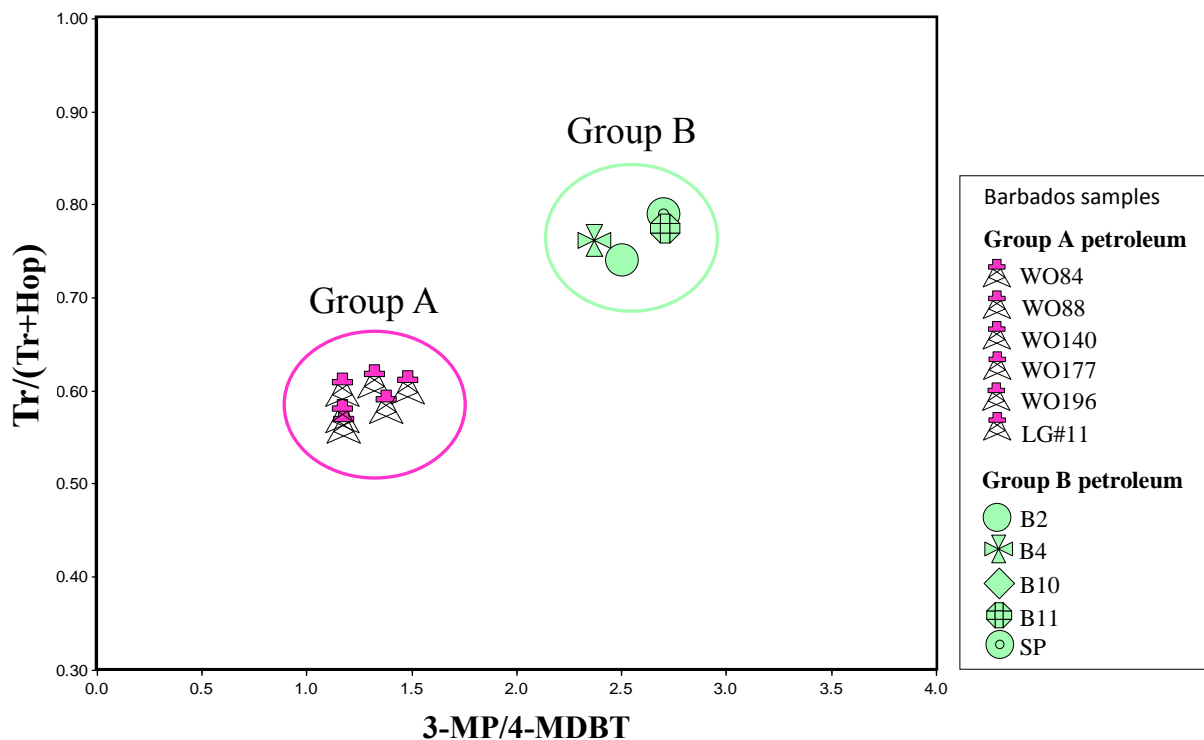


***Fig. 4.2.19.*** *3-MP/4-MDBT versus Tr/(Tr+Hop) cross-plot showing two separate groups of petroleum in the Barbados data set.*

Fig. 4.2.19. shows the correlation between 3-MP/4-MDBT and $C_{23}$-$C_{29}$Tr/($C_{23}$-$C_{29}$Tr+$C_{30}$Hop) ratios for samples in Groups A and B petroleum. The average tricyclic terpanes/$C_{30}$ hopane ratio and 3-MP/4-MDBT are 0.59 and 1.26 respectively for Group A, while the corresponding average values are 0.77 and 2.57 for group B. Two slightly different organofacies coupled with different thermal maturities indicate the existence of two source rocks within independent kitchens.

# 5. DISCUSSION

## 5.1. PETROLEUM SYSTEM ELEMENTS

According to Chaderton (2005), the Mid-Miocene sediments of the Oceanic Formation drape over the Barbados Ridge and extend into the zone of piggyback basins (Fig. 2.2.), forming a regionally-extended seal for hydrocarbons trapped in Eocene deep marine clastic reservoirs of the deformed prism. Paleobathymetric relations of this formation on Barbados proves that the uplift of the Barbados ridge took place in Mid-Miocene time (Chaderton, 2005) when the Barbados accretionary prism thrusted over the Tobago forearc basin (Mudussar, 2016). This compression triggered secondary thrusts and the older western part of the prism (Barbados ridge) became highly deformed. Subsequently, planar-high angle faults formed as a result of gravity collapse of the prism during the Plio-Pleistocene time (Mudussar, 2016).

### 5.1.1. Source rock

No solid evidence exists for the presence of Upper Cretaceous source rocks within the study area. E-W striking normal faults in the basement of the Tobago forearc basin are proposed to have been present at the northern margin of the South American plate before the collision between the Caribbean and South American plates, which started during the Late Cretaceous (Javis et al., 2008). Thus these structures potentially contain Upper Cretaceous organic carbon rich facies (Aitken et al., 2011) similar to those present in northern Colombian and Venezuela. Alternatively, Upper Cretaceous source rocks deposited on the Atlantic floor could have been incorporated into the Caribbean leading edge during it eastward movement (Escalona and Mann, 2011). This scenario would presume the the presence of Upper Cretaceous source rocks at several stratigraphic levels within the accretionary prims.

## 5.2. PETROLEUM SYSTEM ANALYSIS

Exploration drilling as deep as 16.000 feet onshore Barbados (C. Moseley, personal communication, Jan 9, 2017) has not reached Cretaceous aged-rocks. It implies that at the present-day geothermal gradient of ±23°C/km, the Cretaceous source rocks should currently and in the
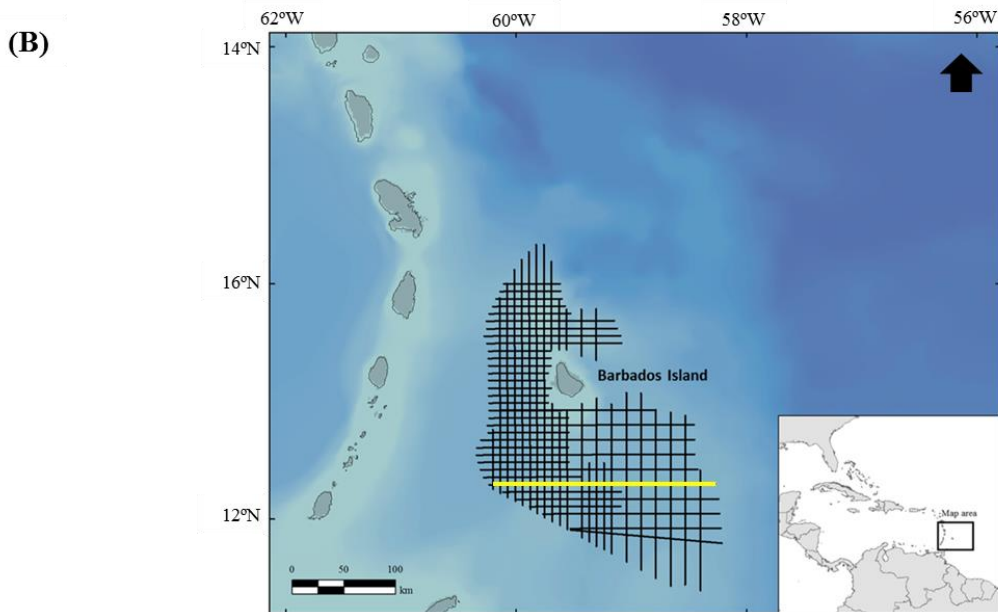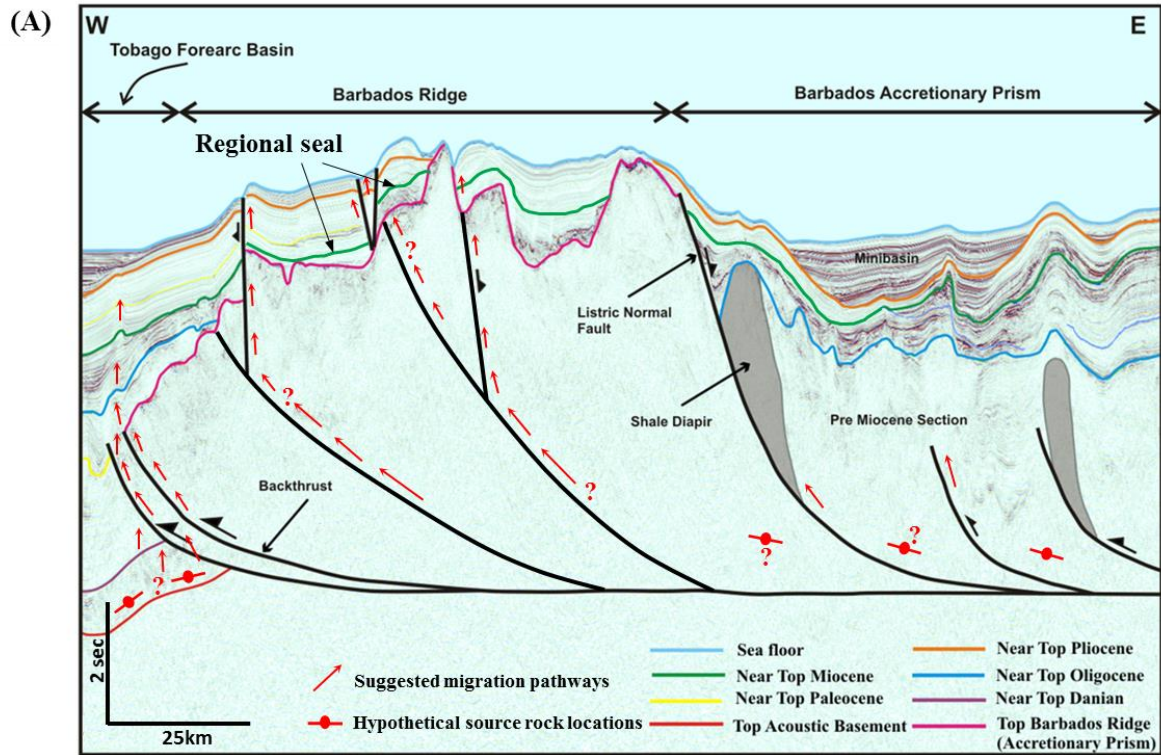
***Fig. 5.1. A.*** *Regional seismic section shows the key structural elements within each geological province (Tobago Forearc basin, Barbados Ridge, and Barbados Accretionary Prism). Deep, western-verging thrusts connect to vertical-high angle faults systems within the Barbados Ridge. Suggested migration pathways and hypothetical locations of Upper Cretaceous source rocks are shown. Modified from Mudussar (2016).* ***B.*** *Base map of the study area highlighting the location of the seismic section in A.*

near past (at least since the Late Miocene), be late mature to over mature beneath the Barbados ridge. Petroleum analyzed in this study is not representative of those elevated temperatures. However, long distance sub-horizontal migration from relatively shallower Upper Cretaceous source intervals may account for the presence of this petroleum onshore Barbados, if facilitated by large thrusts that subsequently feed vertical-high angle faults systems in the prism (Fig. 5.1).

As documented earlier, two main groups of petroleum were identified onshore Barbados. The maturity differences suggest that they originated from different source rock kitchens. This is also supported by the difference in organofacies. Expulsion of petroleum found today in the Woodbourne field (Group A) took place from a kitchen lying within the early to mid-oil window (%$R_c$–ave 0.72-0.76). Petroleum leaking in the Shale Quarry area (Group B) was expelled at higher temperatures from a kitchen within the peak oil window (%$R_c$–ave 0.83-0.94). At the present-day geothermal gradient of ±23°C/km, the mentioned difference in maturity represents a depth difference between the sourcing intervals of approximately 0.8 to 1km. The occurrence of these two groups in separate areas of the island (Fig. 4.2.18.) is probably due to independent migration pathways from the two separate kitchens to the corresponding reservoir.

### 5.2.1.    Pseudo well modeling

Due to the complex tectono-stratigraphic evolution of the area and little available information, the location of the kitchen is fundamentally unknown and so are the timing of generation and eventual migration pathways. In order to obtain a rough timing of hydrocarbons generation, 1D modeling was performed on a pseudo well located at the boundary between the western most extension of the Barbados accretionary prism (Barbados Ridge) and the Tobago basin Fig. 5.2. The model assumes the presence of the Upper Cretaceous source rocks lying on top of the basement. The burial history curve reveals three phases of subsidence:

*Phase 1* – Initial subsidence: subsidence of Upper Cretaceous rocks starts at 65 Ma with thick Paleocene sedimentation during the early stages of extension due to a slab-roll back and subsequent flexural subsidence of the previous forearc basin (Aitken et al., 2011). From Late Eocene to Late Oligocene/Early Miocene subsidence occurred comparatively slowly.
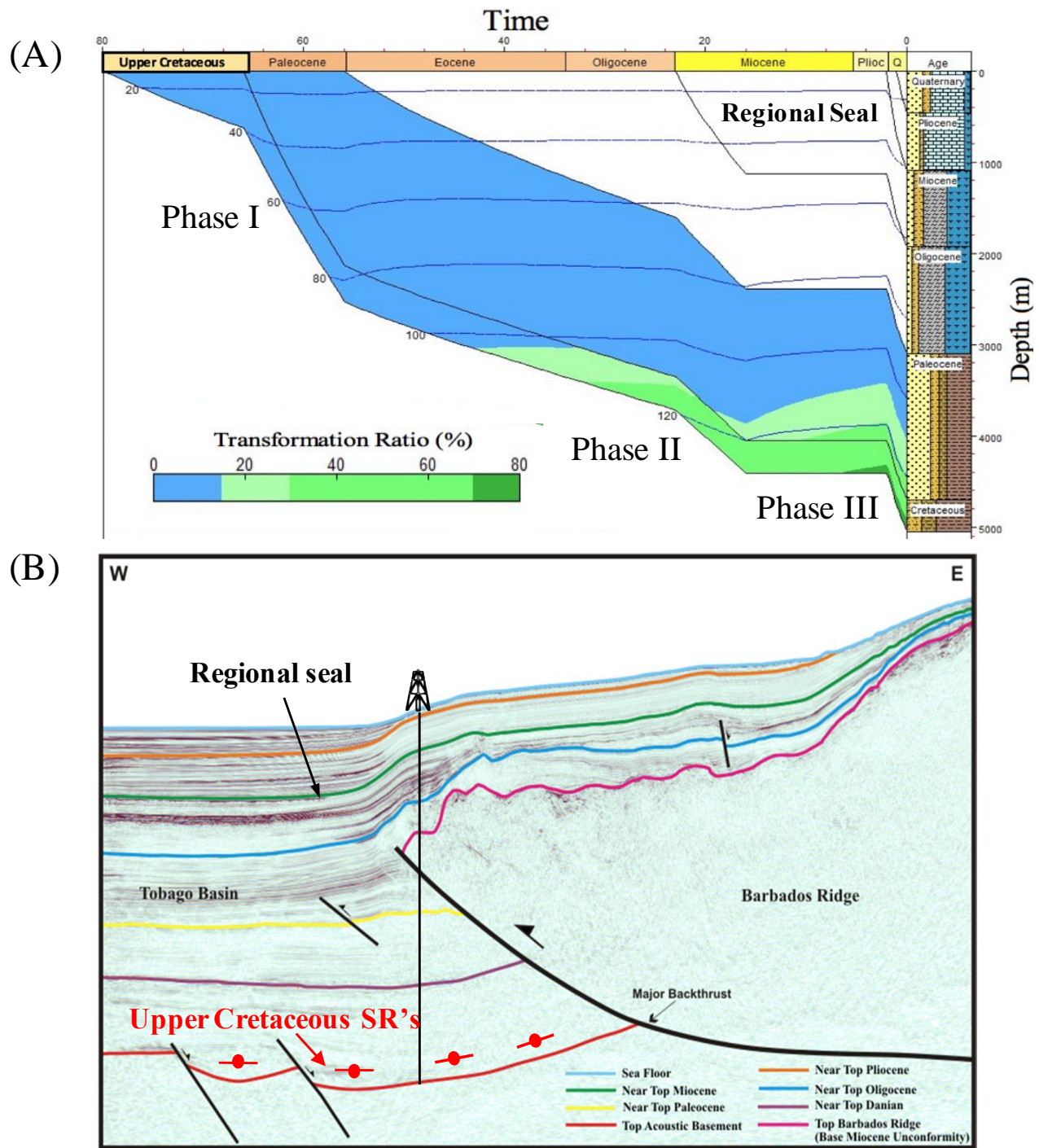
***Fig. 5.2.*** ***A.*** *Burial history with Transformation Ratio overlay for the pseudo well at the junction between the Tobago basin and the western margin of the Barbados Ridge;* ***B.*** *Regional seismic profile across the easternmost extension of the Tobago basin and the western margin of the Barbados ridge (Modified from Mudussar, 2016). Oil generation from Upper Cretaceous source rocks commenced in the Middle Eocene and reached transformation ration of 40% in the Early Oligocene.*

***Phase II*** – Thrust-related subsidence: the initial phase of extension is followed by a period of inversion that started around 23 Ma in the Early Miocene. This phase of inversion was triggered by uplift and westward thrusting of the eastern margin of the Barbados Accretionary Prism over the Tobago forearc basin (Brown and Westbrook, 1987) and caused local subsidence of the Tobago basin.

***Phase III*** – Continuous subsidence: Pliocene-Holocene sedimentation observed in the region since the last ~ 4 Ma has caused further subsidence of the deeply buried rocks on the Tobago basement.

Due to the lack of data, the maturity of the model has not been calibrated and the results, herein, are meant as a rough guideline. Nonetheless, some essential points for the petroleum system are emphasized. Oil generation from Upper Cretaceous source rocks commenced in the Middle Eocene and began to produce significant amounts of hydrocarbons in the Early Oligocene. Petroleum generation proceeded until today and Upper Cretaceous source rocks probably entered the gas window in the Pliocene. Presently, those units still hold potential for generating condensates and gas. A long-term maturation trend combined with various phases of off-scraping may have facilitated entrapment of hydrocarbons with different degrees of thermal maturity at several stratigraphic intervals within the Barbados ridge.

However, preservation of any hydrocarbon accumulation within the Eocene deep marine clastic reservoirs of the Scotland Group prior to the Middle-Miocene uplift event is fairly unlikely due to trap destruction during strong tectonism and the absence of the Oceanic Formation by that time. The timing of other migration-charge events, if existed, prior to the Middle-Miocene is a big question, as is the role of re-migration to shallower traps. The Barbados ridge, as the highest structure in the western margin of the prism is expected to have received significant amounts of oils migrating from the flanks after the Middle-Miocene uplift. However, a complex fault network probably deviated migration toward small accumulations where trap failure causes leakage to the surface.

Preservation of hydrocarbons in the Woodbourne field suggests that the initial filling event (recorded as biodegraded oil in samples above 1000 meters) most likely post-dated the Middle-Miocene uplift of the Barbados ridge (as discussed previously, preservation of earlier accumulations is unlikely due to the Miocene uplift) and charged several stratigraphic levels of the

Woodbourne trap system. The thermal maturity of these oils (0.72-0.77%$R_o$) suggests that they probably represent the early stages of generation and expulsion from a slowly subsiding source rock as indicated by increasing values of the triaromatic steroid (TA) ratio (Table 4.2.2). Later, the light fraction (n-C3 to n-C9) migrated into the Woodbourne trap system most likely facilitated by the last major normal-faulting event, placing this Post-Pliocene, sometimes into the Pleistocene or even more recently. This suggests that there may be a present ongoing charge of the light fraction to the shallower and biodegraded Woodbourne oils. The similar maturity of the light fraction and the heavier indicates that they have the same origin and supports that the light charge to the Woodbourne oils is a result of leakage (faults and/or failing cap rocks) from deeper reservoirs.

Various locations on top of the Less Beholding hill within the Barclays Park (sample B21 of Group C petroleum) (Fig. 4.2.18.) reveal the presence of brownish to dark-black, solid bitumen uniformly spread in clastic sediments of the Scotland Group. They probably represent a paleo accumulation that occurred after the Middle-Miocene uplift and after sedimentation of the regional seal of the Oceanic Formation, but prior to its erosion in the northern part of the island (Fig. 4.2.18.). The relative timing of entrapment in this area and similar maturity ranges with the Woodbourne oils (Group A) could suggest that this petroleum was derived simultaneously from the same source within the early oil window.

Unlike in other locations of the island, in the Shale Quarry, oil impregnated sandstones and seeping oil indicate active leakage in an area where the regional seal formed by Oceanic Formation has been eroded (Fig. 4.2.18.). The calculated vitrinite reflectance values for samples in this area (Group B petroleum) are relatively variable (from 0.87 to 0.94%) (Table 4.2.2.) over a small geographical area. This fact may represent a scenario that involves oil charging and re-migration into vertically stacked reservoirs. Potentially, lower maturity oils flowed earlier into shallower reservoirs, while more mature oils flowed into deeper reservoirs, and today oils are leaking simultaneously to the surface. It is facilitated by the existence of viable traps/reservoirs at virtually all levels drilled in the prism (C. Moseley, personal communication, Jan 9, 2017). As probably occurred in the entire top of the Barbados ridge, migration in the Shale Quarry began after the Middle-Miocene. It is unclear, however, if migration-charge into deeper reservoirs in this area is still taking place or has ceased.

## 5.3.   HYDROCARBON GENERATION POTENTIAL OF CENOZOIC ROCKS

The Paleogene source rocks analyzed in this study show low generation potential and are immature. However, Paleogene deep marine shales delivered by the proto- Maracaibo Delta have been suggested to be efficient source rocks in the Tobago Basin which is proved by the discovery of condensates in the Venezuelan part of the basin (Regueiro and Pena, 1996). Escalona et al., (2011) noted that the heating effect of the rising lesser Antilles during the Miocene may have a positive impact on the maturation of Paleogene source rocks. Thus they can offer an additional source of hydrocarbons within the Barbados accretionary prism.

**Table 6.1.** *GC-MS data available for comparison. Biomarkers parameters used to determine depositional environment, organofacies, lithofacies, and age of the analyzed data set.*

| ID | Sample | m/z 217 | m/z 218 | m/z 191 | C27% | C28% | C29% | C28/29 | Ts/Tm | C29/C30 | C35/C34 | Reference |
|---|---|---|---|---|---|---|---|---|---|---|---|---|
| 0 | La Luna Fm Middle Magdalena basin, SR | x | | x | 37.62 | 27.72 | 34.65 | 1.10 | 0.33 | 0.59 | 0.85 | Rangel et al., 2000 |
| 1 | Mara Oeste, OF | x | | x | 44.21 | 29.18 | 26.61 | 1.10 | 0.21 | 1.1 | 0.98 | López and Mónaco, 2017 |
| 2 | Perija foothills, Cachiri, OS | x | | | 39.59 | 26.02 | 34.39 | 0.76 | | 0.94 | 1.2 | Escobar, M., et al., 2011 |
| 3 | Boscan OF | x | | x | 41.84 | 30.61 | 27.55 | 1.11 | 0.36 | 0.92 | 1.1 | López and Mónaco, 2017 |
| 4 | La Luna Fm Perija, SR | x | | x | 40.00 | 32.74 | 27.26 | 1.20 | 0.41 | 0.95 | 0.88 | Alberdi-Genolet, M., & Tocco, R.,1999 |
| 5 | La Luna Fm Maracaibo basin, SR | x | | | 40.76 | 31.85 | 27.39 | 1.16 | | 1.19 | 1.15 | López and Mónaco, 2017 |
| 6 | Centro Lago OF | | x | x | 40.52 | 31.23 | 28.25 | 1.11 | 0.48 | 0.83 | 0.81 | Tocco and Margarita, 1999. |
| 7 | Eastern Valera, OS | | x | x | 38.05 | 31.19 | 30.76 | 1.01 | 0.54 | 0.96 | 0.94 | Portillo, E., et al., 2008 |
| 8 | Alturitas OF | | x | x | 40.43 | 28.27 | 31.31 | 0.90 | 0.55 | 0.78 | 0.975 | López and Mónaco, 2017 |
| 9 | Los Manueles OF | x | | x | 34.69 | 32.65 | 32.65 | 1.00 | 0.53 | 0.74 | 1.01 | Tocco, R., et al., 1995 |
| 10 | La Guivara, OS | | x | x | 36.70 | 32.11 | 31.19 | 1.03 | | 0.78 | 0.97 | Galarraga, F., et al., 2010 |
| 11 | Playa Grande, OS | | x | x | 30.32 | 36.20 | 33.48 | 1.08 | 0.67 | 0.7 | 0.8 | Tocco, R., et al., 1995 |
| 12 | La victoria OF | x | | x | 48.85 | 32.69 | 18.46 | 1.77 | 0.56 | 0.51 | 0.92 | López and Mónaco, 2017 |
| 13 | Caipe OF | x | | x | 40.55 | 30.93 | 28.52 | 1.08 | 0.57 | 0.58 | 1.18 | Tocco, R., et al., 1995 |
| 14 | Silvestre OF | x | | x | 41.32 | 30.21 | 28.47 | 1.06 | 0.64 | 0.49 | 1.06 | Tocco, R., et al., 1995 |
| 15 | Sinco OF | x | | x | 37.05 | 33.77 | 29.18 | 1.16 | 0.67 | 0.67 | 1 | Tocco, R., et al., 1995 |
| 16 | Silvestre OF | x | | x | 39.44 | 31.10 | 29.46 | 1.06 | 0.56 | 0.45 | 0.77 | López and Mónaco, 2017 |
| 17 | Llanos basin OF | x | | x | 41.44 | 33.08 | 25.48 | 1.30 | 1.05 | 0.52 | 0.91 | Bautista, D.F.G., et al., 2015 |
| 18 | F_C_6_1 OF | | | x | | | | | 0.77 | 0.59 | 0.67 | Bautista, D.F.G., et al., 2015 |
| 19 | F_C_6_1 OF | | | x | | | | | 1.07 | 0.58 | 0.65 | Bautista, D.F.G., et al., 2015 |
| 20 | F_E_5_1 OF | | | x | | | | | 0.37 | 0.56 | 0.76 | Bautista, D.F.G., et al., 2015 |
| 21 | F_W_13_1 OF | | | x | | | | | 1.01 | 0.66 | 0.85 | Bautista, D.F.G., et al., 2015 |
| 22 | F_C_1_1 OF | | | x | | | | | 0.94 | 0.61 | 0.75 | Bautista, D.F.G., et al., 2015 |
| 23 | F_W_6_1 OF | | | x | | | | | 1.20 | 0.6 | 0.75 | Bautista, D.F.G., et al., 2015 |
| 24 | FH_S_11_2 OF | | | x | | | | | 1.01 | 0.76 | 0.64 | Bautista, D.F.G., et al., 2015 |
| 25 | FH_N_9_1 OF | | | x | | | | | 0.78 | 0.61 | 0.67 | Bautista, D.F.G., et al., 2015 |
| 26 | FH_S_1_0 OF | | | x | | | | | 0.64 | 0.58 | 0.63 | Bautista, D.F.G., et al., 2015 |
| 27 | Socororo OF | x | | x | 39.74 | 31.41 | 28.85 | 1.09 | 0.40 | 0.83 | 1.05 | López, et al., 2015 |
| 28 | Junin, Orinoco Belt, OF | x | | x | 33.39 | 31.15 | 35.46 | 0.88 | 0.30 | 0.74 | 0.92 | López, 2014 |
| 29 | Junin, Orinoco Belt, OF | x | | x | 34.29 | 30.91 | 34.80 | 0.89 | 0.29 | 0.75 | 1 | López, 2014 |
| 30 | Maturin, Orinoco Belt, OF | | | x | | | | | 0.33 | 0.79 | 1.19 | López, 2014 |
| 31 | Querequal Fm, SR | x | | | 48.57 | 28.57 | 22.86 | 1.25 | | 0.92 | 0.8 | López and Mónaco, 2017 |
| 32 | Gulf of Paria, TB | | x | x | 34.42 | 33.12 | 32.47 | 1.02 | 0.40 | 0.51 | 0.8 | Rodrigues, 1995 |
| 33 | Coast of Paria, TB | x | | x | 34.33 | 32.65 | 33.02 | 0.99 | 0.40 | 0.66 | 0.77 | Marquez, G., et al., 2013 |
| 34 | Naparima Fm, SR | | x | x | 34.89 | 33.19 | 31.91 | 1.04 | 0.36 | 0.725 | 0.55 | Rodrigues, 1995 |

Type of sample: OF= Oil field; SR= Source rock; TB= Tar balls; OS= Oil seep. Colors correspond to the symbols implemented through the whole chapter for the different basins. References where the corresponding data was obtained are included.
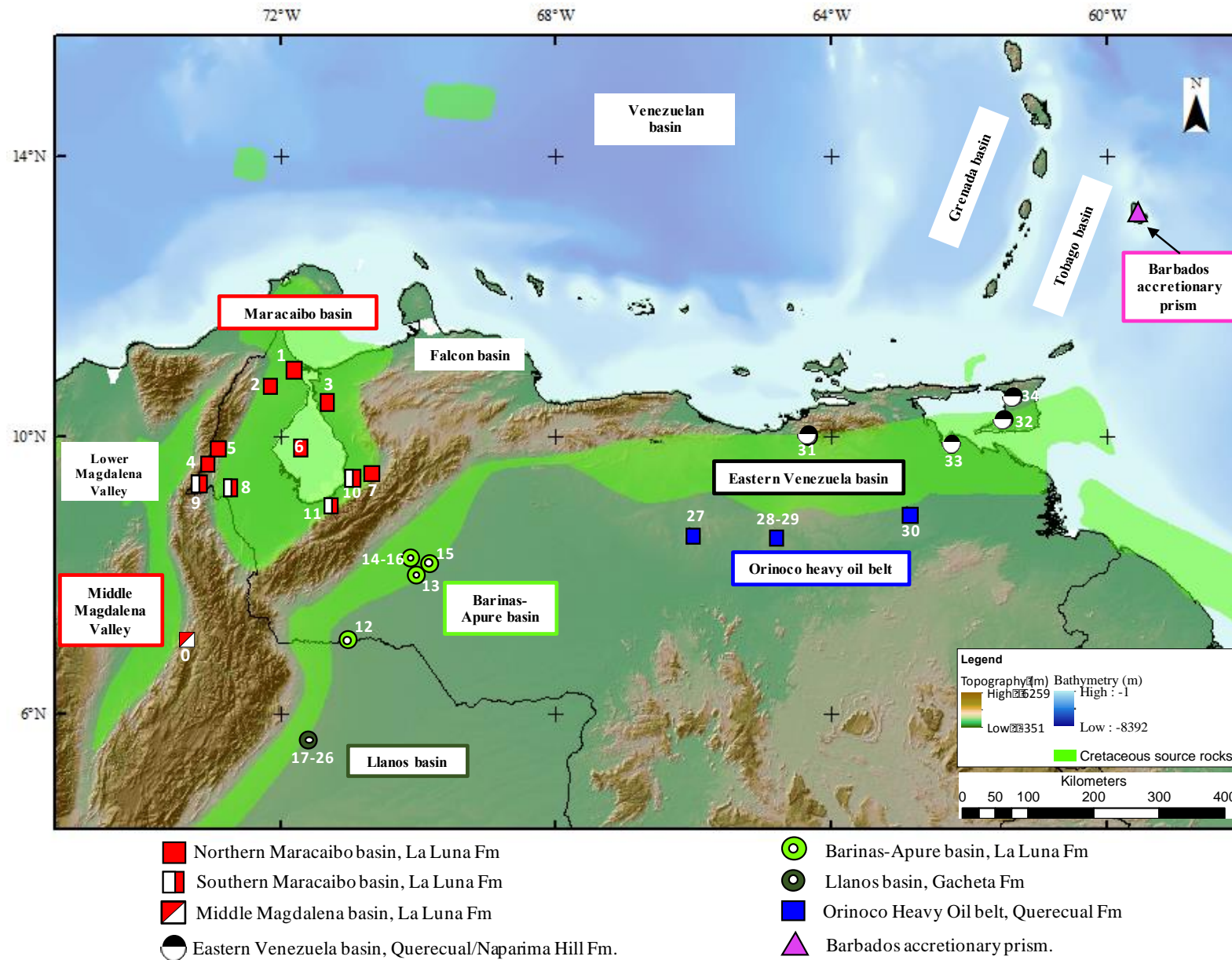
**Fig. 6.1.** *Location of samples included in this study. Distribution of sedimentary basins. Green polygons represent the distribution of Cretaceous source rocks. Next to every basin in the legend, the main Upper Cretaceous source rock is mentioned. For sample ID and types of samples refer to Table 6.1.*

# 6. BARBADOS OILS AND THEIR COMPARISON WITH NORTHERN SOUTH AMERICAN AND CARIBBEAN SOURCE ROCKS AND OILS

Various depositional environments governed sedimentation of Upper Cretaceous source rocks across the northwestern corner of South America. Eustatic sea level changes, local and regional-scale tectonic events, warming sea-surface temperatures, and variations in the sediment supply of fine-grained, hemi-pelagic sediments combined to set distinctive environmental conditions (Erlich et al., 2003) that varied from one basin to another and that are reflected in the composition of today's hydrocarbons.

## 6.1. SETTING THE STAGE FOR COMPARISON

Inherent to the comparison performed in this work using published geochemical data of oils and source rocks there is certain degree of uncertainty regarding accuracy and quality of the information. Published organic geochemical data sets from different studies are limited to *m/z* 191 terpanes fragmetograms along with either *m/z* 217 or *m/z* 218 steranes fragmetograms (Table 6.1). In some areas, the amount of geochemical information is enough to facilitate identification of solid trends, while in other areas data are notoriously limited or is virtually non-existent. Fig. 6.1. shows the distribution of samples included in this study.

Thermal stress may account for variations in the relative concentration of biomarkers, therefore its effects on the available data must be evaluated before any substantive discussion can be made about the age and depositional environments of source rocks. As an attempt to establish thermal maturity differences relative to biomarkers, the Ts/Tm ratio is plotted versus the $C_{35}/C_{34}$ extended hopanes ratio in Fig. 6.2. Most of the samples from the Maracaibo basin, the Barinas-Apure basin, the eastern Venezuelan basin, Orinoco heavy oil belt, the Middle Magdalena basin, and the Woodbourne oils from Barbados (Group A petroleum) are early mature. Samples from the Llanos basin and from the Shale Quarry in Barbados (Group B petroleum) are mid mature, and have the highest maturity in the sample set. From Fig 6.2 it appears that these maturity differences do not account for the substantial variations in the $C_{29}/C_{30}$ and $C_{35}/C_{34}$ hopane ratios existing in the analyzed dataset. These variations may instead suggest inherent characteristics of the depositional environments. Likewise, the abundance of
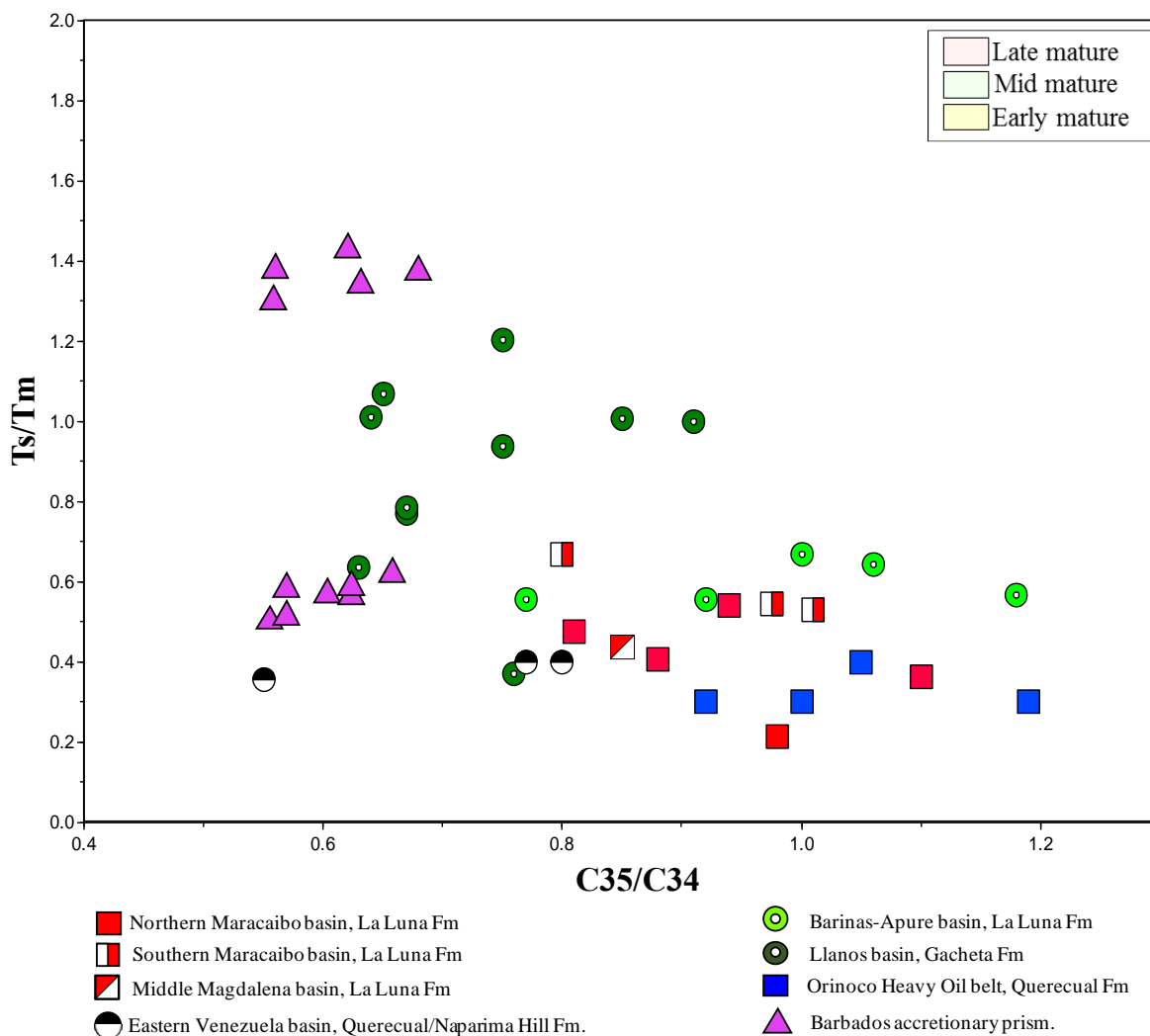
***Fig. 6.2.*** *Cross plot of facies (C35/C34) and maturity (Ts/Tm) parameters using hopane biomarkers shows that variations in maturity do not influence the facies parameters which therefore can be further used for comparison. In general, samples from the Maracaibo basin, the Barinas-Apure basin, the eastern Venezuelan basin, Orinoco heavy oil belt, the Middle Magdalena basin, and the Woodbourne oils from Barbados (Group A petroleum) are early mature. Samples from the Llanos basin and from the Shale Quarry in Barbados (Group B petroleum) are mid mature.*

$C_{28}$ relative to $C_{29}$ regular sterane used for age determination (Table 6.1; Fig.6.3.) is not expected to be significantly altered by the determined thermal stress.

Fig. 6.3. introduces a cross plot of age (my) versus $C_{28}/C_{29}$ sterane distribution used to constrain the age of numerous oils and source rocks from different northern South American and Caribbean basins. This ratio suggests that all the samples represent source rocks and/or oils of Cretaceous age. Solid stratigraphical and paleontological evidence, however, indicates that these rocks (Erlich et al., 2003) and extracted oils are of Upper Cretaceous age.
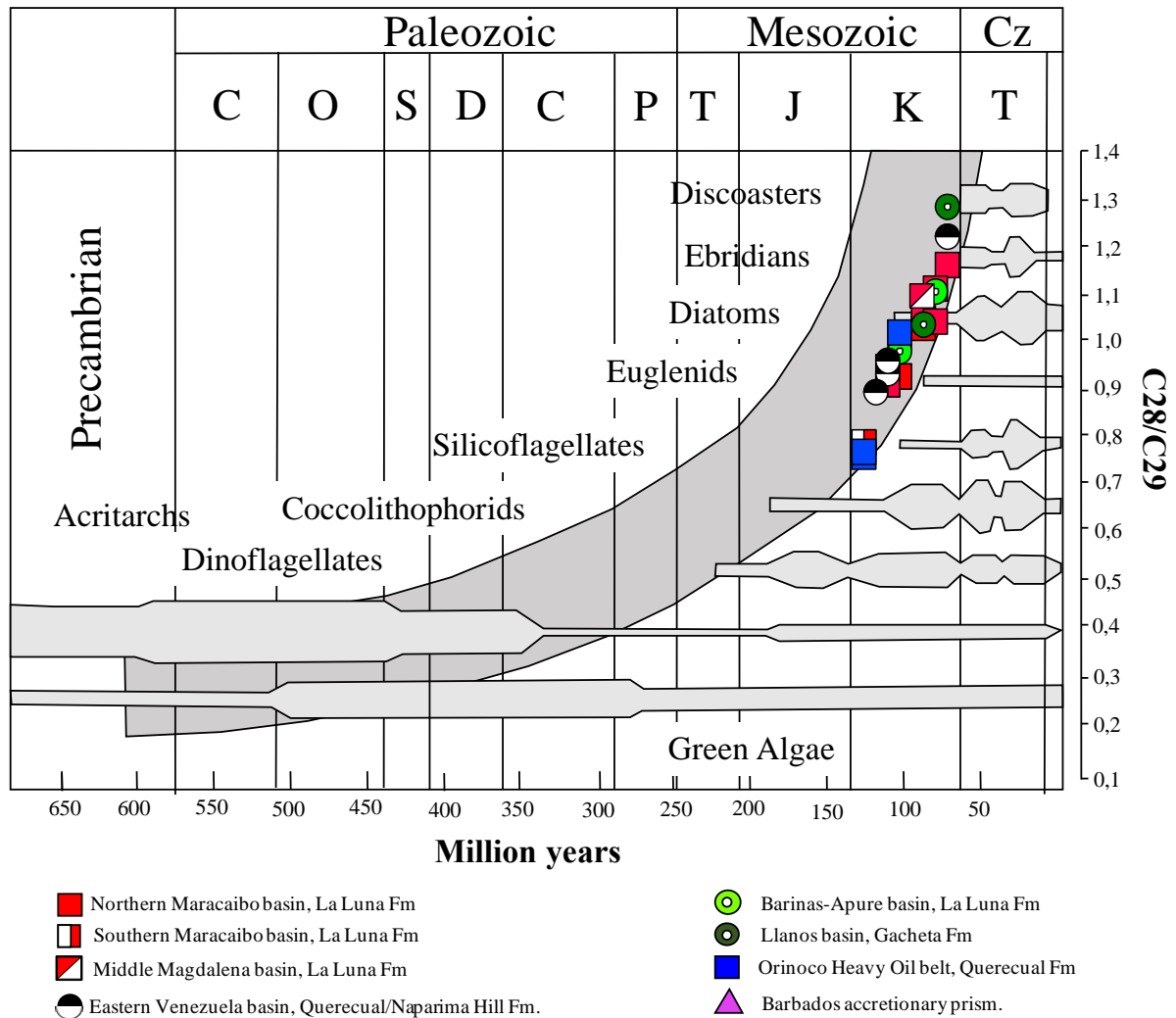
***Fig. 6.3.*** *Determination of source rock age based on $C_{28}/C_{29}$ steranes (Grantham and Wakefield, 1988) indicating Cretaceous age for the sample set.*

## 6.2. BIOMARKERS-BASED COMPARISON

Different authors (Lawrence et al., 2002; Burggraft et al., 2002; Leahy et al., 2004; Hill and Schenk, 2005), have proposed that Barbados oils may be sourced by facies comparable to the Upper Cretaceous La Luna Formation or its regional equivalents onshore the South American plate. In Fig. 6.4., $C_{35}/C_{34}$ hopane ratio is cross-plotted versus $C_{29}/C_{30}$ hopane ratio for several Upper Cretaceous source rocks and derived oils. This plot facilitates comparison that leads to establish factual differences between the carbonate-rich La Luna Formation and its coevals, and their possible resemblance with the rock sourcing the Barbados oils.
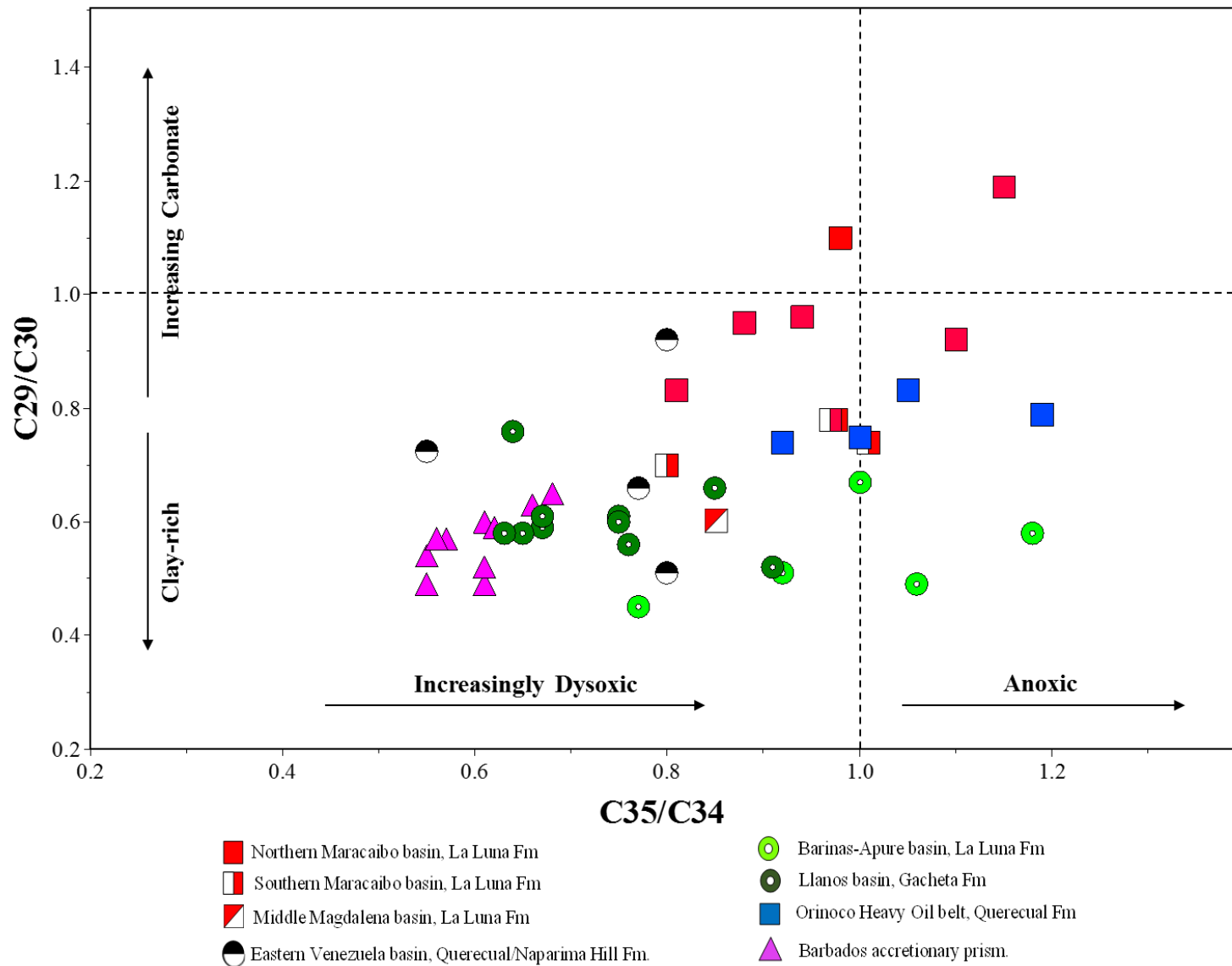
***Fig. 6.4.*** *$C_{35}/C_{34}$ hopane ratio versus $C_{29}/C_{30}$ hopane ratio for the samples set. Barbados samples plot as the most oxic and clay-rich in the data set. By contrast, samples from the Maracaibo basin (derived from La Luna Fm.) and from the Orinoco Heavy oil belt (derived from the Querecual Fm.) plot as the most carbonate-rich and anoxic conditions. It suggests substantial differences between the source rock generating the Barbados oils and La Luna/Querecual/Naparima Hill Formations. Samples from the Llanos basin and Barbados have similar $C_{29}/C_{30}$ ratios, but differ in their $C_{35}/C_{34}$ ratios. See Table 6.1 for CG-MS calculated parameters used in this plot.*

Towards western Venezuela (Fig. 6.1.), samples of the northern Maracaibo basin (red squares in Fig. 6.4.) have average $C_{35}/C_{34}$ and $C_{29}/C_{30}$ ratios around the unity (1 and 0.99 respectively), plotting as carbonate-rich source rocks (or derived oils) deposited in predominantly anoxic conditions. This is in agreement with sedimentation of La Luna Formation in an outer carbonate platform as proposed by Erlich et al., (2003). The low-oxygen conditions extended southwards through the southern Maracaibo basin (half-red squares, average $C_{35}/C_{34} = 0.95$) and the Barinas-Apure basin (light-green rings, average $C_{35}/C_{34} = 0.99$) where the lithology grades into more shaly facies as indicated by the progressively decreasing average values of the $C_{29}/C_{30}$ hopane ratio southwards (southern Maracaibo basin = 0.75; Barinas-Apure basin = 0.59) (Fig. 6.5.). Similar lithofacies were deposited in slightly more oxic conditions (dark-green rings, average $C_{35}/C_{34} = 0.73$) over the northern Llanos basin in eastern Colombia, known as the Gachetá Formation. The aforementioned sedimentary conditions are consistent with sedimentation along a north/south seaway where paleobathymetric highs trapped the basinal water and permitted limited surface-water exchange into the Pacific Ocean (Vergara., 1997a; Johnson, 1999) creating oxygen-depleted waters paired with increasing terrigenous influx southwards.

In eastern Venezuela, oils of the Orinoco heavy oil belt (blue squares in Fig. 6.4.) seem to be derived from predominantly carbonate-rich lithofacies (The Querecual Formation) similar to La Luna Formation in the southern Maracaibo basin, but precipitated under slightly more anoxic conditions as indicated by the average $C_{35}/C_{34}$ hopane ratio = 1.04 (Fig. 6.5.). Vast organic-carbon rich limestones of the Querecual Formation deposited over an extensive flooded shelf (Di Croce, 1996) rather than in a restricted seaway. Towards the eastern Venezuelan basin, the Gulf of Paria, and Trinidad, samples show greater variability (half-black circles) with a general tendency to vary their $C_{29}/C_{30}$ hopane ratio (maximum= 0.94, minimum= 0.5). It may be the result of disturbances in the redox conditions and in the relative abundance of siliciclastic material triggered by catastrophic fluvial discharge into organic-carbon rich slope shales and limestones of the Naparima Hill Formation (Erlich et al., 2003).
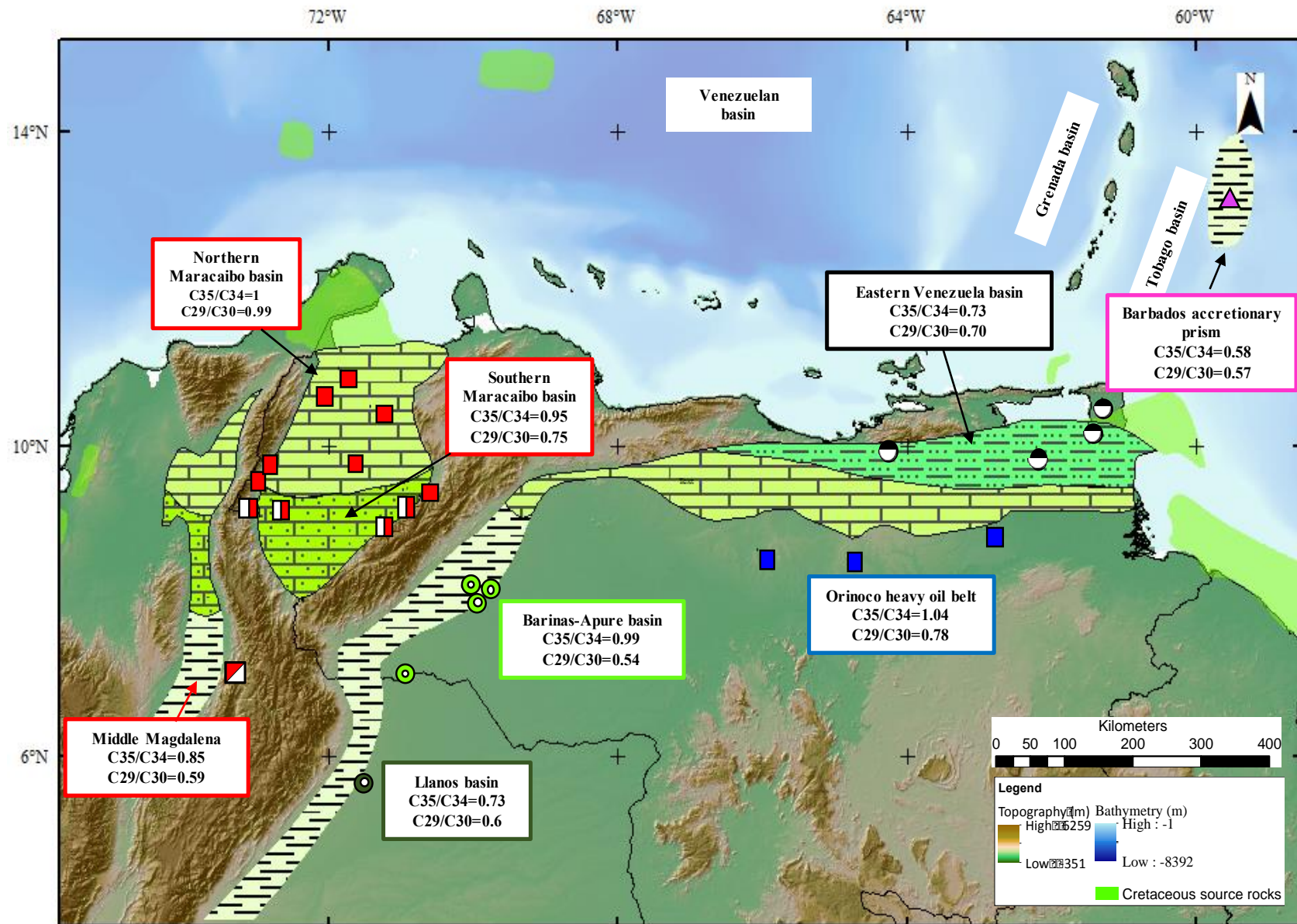
Limestones   Shaly limestones   Shales   Interbedded shales and limestones

Northern Maracaibo basin, La Luna Fm
Southern Maracaibo basin, La Luna Fm
Middle Magdalena basin, La Luna Fm
Eastern Venezuela basin, Querecual/Naparima Hill Fm.

Barinas-Apure basin, La Luna Fm
Llanos basin, Gacheta Fm
Orinoco Heavy Oil belt, Querecual Fm
Barbados accretionary prism.

87

***Fig. 6.5.*** *Map showing depositional and lithological variations interpreted from biomarkers ratios for the basins included in this study. Ratios C29/C30 hopanes for lithology assessment and C35/C34 homohopanes for lithology and redox conditions assessment are displayed for every basin. Starting in the northern Maracaibo basin in Venezuela through the Llanos basin in Colombia, carbonate sedimentation in anoxic conditions grades southwards into more oxic and clay-dominated conditions.*



Legend:
- Northern Maracaibo basin, La Luna Fm
- Southern Maracaibo basin, La Luna Fm
- Middle Magdalena basin, La Luna Fm
- Barbados accretionary prism.
- Llanos basin, Gacheta Fm
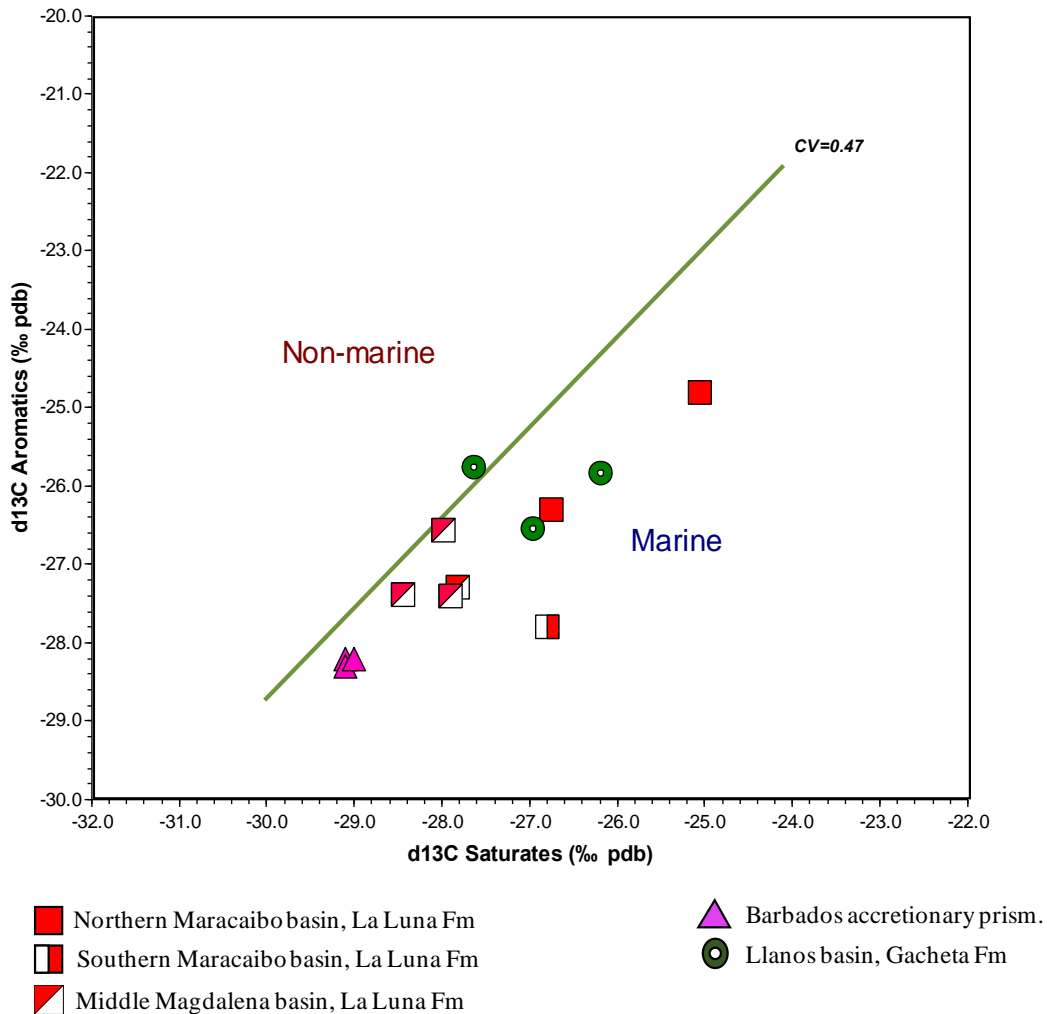
***Fig. 6.6.*** *Saturates versus aromatics isotopic fractions for three Barbados oils and other oils known to be derived from Upper Cretaceous source rocks in northern South America and Caribbean region. Barbados samples plot as the isotopically lightest samples in the data set and differ from La Luna derived oils in the Maracaibo, Middle Magdalena, and Llanos basins.*

The corresponding average $C_{35}/C_{34}$ and $C_{29}/C_{30}$ hopane ratios for 11 samples from Barbados (purple triangles in Fig. 6.4.) are 0.58 and 0.57, significantly lower than the values observed for the anoxic, carbonate-rich rocks of La Luna Formation in the Maracaibo basin (half-red and red squares) and its western equivalent, the Querecual Formation (blue squares). Source rocks generating the Barbados oils seem to be partly comparable with oils derived from the

Gachetá Formation in the Llanos basin (dark green rings), but were deposited under more oxic conditions according to lower $C_{35}/C_{34}$ ratios.

## 6.3.   ISOTOPIC-BASED COMPARISON

Isotopic values for the aromatic and saturate fractions for three Barbados oils from the Woodbourne field and several samples from the Middle Magdalena, Maracaibo, and Llanos basin are plotted in Fig. 6.6. Barbados oils plot consistently as the isotopically lightest samples in the data set. Advance stages of maturity and biodegradation can account for modifications in the isotopic composition of oils and extracts from source rocks. However, it is unlikely that all the plotted samples have experienced extensive biodegradation or extreme temperatures that could modify their original isotopic composition substantially. Barbados oils (Woodbourne oils), for instance, were found to be early mature, while the two oils from the Maracaibo basin are mid-mature. In this respect, differences displayed in the plot are believed to reflect variations in source rock type and facies. These isotopic data support compositional differences between the Barbados oils and other northern South American and Caribbean oils previously inferred from biomarkers data, which in turn reflect differences in the source rocks.

From this discussion, it is clear that the source rock facies generating the petroleum onshore Barbados was deposited in an environment that is definitely different to the typical carbonate-rich environment of La Luna Formation or its eastern equivalent the Querecual Formation. Instead, Barbados petroleum was sourced by a marine shale accumulated in oxic to dysoxic conditions with variable amounts of marine and continental-derived organic matter.

# Southern Llanos basin study case

# 7.   MODEL BUILDING

## 7.1.    AGE ASSIGNMENT AND FACIES DEFINITION

Age of the layers was assigned following the five tectono-stratigraphic sequences model discussed in detail by Moreno and Escalona (2015) (Fig. 3.2.2). The Paleozoic units in this part of the basin are interpreted to contain a coarsening upward sequence predominantly composed of silty and sandy sediments of Cambrian? –Ordovician age (Cooper et al., 1995; Ulloa and Perez, 1982), with marginal to very poor hydrocarbon potential (average TOC = 0.65% and HI ≤ 100 mg/gTOC). However, geochemical data from well 2 suggests the existence of a basal organic carbon-rich interval consisting mainly of black-shales (Fig. 7.1). This interval appears to have higher hydrocarbon generation potential (average TOC = 4% and HI~180mg/gTOC at $\pm 1R_o\%$) relative to the upper section, and is dominated by continental-derived organic matter kerogen type III. Thus the Kinetic reaction of Behar et al., (1997) for Type III (Dogger) source

**Table 7.1.** *Age assignment table for the modeled horizons. Hiatus and erosive events are also included.*

| Age [Ma] | Horizon | - | Layer | - | Event Type | No. of Sublayers | Max. Time Step [Ma] |
|---|---|---|---|---|---|---|---|
| 0.00 | Horizon_219 | | | | | | |
| | | | Pleistocene | | Deposition | 1 | 10.00 |
| 5.00 | Horizon_220 | | | | | | |
| | | | Miocene | | Deposition | 1 | 10.00 |
| 23.00 | Horizon_221 | | | | | | |
| | | | Oligocene | | Deposition | 1 | 10.00 |
| 55.00 | Horizon_222 | | | | | | |
| | | | Upper Cretaceous-Paleocene | | Deposition | 1 | 10.00 |
| 100.00 | Erosion_708_Top | | | | | | |
| | | | Hiatus_708 | | Hiatus | | 10.00 |
| 235.00 | Erosion_544_Top | | | | | | |
| | | | Erosion_544 | | Erosion | | 10.00 |
| 300.00 | Hiatus_626_Top | | | | | | |
| | | | Hiatus_626 | | Hiatus | | 10.00 |
| 458.00 | Horizon_223 | | | | | | |
| | | | Upper Ordovician | | Deposition | 1 | 10.00 |
| 470.00 | Horizon_224 | | | | | | |
| | | | Lower_Ordovician | | Deposition | 1 | 10.00 |
| 495.00 | Hiatus_462_Top | | | | | | |

rocks was adopted. It is, however, noteworthy to mention that due to the advanced thermal maturity (%Ro ~1), the hydrogen indexes (HI) of the source interval have probably been reduced. Therefore, in Table 7.2, a higher hydrogen index (300mg/gTOC) that may approximate that of the original sediments before burial is assigned to the model for the lower Ordovician interval. No other well has reached this interval, but paleogeographic inferences suggest that non-marine to transitional conditions prevailed across the entire southern extension of the Llanos basin (Ulloa and Perez, 1982). Thus for the model it was assumed that the source interval is present along the whole section (Fig. 7.1).

A second Upper Cretaceous-Paleogene source rock was modeled as a combined homogenous section. It contains shales of the Gacheta Formation (Cooper et al., 1995) with TOC contents of around 2-3.5%, but exceeds 4% in some areas. HI above 350 mg/g TOC, but that rarely exceeds 450 mg/g TOC, suggest that these sediments contain kerogen type II. Therefore, the kinetic reaction presented by Behar et al., (1997) for type II (PB) source rocks was applied (Table 7.2).

Facies for the remaining three sequences (Oligocene, Miocene, and Pleistocene) were assigned using literature data (Barrero et al., 2007) and were defined as overburden rocks (Table 7.2).
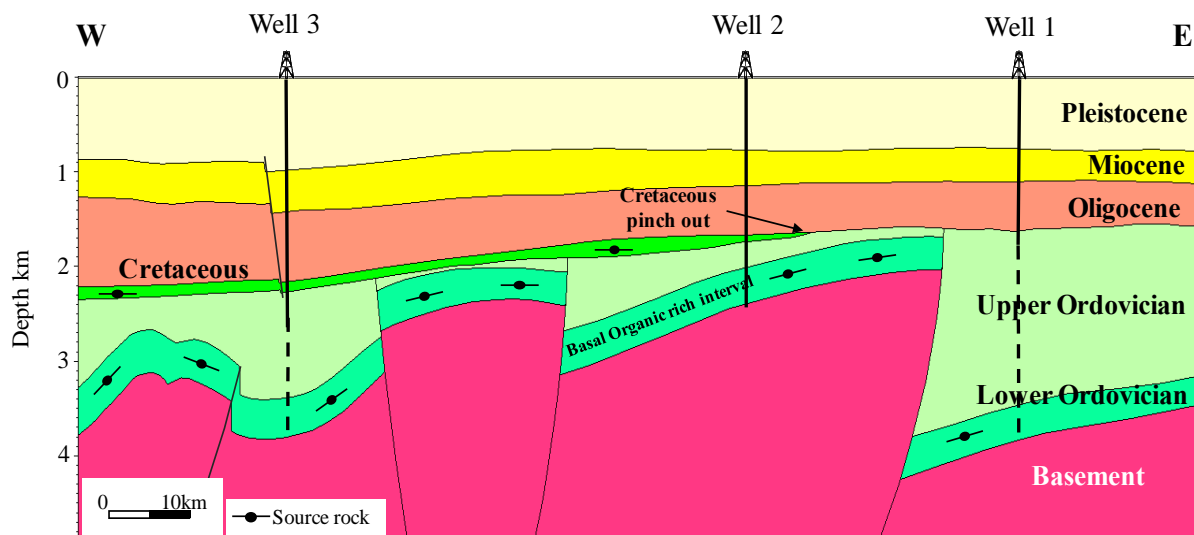


**Fig. 7.1.** *Present-day section showing the different sequences and locations of the three wells used for calibration of the model. Continues lines represent drilled wells, while dotted lines represent pseudo depths used for further simulation purposes. The organic carbon-rich, Lower Ordovician interval is marked. Additionally, the Upper Cretaceous-Paleogene source rock is indicated.*

*Table 7.2. Facies assignment for the modeled horizons.*

| Name | Color | Lithology Value | Kinetics | TOC Mode | TOC Value [%] | TOC Map | HI Mode | HI Value [mgHC/gTOC] | HI Map | Petroleum System Elements |
|---|---|---|---|---|---|---|---|---|---|---|
| Pz_Metamorphic | | Gneiss | | | | → | | | → | none |
| Lower_Ordo | | Shale (organic rich, typical) | Behar_et_al(1997)_TIII-(Dogger) | Value | 4.00 | → | Value | 300.00 | → | Source Rock |
| Upper_Ordo | | Sandstone (clay rich) | | | | → | | | → | Overburden Rock |
| Cretaceous | | Shale (organic rich, 3% TOC) | Behar_et_al(1997)_TII(PB) | Value | 3.00 | → | Value | 400.00 | → | Source Rock |
| Oligocene | | Shale (organic lean, silty) | | | | → | | | → | Overburden Rock |
| Miocene | | Sandstone (subarkose, clay rich) | | | | → | | | → | Overburden Rock |
| Pleistocene | | Siltstone (organic lean) | | | | → | | | → | Overburden Rock |
| | | | | | | → | | | → | |

An important aspect in the geological evolution of the southern Llanos basin is the existence of a long-term hiatus from the Upper Ordovician until the Late Carboniferous (458-300My) followed by uplift and erosion that ceased in the Triassic (235My) (Ruiz et al., 1999; Malone et al., 2002) (Table 7.1). Thereafter, a second hiatus extended until the beginning of the Upper Cretaceous (Cooper et al., 1995).

## 7.2. CALIBRATION AND BOUNDARY CONDITIONS

### 7.2.1. Calibration

The model was calibrated for measured vitrinite reflectance (%$R_o$) and well temperatures. For calculation of the vitrinite reflectance from temperature histories, the EASY %$R_o$ model developed by Sweeney and Burnham (1990) was used.

Fig. 7.2 presents the calibrated values for vitrinite reflectance and well temperatures of the three wells using a variable heat flow model explained in the next section. After calibration, calculated and measured vitrinite reflectance data points show a characteristic pattern of increasing thermal maturity of the entire stratigraphic range from Upper Cretaceous to Pleistocene. A break in the measured vitrinite reflectance values is observed at the unconformity Cretaceous-Paleozoic in wells 2 and 3. This abrupt change in maturity suggests significant uplift (around 2000 meter, discussed in the modeling results section) of the Paleozoic sequence before sedimentation of the Upper Cretaceous-Cenozoic sequence. Vitrinite reflectance data points below the unconformity were also calibrated with calculated values. This break in vitrinite reflectance is not observed in well 1.
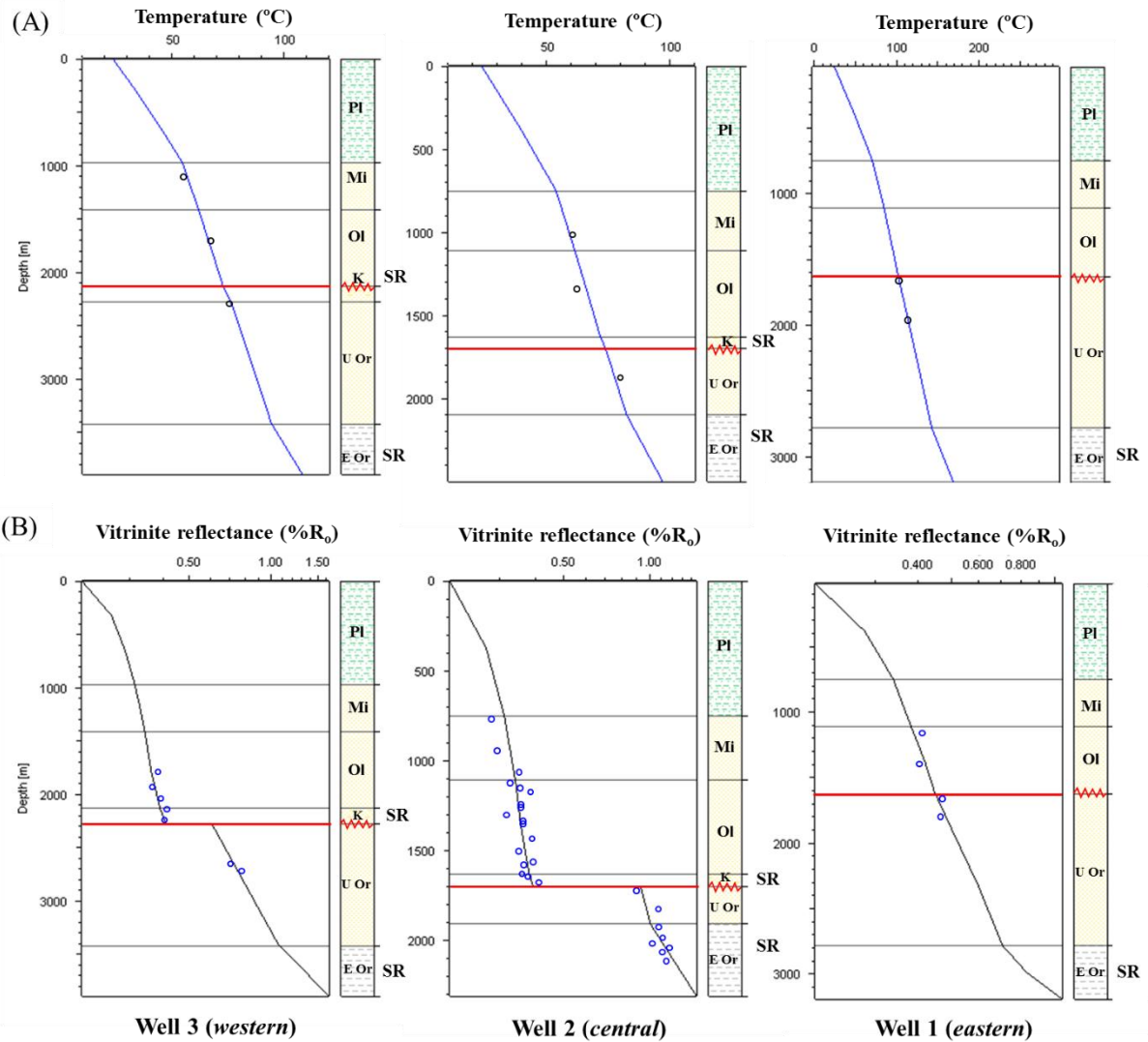
***Fig. 7.2.*** *Calibration of modeled temperature (**A**) and maturity curves (**B**). Continuous and serrated red lines represent the Paleozoic-Cretaceous/Oligocene unconformity. E Or: Early Ordovician. U Or: Upper Ordovician. K: Cretaceous. Ol: Oligocene. Mi: Miocene. Pl: Pleistocene. SR=Source rock intervals. A significant maturity break defined by vitrinite reflectance values (%Rₒ) is observed along the Paleozoic-Cretaceous unconformity in wells 2 and 3. For well locations refer to Fig. 7.1.*

### 7.2.2. Boundary conditions

In Petromod, boundary conditions trends define the basic energetic conditions for the temperature and burial history of the source rock and consequently for the maturation of organic matter through time. The paleo-heat flow (HF) is the lower boundary condition, while the sediment water interface temperature (SWIT) is the upper boundary condition, which was defined using the Auto SWIT function in Petromod. The latitudinal position assigned to the southern Llanos basin was 4°, South America. The mean surface temperature of the area at present day shows that SWIT is around 23.5°C.

Regarding heat flow, no data exist for the Paleozoic-Jurassic period. Based on the geological evolution of the Llanos basin of Cooper et al., (1995), and on the calibrated preset-day values, an approximated heat flow history was generated for the study area (Fig. 7.3). Main inputs were theoretical values from Allen and Allen, (2013), and the magnitude of stretching (calculation of related heat flow) following the approach of Mackenzie (1978). The resulting heat flow history takes account of the four major stages that may have impacted maturation of the source rocks: 1. An Ordovician back arc stage; 2. A Permian orogeny; 3. A Jurassic back arc-related heating episode; and 4. foreland stages during the Upper Cretaceous-present period.
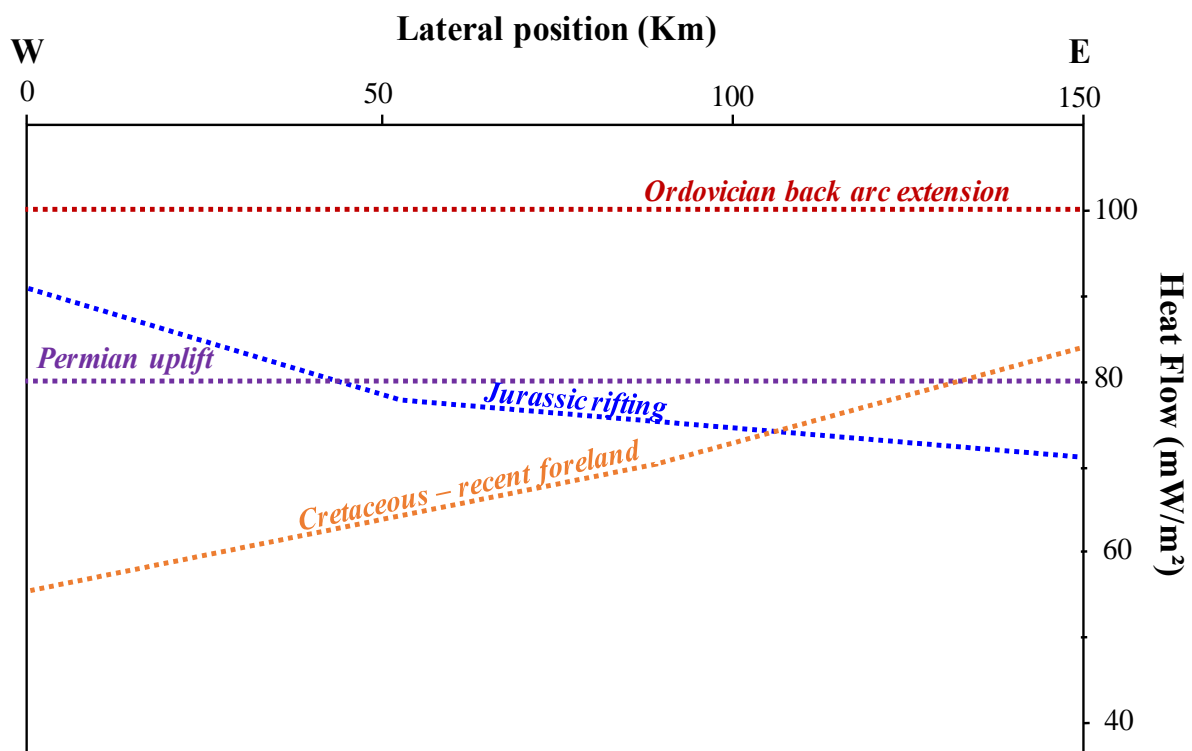


***Fig 7.3.*** *Modeled heat flow history. The highest heat flow occurred in the Ordovician back arc extension. An increase in heat flow took place in the western margin of the basin during the Jurassic rifting. A westwards decreasing trend in heat flow is observed in the present-day heat flow.*

For the calibrated present-day heat flow case, this study found that it varies from $58mW/m^2$ in the western area of the basin (well 3), $72mW/m^2$ (well 2), and $83mW/m^2$ in the east area (well 1) (Fig. 7.3). The same westward decreasing trend was observed for the geothermal gradient. Corresponding values were 25°C in the west area (well 3), 29°C in the central area (well 2), and 39°C in the east area (well 1).

Calculating the heat input in the Ordovician was challenging due to the poor understanding of the amount of back-arc extension. Following the approach of Bachu et al., (1995) on inherent high heat flow for the metamorphic basement of the Llanos basin plus a high typical value for heat flux in back arc basins, the assumption of a maximum of 100 mW/m$^2$ at the model start is plausible (Fig. 7.3).

During the Permian uplift due to the collision between the Americas (Ruiz et al., 1999; Malone et al., 2002) heat flow values likely ranged from of 75 to 85 mW/m$^2$, which are typical values for these tectonic events. The absolute amount of heat flow in the Jurassic back arc extension was determined by the stretching factor β=1 (Bachu et al., 1995) to be approximately 90mW/m$^2$ according to Mackenzie (1978) model. The rifting-derived rise in heat flow most likely had a higher effect on the western margin of the southern Llanos basin (Fig. 7.3), which was closer to the rifting axis.

The Upper Cretaceous to recent period is characterized by two foreland stages (Gomez et al., 2003, 2005; Parra et al., 2009; Horton et al., 2010). Maturity and temperature calibrations (Fig. 7.2) facilitated recognition of a westwards decreasing heat flow trend. No geological arguments were found for supporting any major variation or deviation from normal values during the Upper Cretaceous-recent foreland basin evolution. Therefore, the heat flow values determined by calibration of wells 1, 2, and 3 were held constant through the Cenozoic.

# 8.    MODELING RESULTS

## 8.1. THERMAL AND MATURITY MODELLING, AND HYDROCARBON WINDOWS

Applying the heat flow histories reconstructed by 1D modelling to the entire 2D section resulted in a good match between measured and calculated maturity and temperature. The temperature history model at seven key times is shown in Fig. 8.1. Maturation history of both the type III Early Ordovician and the type II Upper Cretaceous source rocks is presented in Fig. 8.2.

Temperature history shows that by the end of Ordovician (Fig. 8.1-A),  the potential Lower Ordovician source rock interval reached maximum temperatures of about 170°C in the western area of the basin (well 3), and slightly lower values towards the east (150°C, well 1). Consequently, %Ro ranges between 1.0 and 2% in the west, 0.7 - 2% in the basin center, and 0.7 - 1.3% in the east Fig. 8.2-A. Maturity calibration (Fig. 7.5.) supports those values, but also facilitates determination of narrower ranges of 1.1 to 1.6% for the west area, 1 to 1.4% in the center of the basin, and 0.7-1.0% for the eastern area. Thus, by the end of the Ordovician beginning of the Silurian, the Lower Ordovician source interval reached maturity within the wet-gas window toward the west, and within the late oil window toward the east. This study assumes that the oil window ranges from 110°C to 160°C since the main potential source rock (Lower Ordovician) is believed to contain kerogen type III.  Transformation ratios (discussed in the following section) show higher conversion in the west (in excess of 70%) and gradually decrease eastwards (as low as 50%) (Fig 8.4-A).

Since the Mid-Late Silurian the rapid subsidence decelerated and only few sediments accumulated on top of the whole sequence. The Late Ordovician geothermal gradient of ±43°C/Km is believed to have decreased due to a post back arc extension cooling phase. The Lower Ordovician source rocks most likely remained at around 3000 meter depth until the Late Paleozoic.

In the Permian, continent-continent collision triggered uplifting of the central and western areas of the basin (Ruiz et al., 1999; Malone et al., 2002). By the end of the uplift (Late Permian-
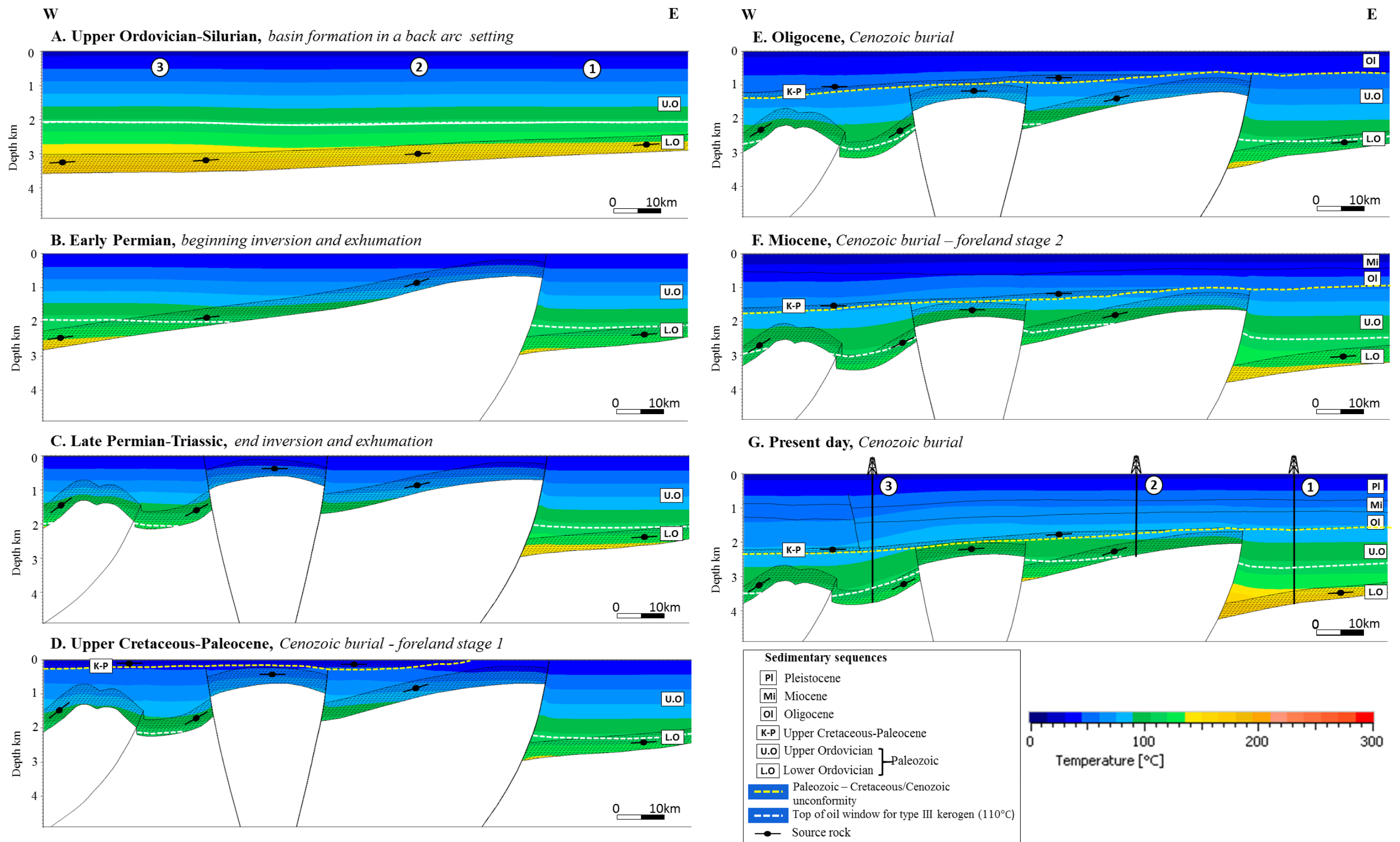
**Fig 8.1**. *Temperature history model at seven key times. Numbers 1, 2, and 3 represent the location of wells used in this study. During the Permian-Triassic uplifting event in the central and eastern areas of the basin, the Lower Ordovician source rock interval experienced significantly lower temperatures than in the Ordovician-Silurian period. During the Upper Cretaceous-Cenozoic burial, Lower Ordovician source rocks have progressively reached temperature higher than ever before in the eastern margin of the basin. Top of the oil window for type III kerogen is highlighted at 110°C.*

**Fig 8.2.** *Maturity history model for the Lower Ordovician and Upper Cretaceous-Paleocene source rock intervals at seven key times. Numbers 1, 2, and 3 represent the location of wells used in this study. The Lower Ordovician source rock interval reached maturity ranging from 0.7 to 1.6%Ro in Upper Ordovician-Silurian time. At present day, Cretaceous-Paleogene source rocks are immature over the entire section.*
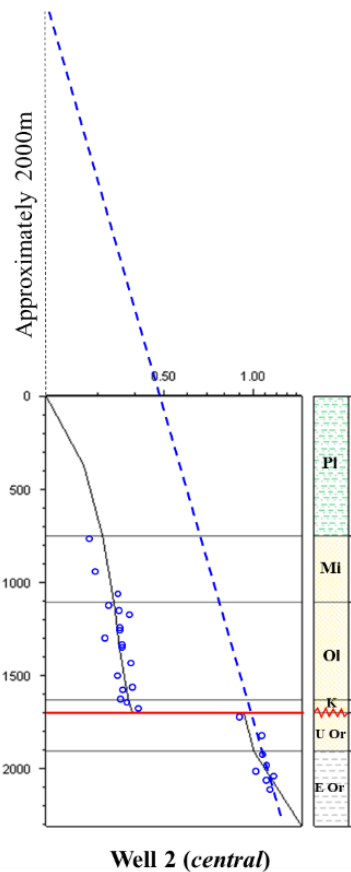
**Fig 8.3.** *Approximate calculation of eroded sediments at the location of well 2 (central area of the basin) using the vitrinite reflectance break at the boundary Paleozoic-Cretaceous.*

Triassic), the Early Ordovician maximum burial was at a depth of around 2000 meters (Fig 8.1-B and C). In the central part of the basin (location of well 2), the source interval was as shallow as 650 meters at temperatures of around 70°C. Due to the uplift, the source rock interval was mostly outside the hydrocarbon window (Fig 8.1- C). Based on the vitrinite reflectance break (Fig. 8.3), erosion of up to 2000 meters took place. A different situation can be inferred for the eastern area of the basin (at the location of well 1), where no major tectonic disturbances seem to have affected the Paleozoic sequence and the source rock kept its depth of around 3000 meters. This conclusion is supported by no break in the vitrinite reflectance values at the Paleozoic-Oligocene unconformity (well 1 in Fig. 7.2).

In the Upper Cretaceous, temperatures are deduced to have been lower due to a systematic decrease in heat flow following the Jurassic back arc extension (Fig. 8.1-D). Renew tectonic activity resulted in increased burial during the Cenozoic (Fig. 8.1-E, F, and G). In the eastern part of the basin, the potential Lower Ordovician source rock interval has reached temperatures up to 175°C(Fig. 8.1-G), and maturity has increased to around 1,2%$R_o$ (1% previous maximum). This increment in maturity is not obvious in Fig. 8.2-G due to the color scale used in the model; however, values of vitrinite reflectance higher than 1% can be seen in Fig. 7.2 for well 1.

Regarding the Cretaceous-Paleogene source rocks, these are immature at a maximum depth of approximately 2300 meters (Fig 8.2-G); Vitrinite reflectance ranges from 0.40% to 0.45%, and present-day temperatures from 70°C to 80°C (Fig. 8.1-G). In order to reach the oil window these layers should have been buried at least 300 meters deeper (considering 90°C as the beginning of the oil window since kerogen type II was assigned to this interval). The Cenozoic

sequence also remains immature over the entire basin. Vitrinite reflectance reaches a maximum of 0.41%, and present-day temperatures range between 23.5°C and 80°C.

## 8.2.    GENERATION OF HYDROCARBONS

The transformation ratio (TR) obtained from the maturation calculations is the fraction of reactive kerogen that has been transformed to hydrocarbons at a certain time. Fig. 8.4 presents the transformation ratio of a potential Lower Ordovician and a Cretaceous-Paleogene source rocks at seven key times through the basin evolution. In Fig. 8.5 transformation ratio at the three well locations is shown.

As expected from the similar temperature and maturity history of Lower Ordovician source rocks, transformation of organic matter followed a similar pattern caused by the high heat flow during the back-arc extension episode (Fig. 8.4-A). By the Late Ordovician-Early Silurian time, around 70% of the total potential was transformed to hydrocarbons in the western area (blue line in Fig. 8.5), around 60% in the central area (green line), and around 50% in the eastern distal area (well 1, black line). According to the organic matter (Type III) simulated, hydrocarbons generated would consist mainly of gas with minor amounts of oil. Migration of generated hydrocarbons into reservoirs may have occurred in vertical and eastwards, updip directions.  In the Silurian-Permian period, transformation reactions froze because of post-rifting cooling followed by uplift of the western and central areas of the basin (Fig. 8.4-B and C).

During Cenozoic reburial, further transformation of the potential Lower Ordovician source rocks did not take place in the western (well 3) and central (well 2) parts of the basin (blue and green in Fig. 8.5 respectively; Fig. 8.4-E, F, and G). In this areas recent temperatures have not exceeded the Ordovician maximum (160°C -170°C) (Fig. 8.1- A and G) required to reactivate transformation. In contrast, within the eastern distal margin of the basin (well 1), transformation has increased since the Miocene (black line on Fig.8.5). During this time, gas has probably been generated as the maturity of the source rock has increased from around 1% to around 1.2% Ro. Potentially, oil that had not been expelled from the source rock would crack to lighter oils or eventually gas. Transformation and generation continues up to the present day reaching values of up to 75%.  Presumably, migration may take place mainly in eastwards

101

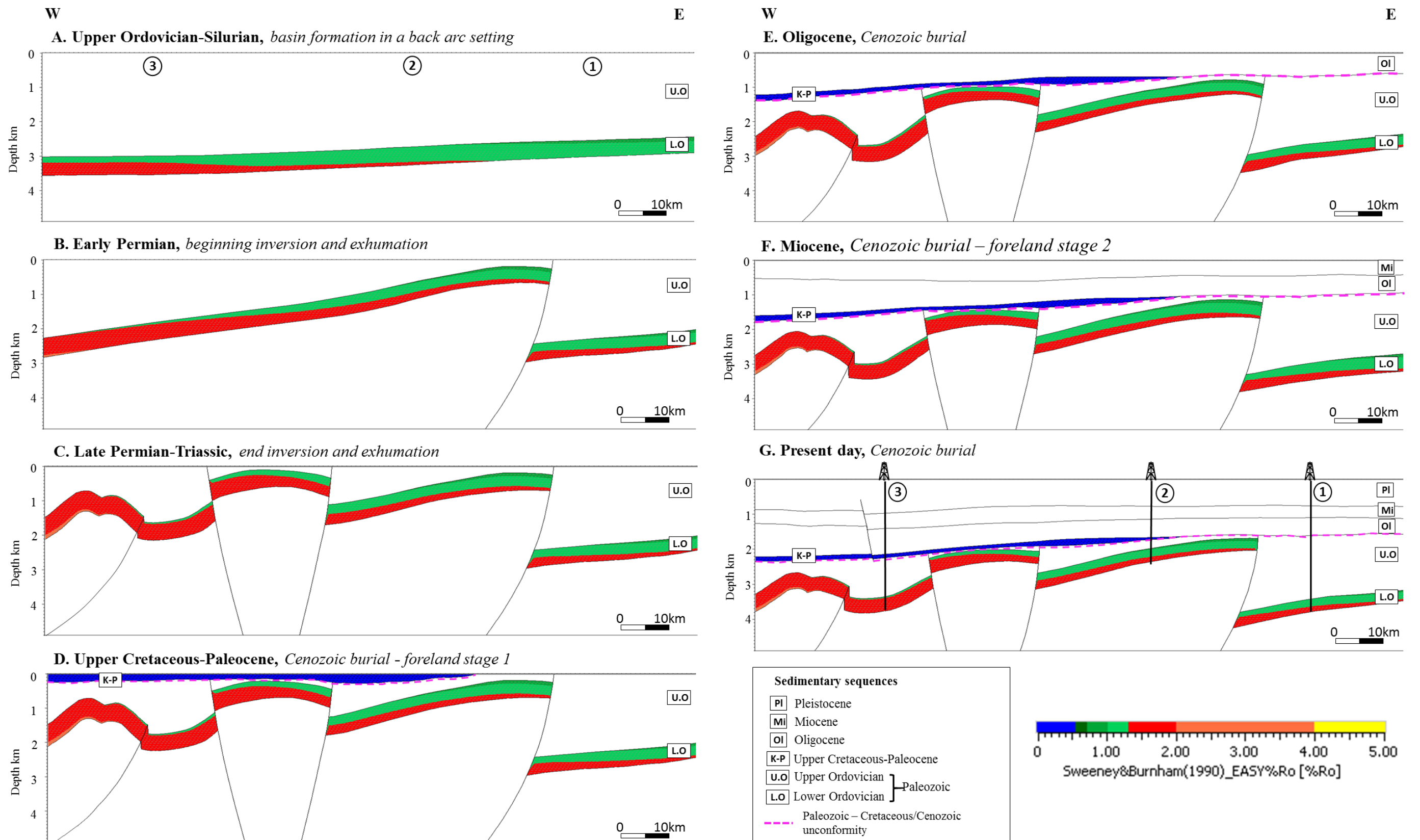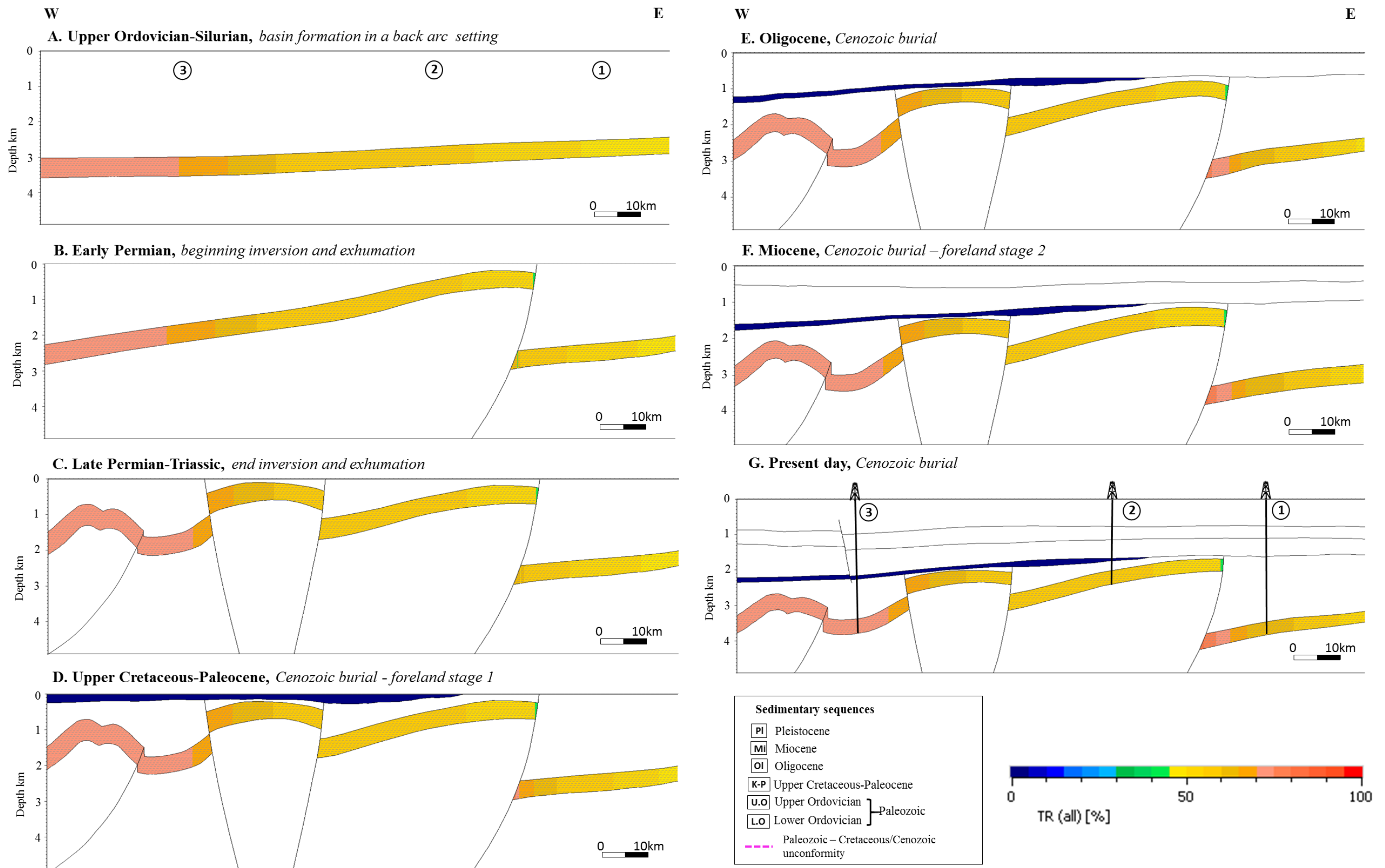**Fig. 8.4.** *Transformation history model for the Lower Ordovician and Upper Cretaceous-Paleocene source rock intervals at seven key times. Numbers 1, 2, and 3 represent the location of wells used in this study. Main observations include an initial transformation phase during the Upper Ordovician- Silurian. Renew transformation is taking place in the eastern margin of the basin.*

direction due to tectonic loading on the west side of the study area.

Given the relatively low maturity of Upper Cretaceous-Cenozoic source rocks, no transformation or generation of hydrocarbons has occurred in this units.
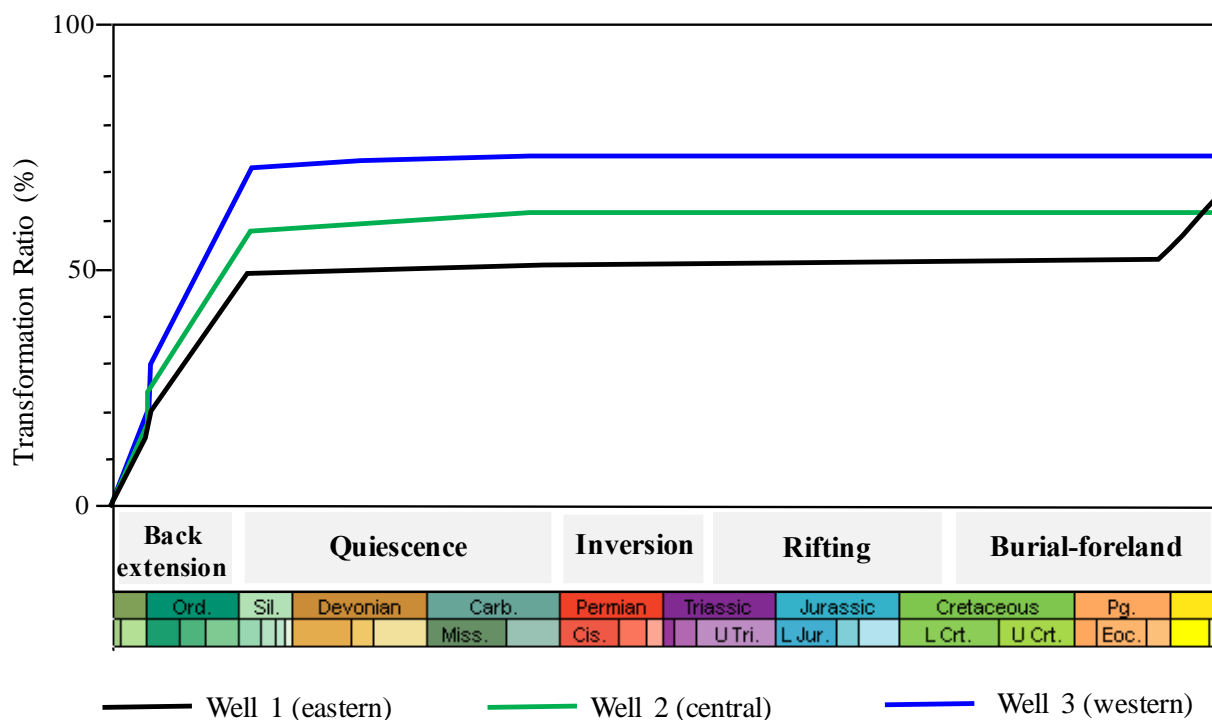


*Fig 8.5. Transformation ration of the Lower Ordovician source rock interval through time.*

## 8.3. IMPLICATIONS FOR THE PETROLEUM SYSTEM

In this section the temperature window for best hydrocarbon preservation potential is evaluated by implementing the concept of the optimum entrapment zone of Nadeau et al., (2005). They suggested that above 120°C pore pressure starts to reach the hydrofracturing pressure, entering the hydrocarbon expulsion zone, whereas biodegradation occurs below 60°C.

In an attempt to estimate the best timing for hydrocarbon generation and migration, with optimum temperatures for preservation in reservoir rocks, plots of transformation ratio of the potential Lower Ordovician source rocks and the temperature history of possible reservoirs at the three well locations are combined in Fig. 8.6. According to this graph, the best time for trapping hydrocarbons in the Upper Ordovician reservoirs of the southern Llanos basin was the end of the Ordovician and Early to Middle Silurian. During this period, kerogen in source rocks

of Lower Ordovician age had been transformed into hydrocarbons (70%, 60%, and 50% at locations 3, 2, and 1 respectively) and the reservoir rocks of Upper Ordovician age were within the optimum entrapment zone at the locations of wells 1 and 2 (green and black dotted lines on Fig. 8.6). The best location for reservoir rocks was between 1000 and 2500 meters because at higher depths elevated temperatures may have caused hydro-fracturing and expulsion of hydrocarbons, as probably occurred at the location of well 3 (blue dotted line on Fig. 8.6).
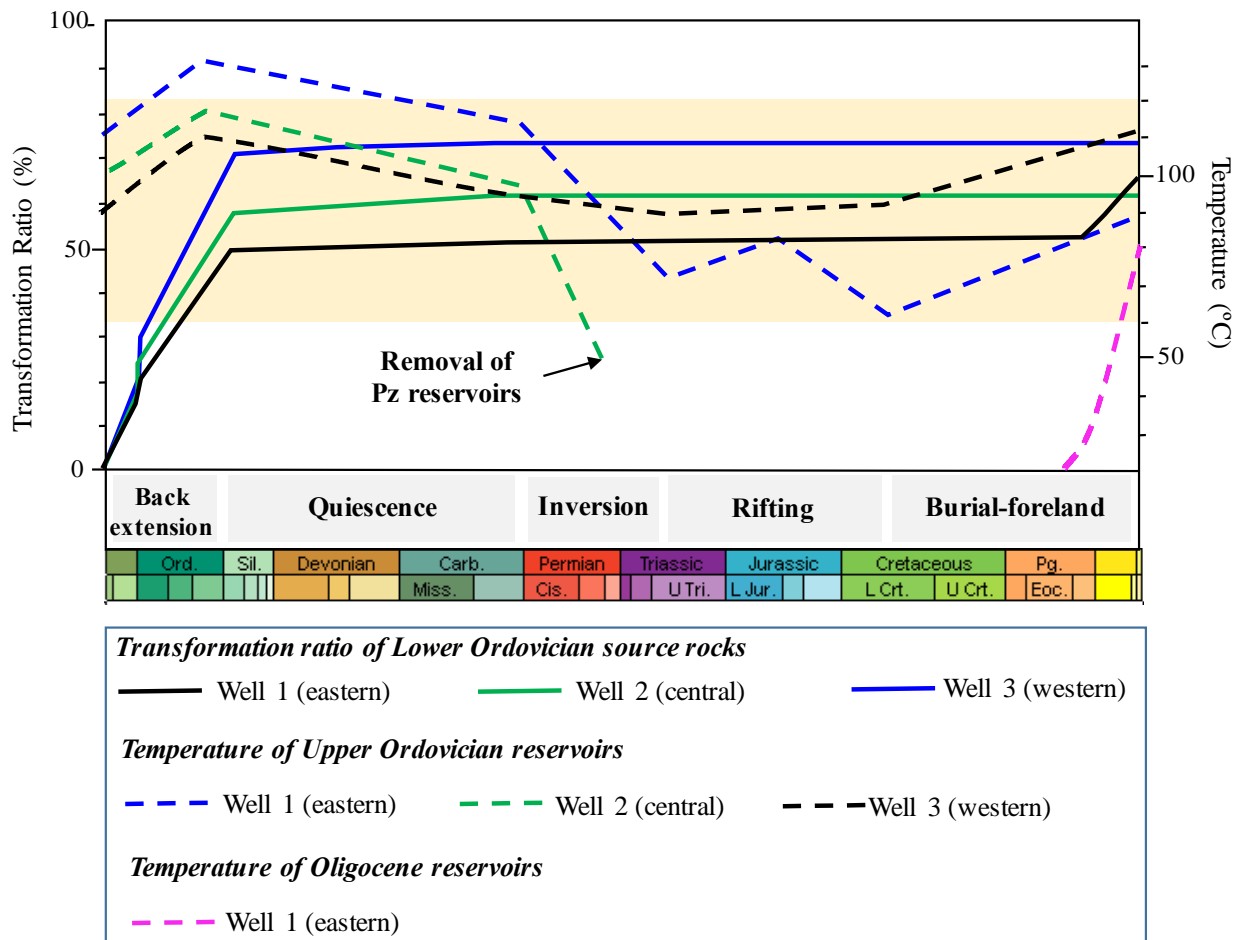


**Fig. 8.6.** *Combined plots of transformation ratio of the Lower Ordovician source rocks and the temperature history of possible reservoirs at the three well locations.*

In the western and central areas of the basin (well 2 and 3), Ordovician reservoirs cooled down rapidly due to the Permian uplift. The resulting erosion of up to 2000 meters (Fig. 8.3) and subsequent pressure release are likely to have caused fracturing and leakage of trapped hydrocarbons. In the central area of the basin (well 2, green dotted line on Fig. 8.6), reservoirs were almost completely eroded. In the case of the distal eastern margin (well 3 location), reservoir rocks have not been affected by tectonism, and have been exposed to relatively steady temperatures (dotted black lines on Fig. 8.6) within the optimum entrapment zone. Long-term

tectonic stability may have favored preservation in deeply-buried reservoirs (tight sand gas?) and/or in the shaly source rock interval (shale gas?).

For Oligocene reservoirs, the only location considered is the eastern area (pink dotted line on Fig. 8.6). Recently these rocks reached temperatures of the optimum entrapment zone. In this area, source rock generation within the early gas window restarted recently at from deep-seated Lower Ordovician rocks. Therefore, migration into these reservoirs is unlikely and is mainly dependent on remigration from deeper reservoirs.

# 9. DISCUSSION

Based on the assumption of a Lower Ordovician source rock over the entire section, this study suggests the existence of a working petroleum system in which tectonism has driven profound changes through time. As shown in Fig 8.1 and 8.2, during Ordovician time, back arc extension favored rapid accumulation and high temperatures to mature the organic matter, but the following Permian uplift destroyed accumulations and impeded further generation in the central and western parts of the basin. More recently, due to Cenozoic foreland sedimentation, burial depth of the Ordovician source rocks has increased and renewed transformation is taking place within the eastern margin of the basin. A potential Paleozoic petroleum system has not experienced the degree of uplift, erosion, and destruction of reservoirs in the eastern part of the basin (Fig. 8.6), making preservation of any petroleum accumulation more plausible.

Compared to the northern part of the basin, hydrocarbons exploration has been unsuccessful in the southern Llanos basin, with only four minor discoveries of Upper Cretaceous-aged heavy oils (Campos, 2011). This study shows that the Upper Cretaceous source rocks are immature and consequently suggests that these oils are a result of long-distance migrations, most likely from the eastern foothills or from the northern deeper part of the basin.

Fig. 9.1 presents the superposition of Upper Cretaceous-Paleogene source rocks and older units in the southern Llanos basin. Based on the map analysis and the combined source–reservoir graphs (Fig. 8.6), within the north-south depocenters in the eastern margin of the basin, Lower Ordovician source rock units are buried deep enough with a temperature range to generate hydrocarbons in an area where the Cretaceous source rocks are completely absent and immature. This area appears to be prospective not only because of renew generation, but also because of the potential existence of preserved gas and/or shale gas accumulations. Based on this study, potential migration of hydrocarbons is believed to occur towards the eastern of the study area where the Paleozoic units pinch out against the metamorphic basement. Therefore, that area should be revised in detail to evaluated the feasibility of hydrocarbons accumulations.
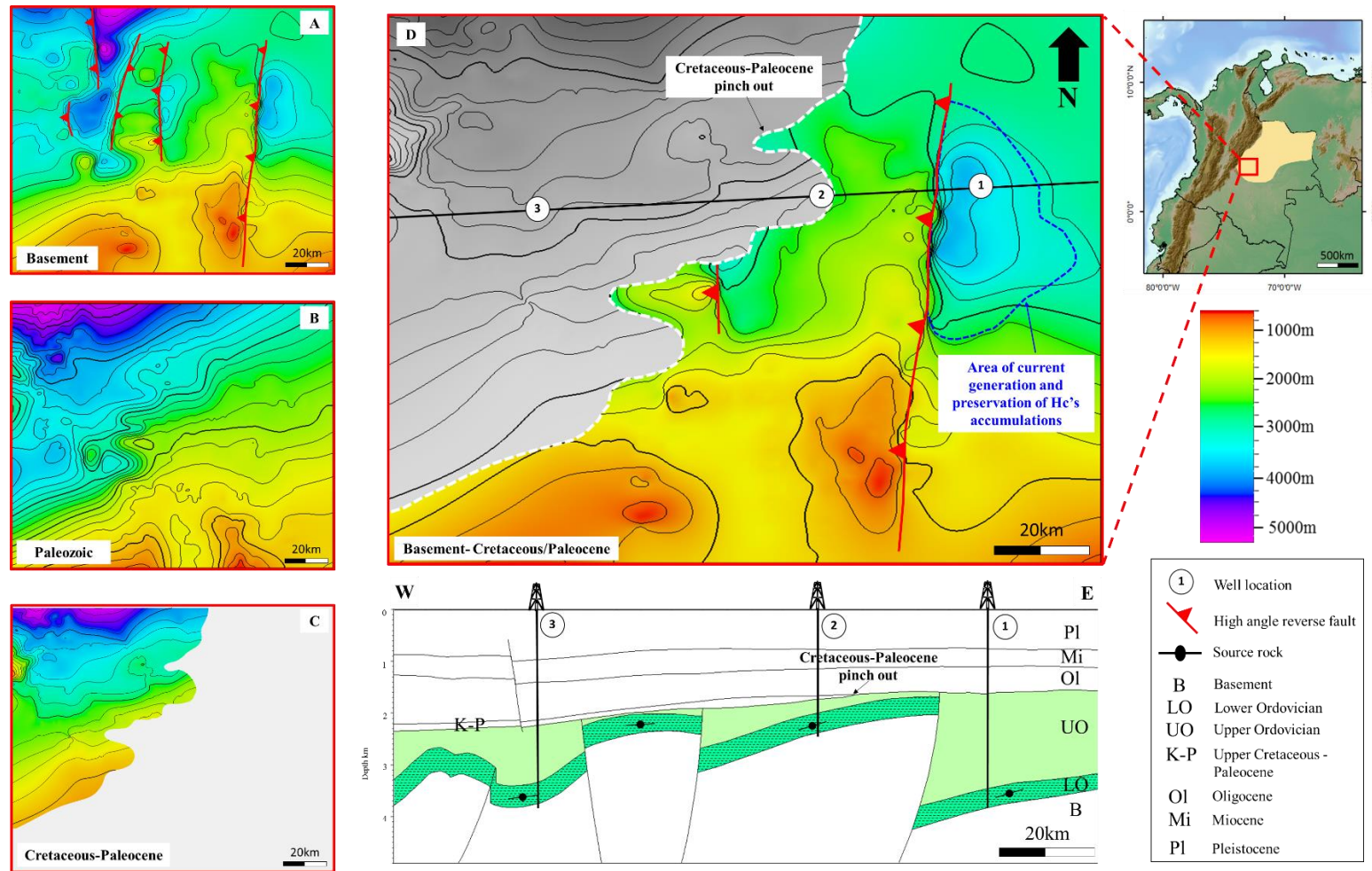
***Fig 9.1.*** *Structural maps in depth (m) of A-Basement, B-Paleozoic, and C- Upper Cretaceous-Paleocene units. D. Structural map showing aerial distribution of the Cretaceous-Paleogene unit relative to basement rocks. E. E-W geological section showing vertical and lateral distribution of Paleozoic units. Numbers 1, 2, and 3 represent the location of wells used in this study. Main observations include the absence of the Upper Cretaceous-Paleocene source rocks in the eastern margin of the basin where Lower Ordovician units are buried deep enough with a temperature range to generate hydrocarbons given the source rock quality.*

107

**Model's limitations**

Due to limited data the model only demonstrates a "what if" scenario and accordingly simulates hydrocarbon generation from a potential Lower Ordovician source rock given the input parameters.

When simulating hydrocarbons generation from an organic carbon rich rock, it is obvious that a process that is critically dependent on heat influx variations can only be an approximation when using theoretical data. In this regard, the most sensitive assumption made was the definition of theoretical values for heat flow during the Early Paleozoic (i.e. Ordovician) as no information on this subject exists.

Migration is a crucial element in any petroleum system modeling exercise. In this case, it is evident that available information was insufficient for performing proper migration analysis. In addition, due to 2D basin modeling limitations in space, migration pathways perpendicular to the section would not be predicted.

# 10. CONCLUSIONS

## 10.1. BARBADOS STUDY CASE

Detailed geochemical characterization leads to the following conclusions:

- ✓ Two petroleum groups were identified. Group A petroleum occurs in the south of the island (Woodbourne oil field) and includes low maturity oils (0.72-0.77%Ro). Group B petroleum occurs in the north of the island (Shale Quarry) and is characterized by higher maturity oils (0.87-0.94%Ro). Slight source rock facies differences were also identified between the two groups.

- ✓ Maturity and facies differences suggest generation within two separate kitchens from either 1- the same source rock with slight facies variations and buried at different depths, or 2- from two different source rocks.

- ✓ Barbados petroleum was generated by a Cretaceous source rock.

- ✓ In the Woodbourne field, an initial filling event is interpreted to have charged the reservoirs after the Mid-Miocene uplift of the Barbados ridge (recorded as biodegraded oil in samples above 1000 meters). Later, due to leakage from deeper reservoirs, the light fraction (n-C3 to n-C9) has migrated and mixed with the biodegraded and shallower oils. The light fraction and the heavier are believed to have the same origin.

- ✓ Geochemical comparison of the Barbados sample set with other northern South American and Caribbean oils/source rocks shows that Barbados petroleum was not derived from the Upper Cretaceous, carbonate-rich La Luna Formation or its eastern equivalent the Querecual Formation as earlier proposed (Lawrence et al., 2002; Burggraf et al., 2002; Leahy et al., 2004; Hill and Schenk, 2005).

- ✓ Barbados oils were derived from a source rock deposited in similar conditions to rocks of the Gacheta formation in the Llanos basin.

- ✓ Analyzed Paleogene source rocks from the northeastern margin of the island do not show significant hydrocarbon generation potential.

## 10.2 SOUTHERN LLANOS BASIN STUDY CASE

Under the assumption that the modeled Lower Ordovician type III source rock is present along the entire profile, the 2D basin modeling leads to the following conclusions.

✓ Hydrocarbons generation began in the Late Ordovician and extended until the Early Silurian with gas as the main generated phase, and probably minors amounts of oil.

✓ In the western and central parts of the basin, Permian regional uplift resulted in erosion and destruction of potential existing accumulations.

✓ The eastern margin of the basin is the only area where Miocene to ongoing hydrocarbon maturation coexists with potential for preservation in reservoirs. The best reservoirs are the Upper Ordovician clastic rocks lying within the optimum entrapment zone.

✓ The eastern tectonically stable area of the basin has potential for hosting hydrocarbons preserved from the initial generation phase, either in convectional reservoirs or within the source rock.

✓ Upper Cretaceous source rocks in this part of the basin are immature, and thus heavy oils of this age found in four minor discoveries correspond to long-distance migrated oils.

The results of this study indicate that Paleozoic units potentially represent an additional source of hydrocarbons in the eastern margin of the basin where traditional Upper Cretaceous-Paleogene source are absent.

# References

1.    Ahmed, M., 2016. Tectonostratigraphic Evolution of the Barbados Accretionary Prism and the Tobago Basin: Implications for Petroleum Systems (Master's thesis, University of Stavanger, Norway).

2.    Aitken, T., Mann, P., Escalona, A. and Christeson, G.L., 2011. Evolution of the Grenada and Tobago basins and implications for arc migration. Marine and Petroleum Geology, 28(1), pp.235-258.

3.    Alberdi-Genolet, M., & Tocco, R., 1999. Trace metals and organic geochemistry of the Machiques Member (Aptian–Albian) and La Luna Formation (Cenomanian–Campanian), Venezuela. Chemical Geology, 160(1), 19-38.

4.    Alberdi, M., Moldowan, J.M., Peters, K.E. and Dahl, J.E., 2001. Stereoselective biodegradation of tricyclic terpanes in heavy oils from the Bolivar Coastal Fields, Venezuela. Organic Geochemistry, 32(1), pp.181-191.

5.    Allen, P.A. and Allen, J.R., 2013. Basin analysis: Principles and application to petroleum play assessment. John Wiley & Sons.

6.    Alfaro, C., Alvarado, I. and Manrique, A., 2015. Heat Flow Evaluation at Eastern Llanos Sedimentary Basin, Colombia.

7.    Arthur, M.A., Dean, W.E. and Pratt, L.M., 1988. Geochemical and climatic effects of increased marine organic carbon burial at the Cenomanian/Turonian boundary. Nature, 335(6192), pp.714-717.

8.    Barker, L.H. and Poole, E.G., 1983. Geology and Mineral Resource Assessment of the Island of Barbados. The Government of Barbados.

9.    Barrero, D., Pardo, A., Vargas, C.A. and Martínez, J.F., 2007. Colombian sedimentary basins: Nomenclature, boundaries and petroleum geology, a new proposal. Agencia Nacional de Hidrocarburos (Vol. 1, p. 92). ANH and B&M Exploration Ltd Bogotá.

10.   Barron, E.J., Fawcett, P.J., Peterson, W.H., Pollard, D. and Thompson, S.L., 1995. A "simulation" of Mid-Cretaceous climate. Paleoceanography, 10(5), pp.953-962.

11.   Bautista, D.F.G., dos Santos Neto, E.V. and Penteado, H.L.D.B., 2015. Controls on petroleum composition in the Llanos basin, Colombia: Implications for exploration. AAPG Bulletin, 99(8), pp.1503-1535.

12.   Brown, K. and Westbrook, G., 1987. The tectonic fabric of the Barbados Ridge accretionary complex. Marine and Petroleum Geology, v. 4: p. 71-81.

13.     Burggraf, A., Lung-Chuan, K., Weinzapfel, A., Senneseth, O., 2002. A new assessment of Barbados onshore oil characteristics and implications for regional petroleum exploration, 16th Caribbean Geological Congress Abstracts, Barbados, West Indies 2002 p. 32.

14.     Bush, A.B. and Philander, S.G.H., 1997. The Late Cretaceous: Simulation with a coupled atmosphere-ocean general circulation model. Paleoceanography, 12(3), pp.495-516.

15.     Cassani, F., Gallango, O., Talukdar, S., Vallejos, C. and Ehrmann, U., 1988b. Methylphenanthrene maturity index of marine source rock extracts and crude oils from the Maracaibo basin. Organic Geochemistry, 13(1-3), pp.73-80.

16.     Chaderton, N., L., Wood, and P. Mann, 2004. The structure and stratigraphy of the Barbados accretionary prism and the Tobago forearc basin in American Geophysical Union, Fall Meeting. San Francisco.

17.     Chaderton, N., 2005. The Evolution of the Tobago Forearc basin: Implications for Sedimentation and Hydrocarbon Prospectivity [unpublished Master of Sciences thesis]: The University of Texas at Austin, Austin, 113 p.

18.     Cooper, M. A., et al., 1995. Basin development and tectonic history of the Llanos basin, Eastern Cordillera, and Middle Magdalena Valley, Colombia: AAPG Bulletin, v. 79, p. 1421–1443.

19.     Cordani, U. G., L. M. Fraga, N. Reis, C. C. G. Tassinari, and B. B. Brito-Neves, 2010. On the origin and tectonic significance of the intraplate events of Grenvillian-type age in South America: A discussion: Journal of South American Earth Sciences, v. 29, no. 1, p. 143–159.

20.     Damsté, J.S.S., Kenig, F., Koopmans, M.P., Köster, J., Schouten, S., Hayes, J.M. and de Leeuw, J.W., 1995. Evidence for gammacerane as an indicator of water column stratification. Geochimica et Cosmochimica Acta, 59(9), pp.1895-1900.

21.     Damsté, J.S.S., Muyzer, G., Abbas, B., Rampen, S.W., Massé, G., Allard, W.G., Belt, S.T., Robert, J.M., Rowland, S.J., Moldowan, J.M. and Barbanti, S.M., 2004. The rise of the rhizosolenid diatoms. Science, 304(5670), pp.584-587.

22.     De Monroy, Z. and Van Erve, A., 1988. Revisión Palinoestratigráfica del Cretácico y Terciario de Apure (Venezuela Suroccidental) Palyno-stratigraphic Revision of Cretaceous and Tertiary de Apure (Venezuela South West).

23.     Deville, E., A. Mascle, S.-H. Guerlais, C. Decalf, and B. Colletta., 2003. Lateral changes of frontal accretion and mud volcanism processes in the Barbados accretionary prism and some implications, in C. Bartolini, R. T. Buffler, and J. Blickwede, eds., AAPG Memoir 79, p. 656-674.

24.     Deville, E., S.-H. Guerlais, Y. Callec, R. Griboulard, P. Huyghe, S. Lallemant, A. Mascle, M. Noble, J. Schmitz, and C. o. t. C. W. Group, 2006. Liquefied vs stratified sediment

mobilization processes: insight from the south of the Barbados accretionary prism: Tectonophysics, v. 428, p. 33-47.

25. Deville, E., and A. Mascle, 2012. The Barbados ridge: A mature accretionary wedge in front of the Lesser Antilles active margin in D. G. Bally, and A. W. Roberts, eds., Regional Geology and Tectonics: Principles of Geologic Analysis: Amsterdam, Elsevier, p. 580-607.

26. Di Croce, J., 1996. Eastern Venezuela Basin: Sequence stratigraphy and structural evolution (Doctoral dissertation, Rice University).

27. Dueñas, H., and S. N. Cesari, 2006. Palynological evidence of Early Carboniferous sedimentation in the Llanos Orientales basin, Colombia: Review of Palaeobotany and Palynology, v. 138, no. 1, p. 31–42.

28. Edgar, N.T., Saunders, J.B., Donnelly, T.W., Schneidermann, N., Maurasse, F., Bolli, H.M., Hay, W.W., Reidel, W.R., SILVA, P., Boyce, R.E. and Prell, W., 1973. Site 146-149. Edgar, NT, Saunders, JB, et al., Initial Reports of the Deep Sea Drilling Project, 15, pp.17-125.

29. Erlich, R.N., Palmer-Koleman, S.E. and Lorente, M.A., 1999. Geochemical characterization of oceanographic and climatic changes recorded in Upper Albian to Lower Maastrichtian strata, western Venezuela. Cretaceous Research, 20(5), pp.547-581.

30. Erlich, R.N., Villamil, T. and Keens-Dumas, J., 2003. Controls on the deposition of Upper Cretaceous organic carbon–rich rocks from Costa Rica to Suriname.

31. Escalona, A., and P. Mann, 2011. Tectonics, basin subsidence mechanisms, and paleogeography of the Caribbean–South American plate boundary zone: Marine and Petroleum Geology, v. 28, no. 1, p. 8–39.

32. Escobar, M., Márquez, G., Inciarte, S., Rojas, J., Esteves, I., & Malandrino, G., 2011. The organic geochemistry of oil seeps from the Sierra de Perijá eastern foothills, Lake Maracaibo basin, Venezuela. Organic geochemistry, 42(7), 727-738.

33. Etayo-Serna, F., 1976. Contornos sucesivos del mar Cretácico en Colombia. In Memorias Primer Congreso Colombiano de Geologia, Bogota, Colombia, 1976.

34. Forero-Suarez, A., 1990. The basement of the Eastern Cordillera, Colombia: an allochtonoous terrane in northwestern South America. Journal of South American Earth Sciences, v. 3, p. 141-151.

35. Frakes, L.A., 1999. Estimating the global thermal state from Cretaceous sea surface and continental temperature data. SPECIAL PAPERS-GEOLOGICAL SOCIETY OF AMERICA, pp.49-58.

36. Galarraga, F., Urbani, F., Escobar, M., Marquez, G., Martínez, M. and Tocco, R., 2010. Main factors controlling the compositional variability of seepage oils from Trujillo State, Western Venezuela. Journal of Petroleum Geology, 33(3), pp.255-267.

37. Gill, F. L., I. C. Harding, C. T. Little, and J. A. Todd, 2005. Palaeogene and Neogene cold seep communities in Barbados, Trinidad and Venezuela: An overview: Palaeogeography, Palaeoclimatology, Palaeoecology, v. 227, p. 191-209.

38. Gomez, E., T. E. Jordan, T. E. Allmendinger, K. Hegarty, and S. Kelley, 2005. Syntectonic Cenozoic sedimentation in the northern Middle Magdalena Valley basin of Colombia and implications for exhumation of the northern Andes: Geological Society of America Bulletin, v. 117, p. 547–569, no. 5.

39. Grantham, P.J. and Wakefield, L.L., 1988. Variations in the sterane carbon number distributions of marine source rock derived crude oils through geological time. Organic Geochemistry, 12(1), pp.61-73.

40. Halpern, H.I., 1995. Development and applications of light-hydrocarbon-based star diagrams. AAPG Bulletin, 79(6), pp.801-815.

41. Herngreen, G.F.W. and Jimenez, H.D., 1990. Dating of the Cretaceous Une Formation, Colombia and the relationship with the Albian-Cenomanian African-South American microfloral province. Review of Palaeobotany and Palynology, 66(3-4), pp.345-359.

42. Hill, R.J., and Schenk, C.J., 2005. Petroleum geochemistry of oil and gas from Barbados; implications for distribution of Cretaceous source rocks and regional petroleum prospectivity Marine and Petroleum Geology v. 22, p. 917-943.

43. Holba, A.G., Ellis, L., Dzou, I.L., Hallam, A., Masterson, W.D., Francu, J. and Fincannon, A.L., 2001, September. Extended tricyclic terpanes as age discriminators between Triassic, Early Jurassic and Middle-Late Jurassic oils. In 20th International Meeting on Organic Geochemistry (Vol. 1, p. 464).

44. Horton, B. K., J. E. Saylor, J. Nie, A. Mora, M. Parra, A. Reyes- Harker, and F. Stockli, 2010. Linking sedimentation in the northern Andes to basement configuration, Mesozoic extension, and Cenozoic shortening: Evidence from detrital zircon U-Pb ages, Eastern Cordillera, Colombia: Geological Society of America Bulletin, v. 122, no. 9–10, p. 1423–1442.

45. Hughes, W.B., 1984. Use of thiophenic organosulfur compounds in characterizing crude oils derived from carbonate versus siliciclastic sources.

46. Ibanez-Mejia, M., J. Ruiz, V. A. Valencia, A. Cardona, G. E. Gehrels, and A. R. Mora, 2011. The Putumayo Orogen of Amazonia and its implications for Rodinia reconstructions: New U-Pb geochronological insights into the Proterozoic tectonic evolution of northwestern South America: Precambrian Research, v. 191, no. 1–2, p. 58–77.

47.    Irving, E. M., ed., 1972. Mapa geológico de la Península de la Guajira, Colombia, (Compilación): Bogotá, Colombia Ins.t. Nac. Inv. Geol. Mineras, scale 1:100,000.

48.    Jarvis, G.T. and McKenzie, D.P., 1980. Sedimentary basin formation with finite extension rates. Earth and Planetary Science Letters, 48(1), pp.42-52.

49.    Javis, A., H. I. Reuter, A. Nelson, A. Escalona, and I. Filina, 2008, Structure and stratigraphy of the Tobago-Barbados Ridge and its implications for hydrocarbons in the Barbados offshore area: AAPG Annual Convention and Exhibition.

50.    Johnson, C.C., 1999. Evolution of Cretaceous surface current circulation patterns, Caribbean and Gulf of Mexico. SPECIAL PAPERS-GEOLOGICAL SOCIETY OF AMERICA, pp.329-344

51.    Klotz, J., Khazaradze, G., Angermann, D., Reigber, C., Perdomo, R., & Cifuentes, O., 2001. Earthquake cycle dominates contemporary crustal deformation in central and southern Andes. Earth and Planetary Science Letters, 193(3-4), 437-446.

52.    Kugler, H. G., P. Jung, and J. Saunders, 1984. The Joes River Formation of Barbados and its fauna: Eclogae Geologicae Helvetiae, v. 77, p. 675-705.

53.    Kvalheim, O.M., Christy, A.A., Telnæs, N. and Bjørseth, A., 1987. Maturity determination of organic matter in coals using the methylphenanthrene distribution. Geochimica et Cosmochimica Acta, 51(7), pp.1883-1888.

54.    Lawrence, S.R., Cornford, C., Kelly, R., Mathews, A., Leahy, K., 2002. Kitchens on a conveyor belt-petroleum systems in accretionary prisms, 16th Caribbean Geological Congress Abstracts, Barbados, Wet Indies 2002 p. 41.

55.    Leahy, K., Lawrence, S., Thrift, J., 2004. Caribbean source rocks may point toward buried treasure. Oil and Gas Journal 102 (8), 35–39.

56.    López, L., 2014. Study of the biodegradation levels of oils from the Orinoco Oil Belt (Junin area) using different biodegradation scales. Organic Geochemistry, 66, pp.60-69.Rodrigues, K., 1995. The Couva Marine oil: a unique, terrestrially sourced, Tertiary oil in Trinidad.

57.    López, L., Mónaco, S.L. and Volkman, J.K., 2015. Evidence for mixed and biodegraded crude oils in the Socororo field, Eastern Venezuela basin. Organic Geochemistry, 82, pp.12-21.e Venezuela: Derivation from Natural Seepages. Journal of Petroleum Geology, 36(2), pp.179-193.

58.    López, L., and Mónaco, S. L., 2017. Vanadium, nickel and sulfur in crude oils and source rocks and their relationship with biomarkers: Implications for the origin of crude oils in Venezuelan basins. Organic Geochemistry.

59. McKenzie, D., 1978. Some remarks on the development of sedimentary basins. Earth and Planetary science letters, 40(1), pp.25-32.

60. Mackenzie, A.S., Patience, R.L., Maxwell, J.R., Vandenbroucke, M. and Durand, B., 1980. Molecular parameters of maturation in the Toarcian shales, Paris Basin, France—I. Changes in the configurations of acyclic isoprenoid alkanes, steranes and triterpanes. Geochimica et Cosmochimica Acta, 44(11), pp.1709-1721.

61. Malone, J. R., R. D. Nance, J. D. Keppie, and J. Dostal, 2002. Deformational history of part of the Acatlan Complex: Late Ordovician–Early Silurian and Early Permian orogenesis in southern Mexico: Journal of South American Earth Sciences, v. 15, no. 5, p. 511–5249.

62. Mann, P., 1999. Caribbean sedimentary basins: Classification and tectonic setting from Jurassic to present, in P. Mann, ed., Caribbean sedimentary basins. Sedimentary Basins of the World, v. 4: Amsterdam, Elsvier Science, p. 3-31.

63. Marquez, G., Galarraga, F., Fernandez, R., De Freitas, K.A., Lorenzo, E., Escobar, M., Sierra, C. and Gallego, J.R., 2013. Geochemical Composition of Beach Tar from the Se Coast of the Paria Peninsula, Ne Venezuela: Derivation from Natural Seepages. Journal of Petroleum Geology, 36(2), pp.179-193.

64. Mello, M.R., Gaglianone, P.C., Brassell, S.C. and Maxwell, J.R., 1988. Geochemical and biological marker assessment of depositional environments using Brazilian offshore oils. Marine and petroleum Geology, 5(3), pp.205-223.

65. Mello, M.R., Telnaes, N., Gaglianone, P.C., Chicarelli, M.I., Brassell, S.C. and Maxwell, J.R., 1988. Organic geochemical characterisation of depositional palaeoenvironments of source rocks and oils in Brazilian marginal basins. Organic geochemistry, 13(1-3), pp.31-45.

66. Moldowan, J.M., 1984. C30-steranes, novel markers for marine petroleums and sedimentary rocks. Geochimica et Cosmochimica Acta, 48(12), pp.2767-2768.

67. Moldowan, J.M., Seifert, W.K. and Gallegos, E.J., 1985. Relationship between petroleum composition and depositional environment of petroleum source rocks. AAPG bulletin, 69(8), pp.1255-1268.

68. Moreno-Sanchez, M., and A. Pardo-Trujillo, 2003. Stratigraphical and sedimentological constraints on western Colombia: Implications on the evolution on the Caribbean plate: AAPG Bulletin, v. 79, p. 891–924.

69. Norabuena, E. O., Dixon, T. H., Stein, S., & Harrison, C. G. A., 1999. Decelerating nazca-South America and nazca-pacific plate motions. Geophysical Research Letters, 26(22), 3405-3408.

70. Parra, M., A. Mora, C. Jaramillo, M. Strecker, R. Sobel, and L. Quiroz, 2009. Orogenic

wedge advance in the northern Andes: Evidence from the Oligocene–Miocene sedimentary record of the Medina basin, Eastern Cordillera, Colombia: Geological Society of America Bulletin, v. 121, no. 5–6, p. 780–800.

71.    Parra, M., A. Mora, C. Jaramillo, V. Torres, G. Zeilinger, and M. R. Strecker, 2010. Tectonic controls on Cenozoic fore- land basin development in the northeastern Andes, Colombia: Basin Research, v. 22, p. 874–903.

72.    Peters, K.E. and Moldowan, J.M., 1991. Effects of source, thermal maturity, and biodegradation on the distribution and isomerization of homohopanes in petroleum. Organic geochemistry, 17(1), pp.47-61.

73.    Peters, K.E. and Moldowan, J.M., 1993. The biomarker guide: interpreting molecular fossils in petroleum and ancient sediments.

74.    Peters, K.E., Walters, C.C. and Moldowan, J.M., 2005. The biomarker guide (Vol. 1). Cambridge University Press.

75.    Pindell, J., R. Higgs, and J. Dewey, 1998. Cenozoic palinspastic reconstruction, paleogeographic reconstruction, and hydrocarbon setting of the northern margin of South America, in J. Pindell and C. Drake, eds., Paleogeographic evolution and non-glacial eustasy, northern South America: Tulsa, Oklahoma, SEPM, v. 58, p. 45–85.

76.    Portillo, E., Torres, J., González, A., Esteves, I., Rojas, J. and Escobar, M., 2008. Origin, thermal maturity and alteration level of oil seeps in the Perijá range foothills, Venezuela. Revista Técnica de Ingeniería de la Universidad del Zulia, 31, pp.97-106.

77.    Rada, R., Mili, H., Bicknell, E. and Blettner, M., 1989. Development and application of a metric on semantic nets. IEEE transactions on systems, man, and cybernetics, 19(1), pp.17-30.

78.    Radke, M., 1988. Application of aromatic compounds as maturity indicators in source rocks and crude oils. Marine and Petroleum Geology, 5(3), pp.224-236.

79.    Rangel, A., Parra, P. and Niño, C., 2000. The La Luna Formation: chemostratigraphy and organic facies in the Middle Magdalena basin. Organic Geochemistry, 31(12), pp.1267-1284.

80.    Regueiro, J., and A. Pena, 1996, AVO in North of Paria, Venezuela: Gas methane versus condensate reservoirs: Geophysics, v. 61, p. 937-946.

81.    Riolo, J., Hussler, G., Albrecht, P. and Connan, J., 1986. Distribution of aromatic steroids in geological samples: their evaluation as geochemical parameters. Organic Geochemistry, 10(4-6), pp.981-990.

82. Rodrigues, K., 1995. The Couva Marine oil: a unique, terrestrially sourced, Tertiary oil in Trinidad.

83. Rubinstein, I., Sieskind, O. and Albrecht, P., 1975. Rearranged sterenes in a shale: occurrence and simulated formation. Journal of the Chemical Society, Perkin Transactions 1, (19), pp.1833-1836.

84. Ruiz, J., R. M. Tosdal, P. A. Restrepo, and G. Murillo-Muñetón, 1999, Pb isotope evidence for Colombia–southern Mexico connections in the Proterozoic, in V. A. Ramos and J. D. Keppie, eds., Laurentia–Gondwana connections before Pangea: Geological Society of America, Special Paper 336, p. 183–197.

85. Saunders, J., Bernoulli, D., Muller-Merz, E., Oberhansli, H., Perch-Nielsen, K., Riedel, W.R., Sanfilippo, A., And Torrini Jr., R., 1984. Stratigraphy of the Late Middle Eocene to Early Oligocene in the Bath Cliff Section, Barbados, West Indies: Micropaleontology, v. 30, p. 390-425.

86. Seifert, W.K. and Moldowan, J.M., 1986. Use of biological markers in petroleum exploration. Methods in geochemistry and geophysics, 24, pp.261-290.

87. Senn, A., 1940. Paleogene of Barbados and its bearing on history and structure of Antillean-Caribbean region: AAPG bulletin, v. 24, p. 1548-1610.

88. Sieskind, O., Joly, G. and Albrecht, P., 1979. Simulation of the geochemical transformations of sterols: superacid effect of clay minerals. Geochimica et Cosmochimica Acta, 43(10), pp.1675-1679.

89. Silva, I.P. and Sliter, W.V., 1999. Cretaceous paleoceanography: evidence from planktonic foraminiferal evolution. Special Papers-Geological Society of America, pp.301-328.

90. Simoneit, B.R., 1977. Diterpenoid compounds and other lipids in deep-sea sediments and their geochemical significance. Geochimica et Cosmochimica Acta, 41(4), pp.463-476.

91. Speed, R., R. Torrini, and P. L. Smith, 1989. Tectonic evolution of the Tobago Trough forearc basin: Journal of Geophysical Research: Solid Earth, v. 94, p. 2913-2936.

92. Speed, R., 1991, Buried accretionary prism drilled on Barbados, JOI/USSAC Newsletter: United States, Joint Oceanographic Institutions Inc. Washington, DC, United States, p. 1.

93. Speed, R., 1994. Barbados and the Lesser Antilles Forearc, in Caribbean Geology an Introduction, S.K. Donovan and T.A. Jackson, Editors. The University of the West Indies Publishers' Association: Kingston.

94. Stein, C.A., 1995. Heat flow of the Earth. Global Earth Physics, pp.144-158.

95. Sweeney, J.J. and Burnham, A.K., 1990. Evaluation of a simple model of vitrinite reflectance

based on chemical kinetics (1). AAPG bulletin, 74(10), pp.1559-1570.

96. Talukdar, S.C., DeToni, B., Marcano, F., Sweeney, J. and Rangel, A., 1993. Upper Cretaceous source rocks of northern South America. AAPG Bulletin (American Association of Petroleum Geologists); (United States), 77(CONF-930306--).

97. Tassinari, C. G., Bettencourt, J. S., Geraldes, M. C., Macambira, M. and Lafon, J. M., 2000. The Amazonian Craton. In: Tectonic evolution of South America. Cordani, U. G., Milani, E. J., Thomaz, A, Campos, D. A (eds). Rio de Janeiro: 31st International Geological Congress, 41-96.

98. Thompson, K.F.M., 1987. Fractionated aromatic petroleums and the generation of gas-condensates. Organic Geochemistry, 11(6), pp.573-590.

99. Tissot, B.P. and Welte, D.H., 2013. Petroleum formation and occurrence. Springer Science & Business Media.

100. Tocco, R., Escobar, M., Ruggiero, A. and Galarraga, F., 1995. Geochemistry of oil seeps and rock samples of the Early Tertiary section from the Northandean Flank of the Venezuelan Andes. Organic geochemistry, 23(4), pp.311-327.

101. Tocco, R. and Margarita, A., 1999. Geochemical study of Misoa Formation crude oils, Centro Lago Field, Lake Maracaibo, Western Venezuelan basin. Marine and petroleum geology, 16(2), pp.135-150.

102. Torrini, R. and R. Speed, 1989. Tectonic Wedging in the Forearc Basin-Accretionary Prism Transition, Lesser Antilles Forearc. Journal of Geophysical Research. 94(No. B8): p. 10, 549 - 10, 584.

103. Ulloa, C., V. E. Perez, and B. Baldis, 1982. Unidades litoestratigráficas del Ordovícico de los Llanos Orientales de Colombia: Memorias V congreso Latinoamericano de Geología, v. 1, p. 109–112 (in Spanish).

104. Van Graas, G.W., 1990. Biomarker maturity parameters for high maturities: calibration of the working range up to the oil/condensate threshold. Organic Geochemistry, 16(4-6), pp.1025-1032.

105. Volkman, J.K., 1988. Biological marker compounds as indicators of the depositional environments of petroleum source rocks. Geological Society, London, Special Publications, 40(1), pp.103-122.

106. Waples, D.W. and Machihara, T.M., 1991. Biomarkers for Geologists. AAPG Methods in Exploration Series No. 9. American Association of Petroleum Geologists, Tulsa, Oklahoma.

107. Weber, J. C., T. H. Dixon, C. DeMets, W. B. Ambeh, P. Jansma, G. Mattioli, J. Saleh, G. Sella, R. Bilham, and Pérez, O., 2001. GPS estimate of relative motion between the

Caribbean and South American plates, and geologic implications for Trinidad and Venezuela: Geology, v. 29, p. 75-78.

108.  Westbrook, G., A. Mascle, and B. Biju-Duval, 1984. Geophysics and the structure of the Lesser Antilles forearc, in B. Biju-Duval, and J. C. Moore, eds., Initial Reports of DSDP 78A: Washington, DC, US Government Printing Office, p. 23-38.

109.  Williams, K., 1995. Tectonic subsidence analysis and Paleozoic paleogeography of Gondwana, in A. J. Ankard, R. Suarez Soruco, and H. J. Welsink, eds., Petroleum basins of South America: AAPG Memoir 62, p. 79–100.

110.  Wilson, D. S., 1996. Fastest known spreading on the Miocene cocos-pacific plate boundary. Geophysical Research Letters, 23 (21), p. 3003-3006.

111.  Zumberge, J.E., 1984. Source rocks of the La Luna Formation (Upper Cretaceous) in the Middle Magdalena Valley, Colombia.